

Aus dem Bereich Molekulare Zellbiologie
Theoretische Medizin und Biowissenschaften
der Medizinischen Fakultät
der Universität des Saarlandes, Homburg/Saar

**Protein Kinase C,
the Spatial and Temporal Modulator of
Intracellular Signal Transduction**

***Dissertation zur Erlangung des Grades eines
Doktors der Naturwissenschaften***

der Medizinischen Fakultät
der UNIVERSITÄT DES SAARLANDES
2014

vorgelegt von: Xin Hui

geb. am: 23.09.1978 in Wuxi, Jiangsu, China

To my dear and loving wife and parents

献给我最亲爱的父母和妻子！

Erklärung gemäß § 7 Abs. 1 Nr. 4

Ich erkläre hiermit an Eides statt, dass ich die vorliegende Arbeit ohne unzulässige Hilfe Dritter und ohne Benutzung anderer als der angegebenen Hilfsmittel angefertigt habe. Die aus anderen Quellen direkt oder indirekt übernommenen Daten und Konzepte sind unter Angabe der Quelle gekennzeichnet.

Weitere Personen waren an der inhaltlich-materiellen Erstellung der vorliegenden Arbeit nicht beteiligt. Insbesondere habe ich nicht die entgeltliche Hilfe von Vermittlungs- bzw. Beratungsdiensten (Promotionsberater/innen oder anderer Personen) in Anspruch genommen. Außer den Angegebenen hat niemand von mir unmittelbar oder mittelbar geldwerte Leistungen für Arbeiten erhalten, die im Zusammenhang mit dem Inhalt der vorgelegten Dissertation stehen.

Die Arbeit wurde bisher weder im Inland noch im Ausland in gleicher oder ähnlicher Form in einem anderen Verfahren zur Erlangung des Doktorgrades einer anderen Prüfungsbehörde vorgelegt.

Ich versichere an Eides statt, dass ich nach bestem Wissen die Wahrheit gesagt und nichts verschwiegen habe.

Vor Aufnahme der vorstehenden Versicherung an Eides Statt wurde ich über die Bedeutung einer eidesstattlichen Versicherung und die strafrechtlichen Folgen einer unrichtigen oder unvollständigen eidesstattlichen Versicherung belehrt.

Ort, Datum

Unterschrift der/des Promovierenden

Unterschrift der die Versicherung an Eides statt aufnehmenden Beamtin bzw. Des aufnehmenden Beamten

Zusammenfassung

In menschlichen Zellen gibt es mehr als fünfhundert simultan arbeitende Kinasen. Das Verständnis ihrer räumlich-zeitlichen Regulation ist nicht nur ein wichtiger Schlüssel zum besseren Verständnis der molekularen Mechanismen menschlicher Erkrankungen, sondern auch für die Entwicklung neuer Therapien notwendig. In dieser Studie konzentrierte ich mich auf die detaillierte Untersuchung der Regulierungsmechanismen der Proteinkinase C (PKC)-Familie, einer ubiquitär vorkommenden Kinase-Familie.

PKC α , ein Mitglied dieser Familie, reagiert auf Ca²⁺-Freisetzung und transloziert diffusionsbegrenzt an die Plasmamembran. Diese Translokation ist ein Schlüsselereignis in der Aktivierung von konventionellen PKCs (cPKCs). Im ersten Abschnitt meiner Dissertation habe ich grundlegende Eigenschaften dieser frühen Schritte der Kinase-Aktivierung untersucht. Für diesen Zweck habe ich mikroskopische Fluoreszenzuntersuchungen an lebenden Zellen durchgeführt und die Kinetik der PKC α -Translokation unter Verwendung von Fusionsproteinen mit unterschiedlichem Molekulargewicht gemessen. Translokationen wurden durch die kontrollierte Ca²⁺-Freisetzung mittels UV-Blitzlicht-Photolyse eingeleitet, welches eine relative Bestimmung der Geschwindigkeit der Ca²⁺-induzierten PKC α -Translokation erlaubte. Das Ergebnis dieser Untersuchungen zeigt, dass die Translokationseigenschaften mit einem ausschließlich diffusionsgesteuerten Prozess kompatibel sind.

Die mögliche Beteiligung des Zytoskeletts an der PKC α -Translokation blieb dennoch eine entscheidende Frage zum besseren Verständnis der PKC α -Aktivierung. Zu deren Beantwortung untersuchte ich die Translokation der PKC α nach pharmakologischer Depolymerisation des Aktins und des Mikrotubuli-Netzwerks. Ich stellte fest, dass keine dieser Zytoskelett-Komponenten die Eigenschaften der PKC α -Translokation beeinflusste und konnte daraus schlussfolgern, dass das Zytoskelett keinen Beitrag zur Kinetik der PKC α Translokation leistet.

Die cPKC-Moleküle funktionieren nicht nur als ein idealer Auslesemechanismus für globale Ca²⁺-Signale, sondern folgen auch räumlich-zeitlich komplexen Ca²⁺-Signalen mit einem ähnlich komplexen Translokationsmuster. Frühere Studien fanden lokale PKC α -Translokationen in Abhängigkeit von kurzlebigen Ca²⁺-Freisetzungseignissen, so genannten Ca²⁺-„Puffs“. Die Lebensdauer dieser Translokationsereignisse überstieg die Länge der „Puffs“ um mehr als das 5-fache. Um dieses Verhalten zu verstehen wollte ich intermolekulare Wechselwirkungen zwischen membrangebundenen PKC α -Molekülen untersuchen. Deren enge Verbindung müsste zu deutlich verlängerten Verweilzeiten an der

Membran und zur Bildung von PKC α -Clustern führen. Um dies zu testen, habe ich Förster-Resonanz-Energie-Transfer (FRET)-Messungen an HEK293-Zellen durchgeführt, die gleichzeitig PKC α -GFP und PKC α -eYFP exprimierten. Nach Stimulation der Zellen mit dem physiologischen Agonisten ATP konnte ich oszillierende FRET-Signale gleichzeitig mit Ca²⁺-Oszillationen und transienten Membranlokalisationen der PKC α messen. Um die alleinige Wirkung von Ca²⁺ zu bewerten, und die Bindung der PKC an Diacylglycerine weitgehend auszuschließen, verwendete ich das Ca²⁺-Ionophor Ionomycin bei verschiedenen extrazellulären Ca²⁺-Konzentrationen. Für sämtliche Ca²⁺-Konzentrationen wurde ein messbarer Anstieg des FRET-Signals beobachtet. Dies spricht für eine direkte Ca²⁺-Abhängigkeit der PKC α -PKC α -Wechselwirkungen an der Plasmamembran. Darüber hinaus zeigten hohe intrazelluläre Ca²⁺-Konzentration unter diesen Bedingungen einen initial starken Anstieg des FRET-Signals, welchem ein spontaner Abfall des Signals folgte. Diese Ergebnisse schlossen einen FRET aufgrund einer Kinase-Anreicherung an der Plasmamembran als den zugrunde liegende FRET-Mechanismus aus und unterstützen ferner das Konzept eines selbstorganisierten PKC α -“Clustering” an der Plasmamembran.

In der ubiquitär exprimierten PKC-Familie teilen sich über 10 PKC-Isoformen ähnliche Grundeigenschaften, einschließlich der eher Substrat-unspezifischen Kinase-Domänen, Lipid-Bindungsdomänen und auto-inhibitorischen Domänen. Wie sie das spezifische Ziel in der Signalkaskade erreichen ist noch unklar. Doch scheint dieses Wissen für unser Verständnis des komplexen Netzwerks von PKC-Signalen in lebenden Zellen essentiell. Ich fand, dass gleichzeitig in einer Zelle exprimierte PKC α - und PKC δ -Fusionsproteine nach physiologischer Stimulation unterschiedliche Muster der Translokation zeigten: PKC α translozierte an die Plasmamembran und PKC δ wurde an intrazelluläre Membranstrukturen rekrutiert, die ich als endoplasmatisches Retikulum (ER) identifizieren konnte. Zum besseren Verständnis dieses Verhaltens verfolgte ich verschiedene Ansätze, die sowohl chemische Stimulation, als auch molekulare und optische Werkzeuge beinhalteten. Meine Ergebnisse zeigten einen bisher unentdeckten G α_s -cAMP-EPAC-PLC ϵ Signalweg, der für die ER-Rekrutierung der PKC δ verantwortlich war. Um die zugrunde liegenden Mechanismen besser verstehen zu können, insbesondere welcher Proteinbereich für das Translokationsverhalten verantwortlich ist, wurden künstliche PKC-Chimären zwischen PKC α und PKC δ durch kreuzweisen Austausch ihrer C1- und C2- oder C1A- und C1B-Domänen konstruiert. Diese Chimären wurden in HEK293-Zellen zur Expression gebracht und ihr Rekrutierungsmuster untersucht. Nach Anwendung einer Vielzahl von spezifischen Stimulationen konnte ich die unterschiedliche Rolle dieser Domänstrukturen für die Erkennung der Zielmembran zeigen. Außerdem habe ich gezeigt, dass ausschließlich die PKC δ -C1B-Domäne für die ER-Rekrutierung verantwortlich und auch hinreichend ist. Die ER-Lokalisierung der PKC δ bewirkt eine lokale Phosphorylierung, die

durch gezielte Phosphorylierungssensoren und die physiologische Verkürzung der ATP-induzierten Ca^{2+} -Oszillationen durch Kinase-vermittelte InsP3-Rezeptor-Phosphorylierung gezeigt wurde. Schlussfolgernd zeigen meine Ergebnisse, dass die vielseitige Kombination eines autonomen C-Domäne-Signalkonstrukts die einzigartigen Funktionen der PKCs ermöglicht. Dies beinhaltet die gleichzeitige Entschlüsselung von Lipid- und Ca^{2+} -Signalen auf der speziellen Zielmembran zur Phosphorylierung spezifischer Zielstrukturen.

Zusammenfassend zeigt die Familie der PKCs ihre Fähigkeit in der Raum-Zeit-Entschlüsselung und der intrazellulären Signalübertragung. Dies führt zu einem neuen und elementaren Verständnis und gewährt Einblicke in das Leben von Zellen.

Abstract

In human cells there are more than five hundred kinases working simultaneously. To understand the spatiotemporal regulation of their activity is the key not only to decode the pathology of human diseases but also for the development of new therapies. In this study, I focused on the protein kinase C (PKC), a ubiquitous expression kinase family, for detailed investigation of their regulatory mechanisms.

As one member of the PKC family, PKC α responds to Ca²⁺ mobilization and translocates to the plasma membrane in a diffusion-limited manner. This translocation is a key event in the activation process of conventional PKCs. In the first part of my thesis I investigated fundamental properties of this early step in the kinase activation. For this purpose I employed fluorescent imaging techniques of living cells to investigate the kinetics of PKC α translocation utilizing fusion constructs with different molecular weight. Translocation was initiated by UV flash photolysis of caged Ca²⁺ that allowed the determination of the relative speed of Ca²⁺-induced PKC α translocation. The result of these studies show that the translocation properties are compatible with solely diffusion-driven process. Nevertheless, whether the cytoskeleton contributes to PKC α translocation remained a critical question for understanding PKC α activation. By pharmacologically depolymerizing the actin and microtubule network I investigated translocation properties of PKC α and found that none of these cytoskeleton components affected PKC α translocation and thus I concluded that the cytoskeleton was not contributing to the kinetics of PKC α translocation.

The cPKC molecules not only work as an ideal read-out mechanism for global Ca²⁺ signal, but also follow spatiotemporally complex Ca²⁺ signals with similar complex translocation regimes. Previous studies found local translocation events of PKC α resulting from short-lived Ca²⁺ release events, so called Ca²⁺ puffs, whose lifetime exceeded the puffs' lifetime by more than 5 fold. To explain this behavior, we proposed intermolecular interactions between membrane-bound PKC α molecules that must be so tight that they significantly prolong membrane residence times of these PKC α molecules and form PKC α clusters. To test this, I used Förster resonance energy transfer (FRET) measurements in PKC α -CFP and PKC α -eYFP co-expressed HEK293 cells and stimulated the cells with the physiological agonist ATP. Oscillatory FRET signals were observed concomitantly with Ca²⁺ oscillations and transient membrane translocations of PKC α . To evaluate the sole effect of Ca²⁺ and largely exclude DAG binding of the PKC, I employed the Ca²⁺ ionophore ionomycin in various extracellular Ca²⁺ concentrations. At all Ca²⁺ concentrations a measurable FRET increase was observed strongly indicating a direct Ca²⁺-dependent PKC α -PKC α interaction

on the plasma membrane. Moreover, high intracellular Ca^{2+} concentrations additionally evoked a spontaneous decay of FRET signal following the strong upstroke of the FRET under these circumstances. These results excluded molecular crowding of the kinase on the plasma membrane as the underlying FRET-generating mechanism and further supported a self-organized PKC α clustering on the plasma membrane.

In the ubiquitously expressed PKC family, over 10 isoforms of PKCs share similar basic construct features, including the rather substrate-unspecific kinase domain, lipid binding domains and autoinhibitory domains. How they achieve the specific target during in signal cascade is still unclear but appears essential for our understanding of the complex network of PKC signaling in living cells. I found that when co-expressing fluorescent protein fusion proteins of PKC α and PKC δ in the same cell treated with physiological stimulation, the PKCs display different patterns of translocation: PKC α translocated to the plasma membrane and PKC δ was recruited to intracellular membrane structures that I identified as the endoplasmic reticulum (ER). To foster understanding of this behavior, I employed several different approaches including chemical compounds, molecular and optical tools. My result demonstrated a novel $\text{G}\alpha_s$ -cAMP-EPAC-PLC ϵ signal pathway that was responsible for the PKC δ ER targeting. To further understand the underlying mechanism and in particular which part of the molecules was responsible for what translocation behavior, artificial PKC chimeras between PKC α and PKC δ were constructed by exchanging their C1 and C2 or C1A and C1B domains crosswise, expressing them in HEK293 cells and investigating their recruitment patterns. Following application of a variety of specific stimuli, I could reveal the independent role of these domain structures for target membrane recognition. Furthermore I demonstrated that it was PKC δ 's C1B-domain that solely and sufficiently determined ER recruitment. The ER targeting of PKC δ caused a local phosphorylation as probed by targeted phosphorylation sensors and physiologically shortening of ATP-induced Ca^{2+} oscillations via kinase-mediated InsP_3 receptor phosphorylation. In conclusion, my results demonstrate that the versatile combination of an autonomous C-domain signaling toolkit enables the unique functions of PKCs as coincidence detectors decoding lipid and Ca^{2+} signaling into phosphorylation on the specific targeted membrane.

Taken together, PKCs as one family of protein kinases display their abilities in spatiotemporal decoding and transduction intracellular signaling, which provide novel and elementary understanding and insights into the life of cells.

Contents

Zusammenfassung	I
Abstract	IV
Contents	VI
Figure list	X
Tabel list	XII
Abbreviation list	XIII
1 Introduction	1
1.1 Protein kinase C family	1
1.2 Domain structure of PKCs	3
1.2.1 The pseudosubstrate	4
1.2.2 The C1 domain	4
1.2.3 The C2 domain	6
1.2.4 The kinase domain	7
1.2.5 The V5 domain	9
1.3 Regulation of PKCs	11
1.3.1 Maturation of PKCs	11
1.3.2 Activation and translocation of PKC	14
1.3.3 Inactivation of PKC	16
1.3.4 PKC and protein binding	16
1.4. Cytoskeleton and diffusion-driven PKC α distribution in Ca ²⁺ induced plasma membrane translocation	18
1.5. Self-organized clustering of membrane-bound cPKC	19
1.6. C-domain toolkit of PKC decoding spatiotemporal signal	21
2 Material and methods	23
2.1 Material	23

2.1.1 Chemical compounds and solutions	23
2.1.2 Enzymes and kits for molecular cloning	24
2.1.3 Small interfering RNA	24
2.1.4 Primers.....	24
2.1.5 DNA vectors and fluorescent labeled proteins.....	24
2.2 Microscopy devices.....	26
2.2.1 Video-imaging system (TILL Photonics Imago)	26
2.2.2 Confocal microscope (Leica TCS SP5).....	26
2.2.3 Kilobeam scanning confocal system (VisiTech-VTinfinity)	26
2.3 Methods.....	28
2.3.1 Recombination of the Chimera construction.....	28
2.3.2 PKC δ mutagenesis	31
2.3.3 Construct of PKC δ -eGFP and Rap1GAP co-expression vector.....	31
2.3.4 Generation of the ER localized CKAR	32
2.3.5 Cell culture and transfection.....	34
2.3.6 Immunocytofluorescence labeling of actin filaments.....	35
2.3.7 Confocal imaging of living cells on Leica TCS SP5	35
2.3.8 Intracellular Ca ²⁺ flash photolysis assay	35
2.3.9 Intracellular InsP ₃ flash photolysis assay	36
2.3.10 Fura-2 based Calcium imaging.....	36
2.3.11 Förster resonance energy transfer (FRET)	37
2.3.12 Image analysis	37
2.3.13 Statistic analysis	38
3 Results	39
3.1 Mechanisms of PKC α translocation	39
3.1.1 Ca ²⁺ -induced redistribution of PKC α to plasma membrane	39
3.1.2 Dynamics of PKC α translocation.....	43
3.1.3 PKC α translocation and the cytoskeleton	45
3.2 Self-organized clustering of membrane-bound cPKC	48
3.2.1 Transient interaction of plasma membrane-bound cPKC upon ATP stimuli. 48	
3.2.2 Persistent interaction of membrane-bound cPKC following Ca ²⁺ influx.....	49
3.2.3 Self-organized formation of membrane-bound cPKC.....	51

3.3 C-domain toolkit of PKC decoding spatiotemporal signal	83
3.3.1 PKC α and PKC δ target distinctive compartments of cell.....	53
3.3.2 PKC δ targets the ER-membrane following ATP stimulation	56
3.3.3 ER recruitment of PKC δ is mediated by a cAMP-Epac-PLC ϵ signal pathway.....	58
3.3.4 The C1 and C2 domain of PKC α and PKC δ can signal independently of one another	63
3.3.5 The C1B domain of PKC δ is responsible for ER recognition.....	68
3.3.6 PKC phosphorylation at subcellular compartments	71
3.3.7 Recruitment of PKC δ to the ER reduced InsP $_3$ -sensitivity of the InsP $_3$ R.....	73
4 Discussion	79
4.1 PKC α translocation is diffusion-driven and independent of the cytoskeleton	79
4.1.1 Diffusion-driven Ca $^{2+}$ -dependent PKC α translocation	79
4.1.2 Kinetics of oligomerized PKC α in the process of plasma membrane translocation	80
4.1.3 PKC α translocation is independent of an intact cytoskeleton.....	81
4.1.4 Summary and perspective.....	82
4.2 Self-organized clustering of membrane-bound cPKC	83
4.2.1 The novel theoretical model of membrane-bound cPKC	83
4.2.2 Properties of PKC α -plasma membrane interactions.....	84
4.2.3 Self-organized clustering of membrane-bound PKC α	85
4.2.4 Summary and perspective.....	86
4.3 C-domain toolkit of PKC decoding spatiotemporal signal	88
4.3.1 PKC α and PKC δ target distinctive compartments of the cell.....	88
4.3.2 Following ATP stimulation PKC δ targets the ER-membrane	88
4.3.3 ER specific DAG production recruits PKC δ	89
4.3.4 The C-domain composition of PKCs determine their translocation pattern ..	90
4.3.5 Activation model of PKC δ ER translocation	91
4.3.6 Local PKC phosphorylation at their distinct subcellular compartment.....	92
4.3.7 Recruitment of PKC δ reduced sensitivity of the InsP $_3$ R towards InsP $_3$	92
4.3.8 Summary and perspective.....	94
References.....	95

Appendix I Publication	i
Appendix II Acknowledgement.....	ii
Appendix III Curriculum Vitae	iii

Figure List

Fig. 1.1.1 Protein kinase C (PKC) family members are located on a branch of the AGC kinome.....	2
Fig. 1.2.1 Domain structures of Protein kinase C (PKC) family members.....	3
Fig. 1.2.2 Alignment of PKC C1 domains.....	5
Fig. 1.2.3 Alignment of PKC kinase domains.....	8
Fig. 1.2.4 Alignment of the kinase domain V5.....	10
Fig. 1.3.1 Classical mechanism of PKCs maturation.....	11
Fig. 1.3.2 Activation model of conventional PKC.....	14
Fig. 1.4.1 Schematic diagram of two transport models of PKC.....	18
Fig. 1.5.1 Spatiotemporal variety of LTEs.....	20
Fig. 2.1.1 Map of plasmids encoding fluorescent labeled PKC proteins.....	25
Fig. 2.2.1 Illustration of the kilobeam scanning confocal microscopy.....	27
Fig. 2.3.1 Structure of chimeras.....	28
Fig. 2.3.2 Scheme of chimera construction.....	29
Fig. 2.3.3 Scheme of the bidirectional expression vectors.....	32
Fig. 2.3.4 Scheme of erCKAR generation.....	33
Fig. 3.1.1 Photolysis of caged Ca^{2+} in living cells.....	40
Fig. 3.1.2 Quantitative analysis of PKC α -eGFP translocation.....	41
Fig. 3.1.3 The C2 domain of PKC α is essential for Ca^{2+} -induced PKC α translocation.....	42
Fig. 3.1.4 DsRed2 tetramer structure.....	43
Fig. 3.1.5 Dynamic process of PKC α monomer and tetramer translocation.....	44
Fig. 3.1.6 Effects of Cyto-D and nocodazole on the cytoskeleton.....	45
Fig. 3.1.7 Effects of Cyto-D and nocodazole on intracellular Ca^{2+} photolysis.....	46
Fig. 3.1.8 PKC α translocation independent of the depolymerization status of actin filaments or microtubules.....	47
Fig. 3.2.1 Transient interaction of plasma membrane-bound cPKC upon ATP stimuli.....	49
Fig. 3.2.2 Consistent FRET signals with PKC α -membrane binding.....	50
Fig. 3.2.3 Spontaneous decay of the FRET signal within a constant PKC α membrane binding.....	52
Fig. 3.3.1 PMA-induced PKC translocation.....	53
Fig. 3.3.2 PKC α and PKC δ are differentially targeted following ATP stimulation.....	54

Fig. 3.3.3 Bryostatin 1 specifically recruits PKC δ to intracellular membrane.....	55
Fig. 3.3.4 PKC δ targets the ER membrane following ATP stimulation.....	57
Fig. 3.3.5 PLC is engaged in the targeting of PKC δ to the ER.	59
Fig. 3.3.6 The involvement of cAMP-Epac in PKC δ ER recruitment.	60
Fig. 3.3.7 Inhibitory effects of Rap1GAP protein on ATP-induced PKC δ recruitment to the ER.....	62
Fig. 3.3.8 Intracellular distribution of Chimera III following different stimulation regimes.....	64
Fig. 3.3.9 Translocation of Chimera II following various stimulation regimes in HEK293 cells.....	65
Fig. 3.3.10 Distribution of Chimeras I and IV following PMA stimulation.	66
Fig. 3.3.11 The C1B domain of PKC δ is responsible for ER targeting..	69
Fig. 3.3.12 Effects of mutation in PKC δ C1B domain on the ER translocation..	70
Fig. 3.3.13 Directed PKC translocation is associated with kinase activity at the target membrane.	72
Fig. 3.3.14 Bryostatin 1 alters Ca ²⁺ mobilization.....	75
Fig. 3.3.15 Sensitivity of InsP ₃ R towards InsP ₃ is decreased by Bryostatin 1 pre- stimulation.	76
Fig. 3.3.16 PKC δ activation desensitizes the InsP ₃ R towards InsP ₃	77
Fig. 4.2.1 Schematic representation of PKC α protein–protein interaction on the plasma membrane.....	84
Fig. 4.3.1 Proposed scheme of signaling cascades for cPKC and nPKC activation in HEK293 cells	89

Table List

Table 1.1 Summary of phosphorylation of A-loop, TM and HM effects on catalytic activity of PKC isoforms.....	13
Table 1.2 RACK-PKC isoform protein-protein interaction.	17
Table 2.1 The list of primers for PKC Chimeras construction.....	30
Table 2.2 List of primers for PKC δ mutations.	31
Table 2.4 Primers for vector pBI-Rap1GAP-PKC δ -eGFP.....	32
Table 2.4 Primers for DNA plasmid ER-CKAR..	33
Table 3.3.1 Summary of the translocation pattern of Chimera I-IV.....	67
Table 3.3.2 Summary of translocation pattern from Chimera A-D.....	68

Abbreviation List

[Ca ²⁺] _i	Intracellular Ca ²⁺ concentration
AC	Adenylyl cyclase
AKAP	A-Kinase Anchoring Proteins
AOBS	Acousto Optic Beam Splitter
AOTF	Acousto Optic Tunable Filter
aPKC	atypical Protein Kinase C
ATP	Adenosine Triphosphate
Ca ²⁺	Calcium Ion
cAMP	Cyclic adenosine monophosphate
CCD	Charge-Coupled Device
CFP	Cyan Fluorescent Protein
CKAR	C kinase activity reporter
cPKC	Conventional/classical protein kinase C
cPLA	Cytosolic Phospholipase A
Cyto-D	Cytochalasin D
DAG	Diacylglycerol
DMEM	Dulbecco's modified Eagle's medium
DMSO	Dimethylsulfoxide
DNA	Deoxyribonucleic acid
EDTA	Ethylenediaminetetraacetic acid
eGFP	Enhanced green fluorescent protein
EGTA	Ethylene glycol tetraacetic acid
Epac	Exchange protein activated by cAMP
ER	Endoplasmic reticulum
ERK	Extracellular signal-regulated kinase
FBS	Fetal bovine serum
Fluo-4/AM	Fluo-4-acetoxymethyl ester
FP	Fluorescent protein
fps	frames per second
FRAP	Fluorescence recovery after photobleach
FRET	Förster resonance energy transfer

Fura-2/AM	Fura-2-acetoxymethyl ester
FW	Forward primer
GAP	GTPase-activating proteins
GEF	Guanine nucleotide exchange factor
GPCR	G protein-coupled receptor
GRK	G protein-coupled receptor kinases
GTP	Guanosine triphosphate
GTPase	Guanosine triphosphatase
HEK293	Human Embryonic Kidney 293 cells
HEPES	2-[4-(2-hydroxyethyl)piperazin-1-yl]ethanesulfonic acid
HM	Hydrophobic motifs
Indo-1/AM	Indo-1-acetoxymethyl ester
InsP3	Inositol-1,4,5-trisphosphate
IP3R	Inositol-1,4,5-trisphosphate receptor
K ⁺	Potassium ion
Li ⁺	Lithium ion
LTEs	Local translocation events
MCS	Multiple cloning site
ms	Millisecond
mTOR	mammalian Target of Rapamycin
Na ⁺	Sodium Ion
NCX	Sodium/Calcium Exchanger
NLS	Nuclear location sequence
NP-EGTA	o-Nitrophenyl ethylene glycol tetra acetic acid
nPKC	novel Protein kinase C
PBS	Phosphate buffered saline
PCR	Polymerase chain reaction
PDK1	Phosphoinositide-dependent protein kinase 1
PH	Pleckstrin homology
PIP2	phosphatidylinositol 4,5-bisphosphate
PKA	Protein kinase A
PKC	Protein Kinase C
PLC	Phospholipase C

PLD	Phospholipase D
PMA	12-O-Tetradecanoylphorbol-13-acetate
PS	Phosphatidylserine
RACK	Receptors for activated C kinase
roi	Region of interest
RV	Reverse primer
SERCA	Sarco/Endoplasmic Reticulum Ca ²⁺ -ATPase
siRNA	small interfering RNA
SR	Sarcoplasmic reticulum
TM	Turn motifs
WT	Wild type
YFP	Yellow fluorescent protein

Chapter 1

INTRODUCTION

Protein kinases are catalytic enzymes that have the capability to modify other proteins by chemically adding a phosphate group to their serine/threonine (Ser/Thr) or tyrosine (Tyr) residues. The human genome contains more than 500 genes for protein kinases and constitute about 2% of all human genes [1]. Most of the human proteins can be modified by kinase activity, and protein kinases are known to mediate most of the signal transduction in eukaryotic cells. Protein kinases control many cellular processes by modification of substrate activity, including metabolism, transcription, cell cycle progression, cytoskeletal rearrangement and cell movement, apoptosis, and differentiation [2]. Protein phosphorylation also plays a critical role in intercellular communication during development, in physiological responses, in homeostasis, and in the functioning of the nervous and immune systems. As such, dysregulation and mutations of protein kinases play causal roles in human diseases, thus offering the possibility of developing agonists and antagonists of these enzymes for use in disease therapy [3-7]. Therefore fully understanding the regulation of human protein kinases will aid in deciphering human diseases and in the development of therapeutics. In my thesis, I focused on one family of protein kinase, the protein kinase C (PKC).

1.1 Protein kinase C family

The first member of the PKC family was discovered by Nishizuka and co-workers in 1977 [8] and described as the receptors for the potent tumor promoter the phorbol esters and mediators of signaling by the lipid second messenger diacylglycerol (DAG). Since then more than 54,000 research articles have been published, which makes PKCs one of the most studied enzyme family. PKCs are ubiquitously expressed and contribute/regulate a remarkable range of signaling pathways, including, but not limited to, gene expression, cell

polarity, cell migration, proliferation and differentiation, T cell recognition, neuronal signaling, and metabolism [9-14].

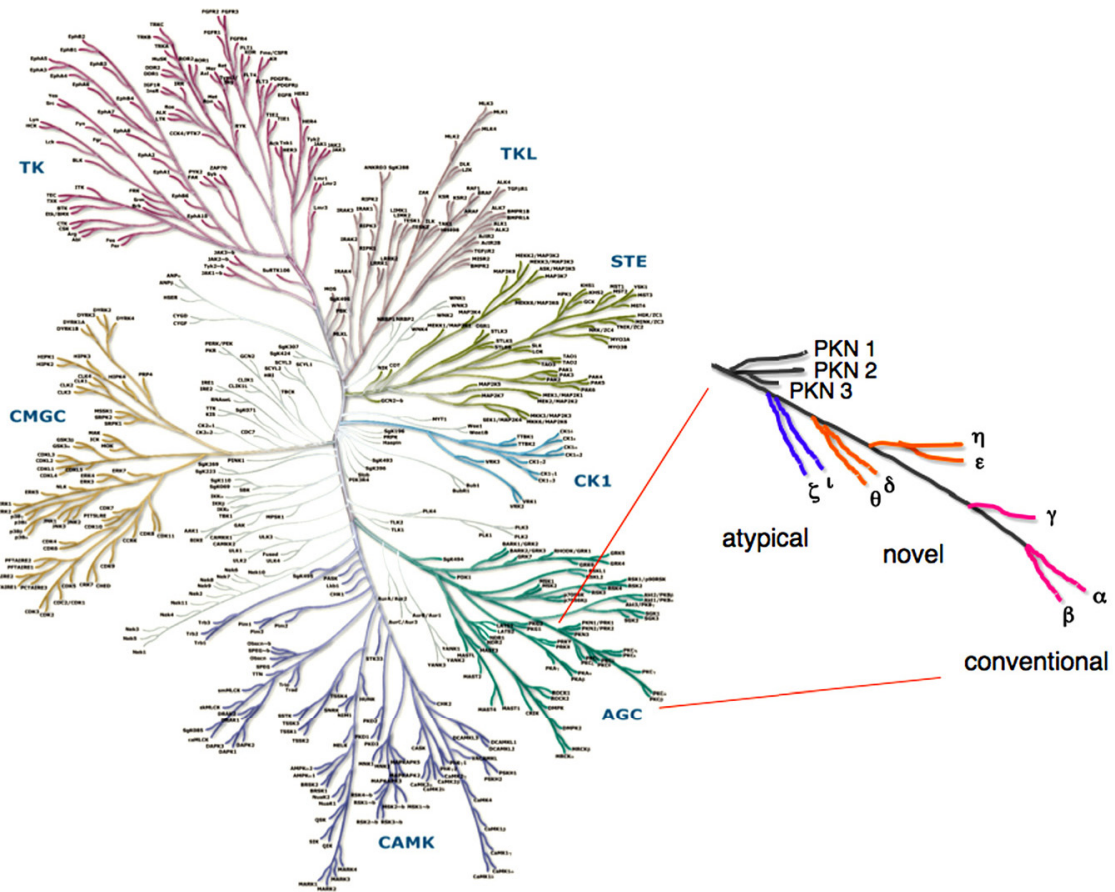


Fig. 1.1.1 Protein kinase C (PKC) family members are located on a branch of the AGC kinome (reproduced from www.cellsignal.com/reference/kinase). PKC isoforms enlarged at the position of the AGC kinases on the right. Modified from *Am J Physiol Endocrinol Metab* 298: E395–E402 [15]

The PKC family is belonging to the serine/threonine protein kinase family, classified to the AGC kinase superfamily [16], which account for 60 of the 518 human protein kinases [1]. In mammals, 10 isoforms of PKC have been identified so far, which occupy the tip of a branch of the AGC kinases from which the related kinases protein kinase N (PKN), Akt/PKB, p70 S6 kinase, protein kinase G (PKG), and protein kinase A (PKA) diverge (Fig. 1.1.1) [1, 15]. These 10 members are highly conserved throughout eukaryotic evolution, evolved from a single PKC, PKC1, in *saccharomyces cervisiae* [17, 18], and are grouped into three classes based on their related domain structure: the conventional or classical PKCs (cPKC), novel PKCs (nPKC), and atypical PKCs (aPKC) [15, 19-21]. When investigating the phylogenetic tree (Fig. 1.1.1), at the very tip of as mentioned branch there are the four conventional PKCs: PKC α , the first cloned enzyme of PKC family; the alternatively spliced PKC β I and PKC β II, which differ in the last 43 amino acids, and PKC γ . cPKCs can be activated by Ca²⁺ and/or by DAG and phorbol esters. Next in the

branch are the four novel PKCs, PKC δ , ϵ , η , and θ , which are not regulated by Ca²⁺ but can be activated by DAG and phorbol esters. The closest subfamily to the branching point are the atypical PKCs, PKC ζ and PKC ι (human; murine isoform is PKC λ), which are unresponsive to Ca²⁺, DAG and phorbol esters. All PKC isoforms are reported to require phosphatidylserine (PS) for optimal activity (Fig. 1.2.1) [22].

1.2 Domain structure of PKCs

In general, all PKC isoforms share basic structural features, such as an N-terminal regulatory domain coupling to a highly conserved C-terminal kinase domain with a C-terminal tail (Fig. 1.2.1). The structure of the N-terminal regulatory domain determines the classification of the 10 isoforms of PKCs and plays an essential role in kinase regulation and activity.

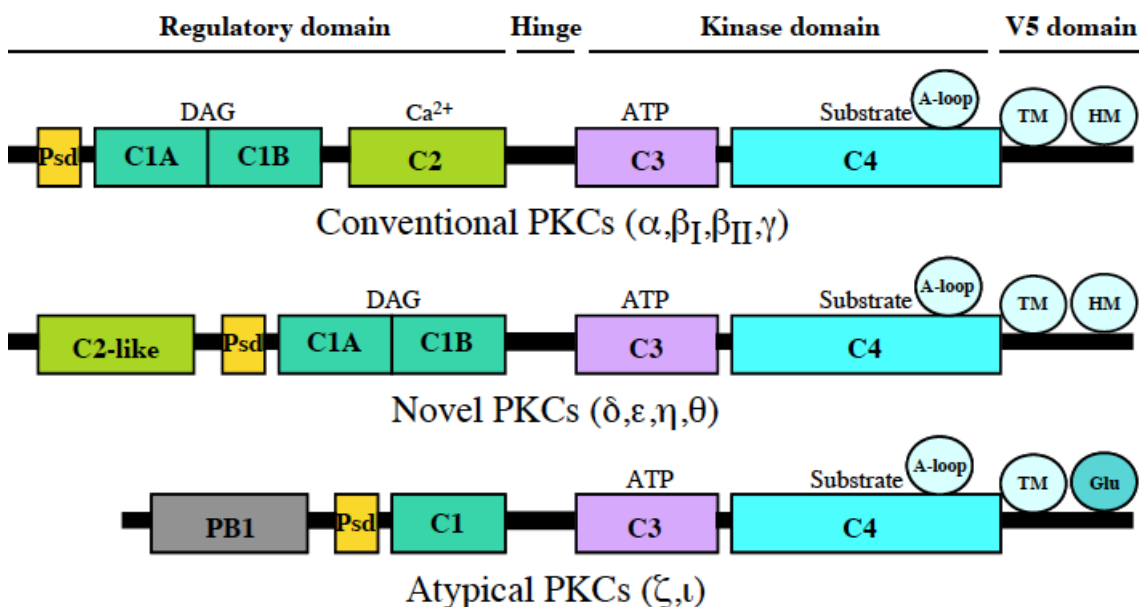


Fig. 1.2.1 Domain structures of Protein kinase C (PKC) family members. Shown are the conventional, novel and atypical PKC subfamilies and their corresponding domains in the regulatory domain and C-terminal domain. Psd: pseudosubstrate site. Modified from Cellular Signalling 23:753–762 [23].

In cPKCs, the N-terminal regulatory domain comprises a C1A and a C1B domain, which binds to DAG or phorbol ester respectively, and a C2 domain, which binds to Ca²⁺, phosphatidylserine, or phosphatidylinositol 4,5-bisphosphate (PIP₂). Both cPKCs and nPKCs share a similar pattern of regulatory domains, containing C1 and C2 domains, and pseudosubstrate peptides, but in different order. In nPKCs the C2 domain is in front of the pseudosubstrate and C1 domain. Importantly, the C2 domains of nPKCs lack the critical Ca²⁺-coordinating amino acids causing nPKCs inability to bind to Ca²⁺ [24]. These

differences in C2 domain structure may underlie the distinct pharmacology of cPKC and nPKC isoforms. Characterized with short regulatory domains, the aPKCs contain an atypical C1 domain with only one cysteine-rich motif binding to phosphatidylinositol 3,4,5-bisphosphate and a protein-protein interaction domain named PB1 (Phox and Bem 1) interacting with other proteins [22, 25]. In all PKCs, pseudosubstrate sequences exist in the regulatory domain that under resting conditions occupy the substrate-binding pocket in the C-terminus and block their catalytic activity [26-29]. The detailed properties of each domain are described below.

1.2.1 The pseudosubstrate

The pseudosubstrate, present in all PKC isoforms, was originally identified in the regulatory region of cPKC by a stretch of amino acids that were competitive inhibitors of PKCs [30, 31]. Further evidence revealed that this sequence served an auto inhibitory role in PKC's activation [27]. By biochemical approaches, it was established that activation of cPKC is accompanied by the release of the pseudosubstrate sequence from the kinase activity pore [32]. Recently the crystal structure of intact PKC β II eventually confirmed the hypothesis that the pseudosubstrate occupied the substrate-binding cavity of PKCs, thus maintaining the enzyme in an inactive conformation [33].

1.2.2 The C1 domain

In PKCs, the C1 domain was identified as a DAG and phorbol ester binding site in PKCs with a conserved motif, HX₁₂CX₂CX_nCX₂CX₄HX₂CX₇C, (H stands for histidine, C stands for cysteine, X is any other amino acid, and n is 13 or 14 (Fig. 1.2.2). In cPKC and nPKC isoforms, this motif occurs as a tandem and forms C1A and C1B domains.

According to the high-resolution crystal structure of the C1B domain from PKC α , PKC β I and II, PKC γ , and PKC δ , these C1 domains share similar tertiary structures and functionally anchor the PKCs to membranes by hydrophobic switches [34-36]. Briefly, the positive charged C1 domain residues are able to interact with anionic membrane phospholipids and penetrate the membrane bilayer to bind DAG, which is located more deeply within the membrane leaflet. Lipid cofactors such as phorbol esters then bind to a narrow polar groove at the top of the C1 domain [37].

The C1A and C1B domains of PKCs display a broad range of intrinsic affinities, from 1 nM to more than 3 μ M, for lipid cofactors, *e.g.*, DAG and phorbol esters. For instance, the C1B domain of PKC α and PKC β II has such a weak DAG binding affinity that under physiological conditions it merely contributes to membrane binding. In addition, C1B is

more sensitive to PMA than the C1A domain [38, 39]. However, for nPKC isoforms, it was variously reported that the C1B domain of PKC δ and PKC θ display a higher affinity for both DAG and PMA than their C1A domain. In contrast, the PKC ϵ C1A domain has a higher affinity for DAG than its C1B domain [40-44]. Interestingly, there are several amino acids which are highly conserved and critical for maintaining the DAG binding affinities in both C1A and C1B domains, as shown in Fig. 1.2.2.

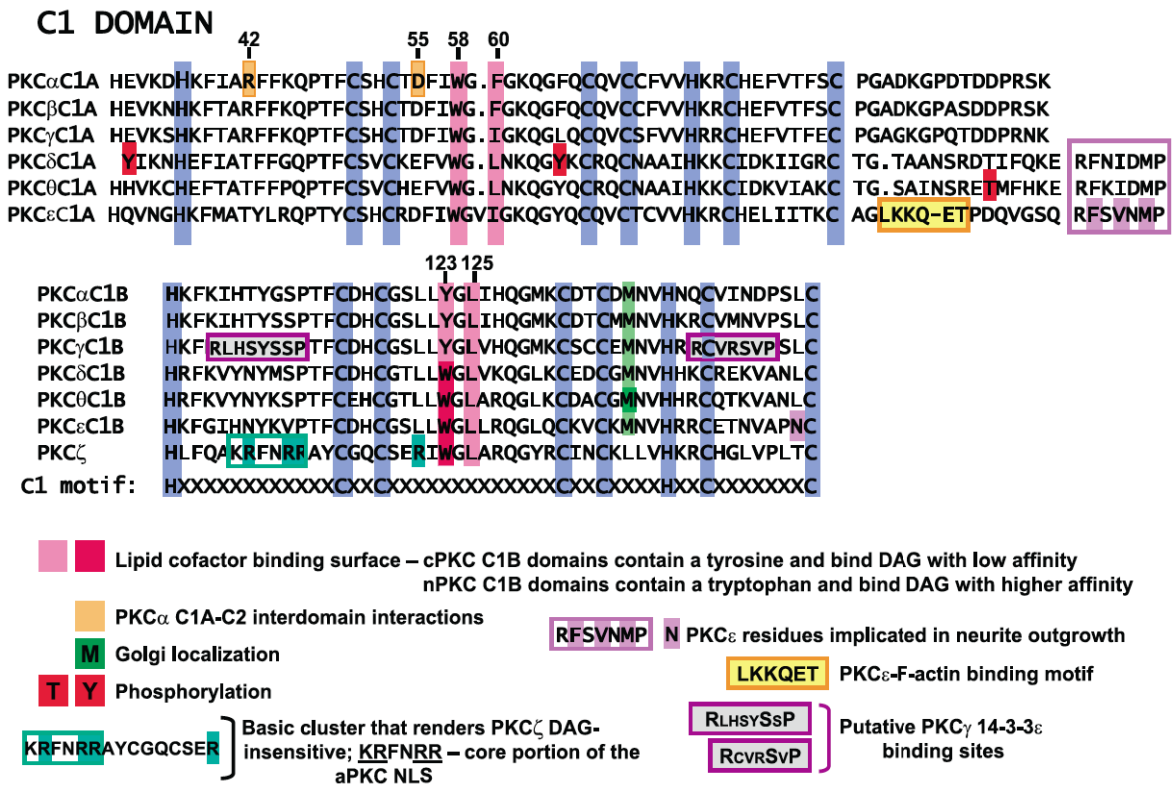


Fig. 1.2.2 Alignment of PKC C1 domains. Numbering is based on PKC α . Conserved cysteine and histidine residues are in blue. Other structural determinants of C1 domain function are as indicated on the figure. Modified from Physiol Rev 88: 1341–1378 [20].

With respect to the electrostatic interactions between the C1 domains of PKCs and anionic phospholipids of membrane, phosphatidylserine is an important player especially for PKC α , PKC β I, and β II [42, 43, 45, 46]. Studies with PKC α have shown that phosphatidylserine plays an essential role to disturb intra molecular interactions, which form between C1A-C2 pairs, *e.g.*, Asp⁵⁵-Arg²⁵², Arg⁴²-Glu²⁸², and Phe⁷²-Phe²⁸² residues [47]. PKC isoforms also have the abilities to interact with other lipids such as ceramide and arachidonic acid via their C1 domains. As previously reported, ceramide is not only able to recruit PKC α from the cytosol to the plasma membrane, but can also cause translocation of PKC δ /PKC ϵ from the cytosol to the Golgi or other intracellular membrane [11, 48]. Arachidonic acid also mimics the effects of ceramide in recruiting PKC ϵ from the cytosol to the Golgi, but displays no effects on PKC δ . Interestingly, it inhibits translocation

of PKC γ to the plasma membrane [42, 49]. Further studies revealed that ceramide binds to the C1B domain of PKC δ /PKC ϵ , whereas arachidonic acid inhibits PKC γ translocation by its C1A domain.

In contrast, the C1 domain of aPKCs contains a cluster of basic residues (HLFQAKRFNRRAYCGQCSEIRI, shown in Fig. 1.2.2) that appear neither in cPKCs nor in nPKCs. It was noted that this part in the C1 domain of PKC λ might function as a nuclear location sequence (NLS) instead of lipid binding [50]. Although the analysis of primary sequences of C1 domains in aPKCs can't entirely explain their inability to bind phorbol esters, it appears obvious that there are crucial elements missing in their sequence, such as residues that maintain the structure of ligand binding sites or hydrophobic residues involved in membrane insertion.

1.2.3 The C2 domain

C2 domains were initially identified in the regulatory domain of cPKCs as a Ca²⁺-dependent membrane-binding motif of about 130 residues [8]. Afterwards, C2 domains were found in many proteins, where they participate in membrane trafficking and signal transduction. In general, C2 domains share a common tertiary structure comprised of eight anti-parallel β -strands connected by variable loops, in which the sequences of the core β -strands portion are more homologous than the loop sequences, which are more divergent and dictate functional specificity.

Detailed crystal structure studies of PKC α suggest that several highly conserved Asp residues Asp¹⁸⁷, Asp¹⁹³, Asp²⁴⁶, Asp²⁴⁸, and Asp²⁵⁴, in the Ca²⁺-binding loops bind to two or three calcium ions in a highly cooperative manner [51]. Other amino acids are important for membrane association. For example, Asn¹⁸⁹ is essential for the PS selectivity of PKC α , Arg²⁴⁹/Arg²⁵² contribute to PKC α 's electrostatic interactions with the anionic membrane surface, Trp²⁴⁵/Trp²⁴⁷ are involved in hydrophobic interactions with the membrane, and the highly basic lysine-riched β 3- and β 4-sheets contribute to PKC α -PIP₂ binding at the membrane [51-54].

In contrast to cPKCs, the C2 domain of nPKCs, also called as C2-like domain, is deficient of those Ca²⁺-binding residues in the loop sequences and therefore binds membranes in a Ca²⁺-independent manner. Moreover, the C2 domain of PKC δ is also unable to bind lipids. This is presumably compensated by the high intrinsic affinity of the PKC δ C1 domain for lipid-membrane [41].

1.2.4 The kinase domain

The amino acid sequence of PKC catalytic domains highly aligns with most of the residues that are invariant across AGC kinase family members such as PKA and AKT [16, 55, 56]. Such sequences cluster at sites of ATP binding and activation (Fig. 1.2.3). Similar to other AGC kinases, the catalytic domain of PKCs consists of an N-terminal small lobe, known as N-lobe, a C-terminal large lobe, known as C-lobe, and one sandwiched molecule of ATP, which serves as the phosphate donor during phosphorylation. The N-lobe contains β -sheets and the glycine-rich ATP-binding loop with a consensus GXGXXG sequence, which is a marker for nucleotide binding proteins, and an invariant lysine, which forms the active residue to transfer the phosphoryl group. At the C-lobe, α -helices are predominant and form an activation loop for magnesium binding and substrate catalysis. Between these two main lobes of the kinase domain, there is a “gatekeeper” residue to control access to a preexisting cavity in the ATP binding pocket [57]. The “gatekeeper” residue is conserved as a large hydrophobic amino acid in the human kinome [58]. Most notably, mutations at this position are the basis of strategies to engineer artificial kinases that are uniquely sensitive to certain unnatural ATP analogs to specially inhibit or activate kinases in cell [6].

The activation segment of the kinase locates in the C-lobe, adjacent to the ATP-binding site, and contains important catalytic elements such as the DFG (Asp–Phe–Gly) motif. The Asp residue in the motif is an invariant catalytic residue and responsible for chelating one Mg^{2+} ion that positions the phosphates for phosphotransfer. The activation segment is connected to the N-lobe through the αC helix, and its own phosphorylation leads to conformational changes, especially in the αC helix. These changes coordinate the formation of a crucial network of hydrogen bonds between a Glu residue on the αC helix, a Lys residue in the N-lobe and the phosphates of the ATP; this network is required for the catalytic activity of the enzyme [16, 56].

KINASE DOMAIN

A

	ATP Binding site GxGxxG	Invariant Lysine	Gatekeeper Residue
PKC α	MVLGKGSF GKVMLADRKGTEELYAIK ³⁶⁸	ILKKDVIQDDV	TVDRLYFVMEYVNGGDLMYHIQQV
PKC β	MVLGKGSF GKVMLSERKGTDELYAVK ³⁷¹	ILKKDVIQDDV	TMDRLYFVMEYVNGGDLMYHIQQV
PKC γ	MVLGKGSF GKVMLAERRGSDELYAIK ³⁸⁰	ILKKDVIVQDDV	TPDRLYFVMEYVTGGDLMYHIQQL
PKC δ	KVLGKGSF GKVLLGELKGRGEYFAIK ³⁷⁶	ALKKDVLIQDDV	TKDHLFFVMEFLNGGDLMYHIQDK
PKC θ	KMLGKGSF GKVFLAEFKTNQFFAIK ⁴⁰⁹	ALKKDVLMDDV	TKENLFFVMEYLNNGDLMYHIQSC
PKC ϵ	KVLGKGSF GKVMLAELKGDVEYAVK ⁴³⁶	VLKKDVILQDDV	TKDRLFFVMEYVNGGDLMFQIQRS
PKC η	KMLGKGSF GKVFLAEFKRNQFFAIK ³⁸³	ALKKDVLMDDV	TPDRLFFVMEYVNGGDLMFHIQKS
PKC ζ	GLGLODFDL IRVIGRGSYAKVLLVRLKKNQIYAMK ²⁸¹	VVKKELVHDDEDI	TTSRLFLVIEYVNGGDLMFHMQRQ
PKC ι	SLGLODFDL LRVIGRGSYAKVLLVRLKKTDTIYAMK ²⁷⁴	VVKKELVNDDEDI	TESRLFFVIEYVNGGDLMFHMQRQ
PKA	KTLGTGSFGRVMLVKHKESGNHYAMK ⁷³	ILDKQKVVKLQKI	DNSNLYMVEYVAGGEMFSLRRI
AKT1	KLLGKGTFFGKVLVKEKATGRYYAMK ¹⁷⁹	ILKKEVIVAKDEV	THDHLCFVMEYANGGELFFHLSRE



Known PKC ι phosphorylation sites (Y²⁵⁶, Y²⁷¹ and Y³²⁵) that are conserved in PKC ζ



aPKC Nuclear Export Sequences; * hydrophobic Phe and Leu residues required for NES function

B

	Mg positioning loop	Activation loop
PKC α	DFGMCKEHMMDGVTTTRT ⁴⁹⁷	FCGTPDYIAPEIIAYQPYGKSVDWWAY
PKC β	DFGMCKENIWDGVTTKT ⁵⁰⁰	FCGTPDYIAPEIIAYQPYGKSVDWWAF
PKC γ	DFGMCKENVFPGSTTRT ⁵¹⁴	FCGTPDYIAPEIIAYQPYGKSVDWWSF
PKC δ	DFGMCKENIIFGENRAST ⁵⁰⁵	FCGTPDYIAPEILQGLKYSF ⁵³² SVDWWSF
PKC θ	DFGMCKENMLGDAKTNT ⁵³⁸	FCGTPDYIAPEILLGQKYNHSVDWWSF
PKC ϵ	DFGMCKEGILNGVTTT ⁵⁶⁶	FCGTPDYIAPEILQELEYGPSVDWWAL
PKC η	DFGMCKEGICNGVTAT ⁵¹²	FCGTPDYIAPEILQEMLYGPVAVDWWAM
PKC ζ	DYGMCKEGLPGDTTST ⁴¹⁰	FCGTPNYIAPEILRGEY ³³² GFSVDWWAL
PKC ι	DYGMCKEGLRPGDTTST ⁴⁰³	FCGTPNYIAPEILRGED ³³² YGFSVDWWALG
PKA	DFGFAKRVK.G.RTW.T ¹⁹⁸	LCGTPEYLAPEIILSKGYNKAVDWWAL
AKT	DFGLCKEIKDGATMK ³⁰⁸	FCGTPEYLAPEVLEDNDYGRAVDWWGL

RESIDUES PROPOSED TO SUBSTITUTE FOR T ⁵⁰⁵ PHOSPHORYLATION IN PKC	I497	Residues that form a hydrophobic stack (with PKC δ -Y ³³²) to stabilize the activation loop
	F498	
	F525	
	E500	Charged residue that may substitute for T ⁵⁰⁵ phosphorylation

Fig. 1.2.3 Alignment of PKC kinase domains. (A) The ATP binding site, invariant lysine, and gatekeeper residues of PKCs are highlighted in yellow. (B) The Mg²⁺ positioning loop is shown in green. The phosphorylation site of the activation loop, invariant tyrosine that is phosphorylated in certain PKCs, is depicted in red. Other important residues are indicated in the figure. Modified from Physiol Rev 88: 1341–1378 [20].

1.2.5 The V5 domain

Following further studies on the PKC family, V5 domains recently attract increasing interests. In general, V5 domains contain 50 to 70 amino acids following the C-terminus of the catalytic core of the kinase domain, which mainly consists of the highly conserved turn motifs (TM) and hydrophobic motifs (HM) as well as an additional 7–21 residues at the extreme C-terminus that are highly divergent both in their length and sequence (Fig. 1.2.1). Due to such a property, the extreme C-terminal regions of the V5 domain have been implemented as epitopes to raise the specificity of antibodies for different PKC isoforms in Western blot and immunolabeling studies.

The C-terminal V5 domain is the only difference between the two spliced PKC β isoforms, PKC β I and PKC β II. Although PKC β I and PKC β II are expressed in a tissue-specific and developmentally regulated manner [59], they display distinct translocation patterns upon stimulation of metabotropic glutamate receptor-1a (mGluR1a), which couple to the hydrolysis of phosphoinositides via G α_q proteins. Furthermore, two specific residues, Asn⁶²⁵ and Lys⁶⁶⁸, in the V5 domain of PKC β II are required for the PKC β II-like translocation pattern. This can be switched to PKC β I-like translocation pattern simply by mutating one of the two residues [60, 61].

The C-terminal V5 domain also works as a cis-regulatory element of the enzyme activity of PKCs, containing a hydrophobic motif (HM) and a “turn motif”. The hydrophobic motif, consisting of a phosphorylatable Ser flanked by hydrophobic residues, locates at the C-terminus of the V5 domain, which is found in most AGC kinases [62, 63]. The HM wraps around the N-lobe of the kinase domain to insert two aromatic residues into the hydrophobic motif pocket. The phosphorylation of their Ser residue is required for keeping the α helix in the active conformation. Since the phosphorylation site in the HM is absent in aPKC (Fig. 1.2.4), the negatively charged Glu residue takes its place, structurally mimicking the phosphorylated serine/threonine to perform a similar function. Meanwhile, the “turn motif”, consisting of a phosphorylatable serine/threonine residue precedes the hydrophobic motif, where it assists the C-terminal tail to find its way around the entire N-lobe. The phosphorylation of the “turn motif” and the corresponding positively charged patch on the N-lobe of the kinase is required for kinase stability and may also protect the hydrophobic motif site from dephosphorylation [64]. In all PKCs, the intramolecular interactions between the V5 domain and the N-lobe are essential for full kinase activity.

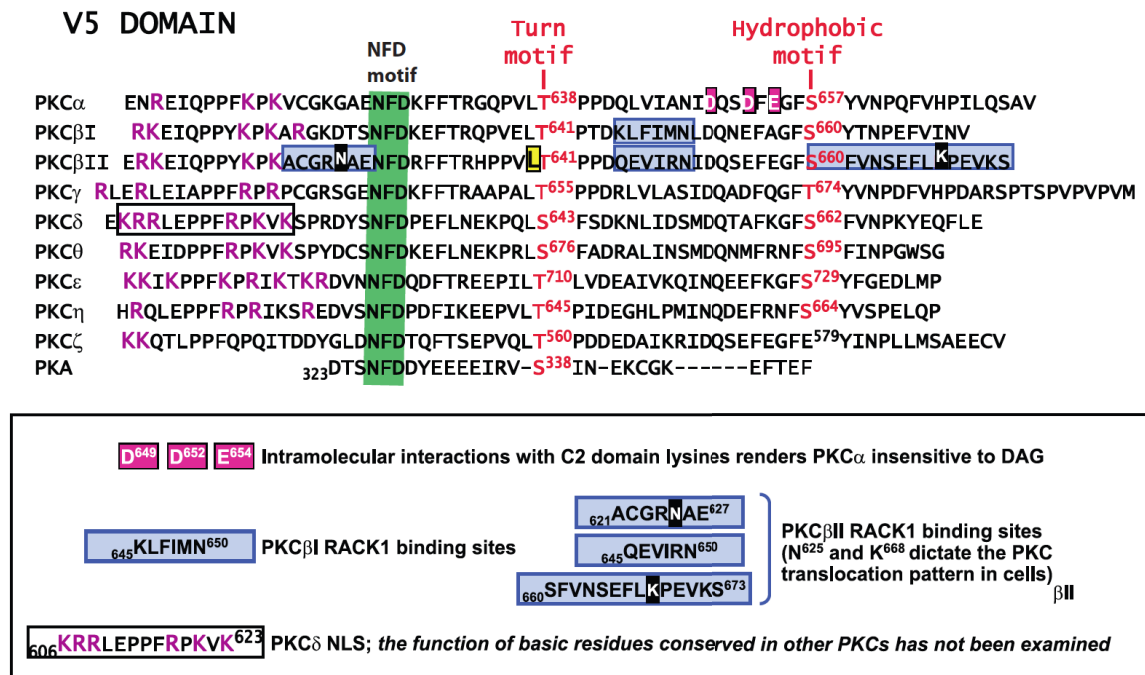


Fig. 1.2.4 Alignment of the kinase domain V5. The NFD motif is highlighted in green and the phosphorylation sites in TM and HM motif are in red. Other important residues are indicated in the figure. Modified from Physiol Rev 88: 1341–1378 [20].

Recently, Leonard et al. reported a novel intramolecular interaction between the C1B domain and V5 domain around residues 628-630 of PKC β II, referred to NFD (Asn(N)-Phe(F)-Asp(D)) motif. As a highly conserved catalytic element in the AGC kinases, the NFD motif reportedly involves an α helix. Here, the Phe⁶²⁹ residue is involved in the active site and binds the adenine of ATP in the inhibitor-bound kinase domain of PKC β II. Leonard et al. found the NFD motif to form a “clamped” conformation that keeps the Phe⁶²⁹ out of the active site, intimately contacting with both the C1B and catalytic domains. This conformation prevents the NFD motif from participating in ATP binding and eventually stabilizes the active site of the kinase domain [33].

The V5 domain not only regulates the kinase activity of PKCs, but also modulates PKC-DAG binding. An intramolecular interaction between V5 domain residues (Asp⁶⁴⁹, Asp⁶⁵², and Glu⁶⁵⁴; Fig. 1.2.4) and C2 domain lysine-rich cluster stabilizes the “closed” conformation of PKC α and reduces its sensitivity to DAG, which can be reversed by V5 domain truncation or mutations [41, 65].

In addition, there are six amino acids (⁶¹¹KRKVEPPFKPKVK⁶²³, shown in Fig. 1.2.4) in the V5 domain of PKC δ that act as a nuclear localization sequence (NLS), which results in some nuclear expression of PKC δ [66]. Although many of these basic residues are conserved in other cPKCs and nPKCs, their function still needs to be elucidated.

1.3 Regulation of PKCs

Considering their ubiquitous expression and vital functions in cells, the activity of PKCs must be under a precise regulation in living cells. From what we know today, the function of PKCs is regulated by priming phosphorylation, pseudosubstrate exposure, subcellular location and its protein degradation in the intracellular context.

1.3.1 Maturation of PKCs

It is believed that all PKC isoforms are rendered mature only after a series of ordered, tightly coupled and constitutive phosphorylations, by which the enzyme eventually obtains the stability and catalytic competence [67, 68]. The earliest step for PKC's maturation is the binding of the chaperone HSP90 and the co-chaperone Cdc37 to a conserved PXXP motif in the C-terminal tail of PKCs to form a molecular clamp in the kinase domain, which is essential for phosphorylation occurring [69]. Perturbation of this key regulatory step causes either PKC degradation or dysregulation, which provides one mechanism in PKC-related diseases: a mutation at the first Proline of this motif in PKC α was identified as a mutation driving glioblastoma [70].

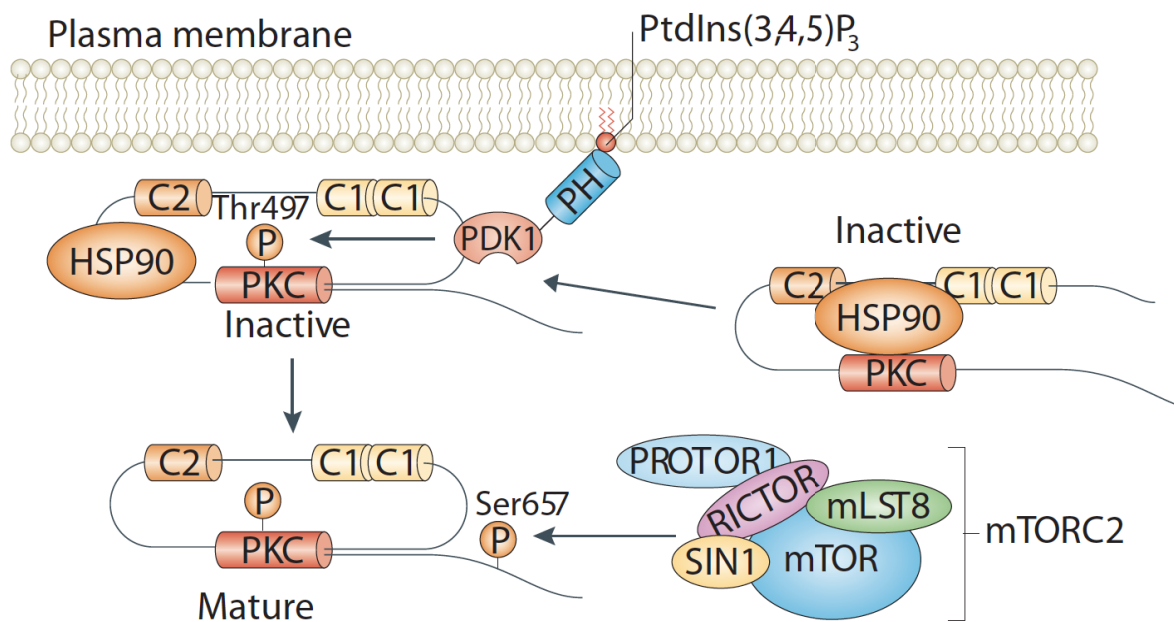


Fig. 1.3.1 Classical mechanism of PKCs maturation. Premature PKC is bound to chaperone proteins and phosphorylated by PDK1 at A-loop around the plasma membrane. Then the protein is phosphorylated by mTORC2 complex subsequently at the C-terminal tail to stabilize its conformation. Modified from Nat. Rev. Mol. Cell Biol. 11:9–22. [16]

Priming phosphorylations of PKC are central steps for PKCs maturation. Among the multiple predicted phosphorylation residues in the protein, three key phosphorylation sites on the C-terminus of PKC were identified as essential for the kinase activity by mutational analysis and mass spectrometry [71, 72]. These are known as the activation loop (A-loop), the turn motif (TM), and the hydrophobic motif (HM) (Fig. 1.2.1). Although all three sites are conserved in cPKC and nPKC isoforms, the aPKCs do not contain an HM residue but instead of a negatively charged glutamic acid, which may mimic a constitutive phosphorylation (Fig. 1.2.1, Fig.1.2.4).

The activation loop in the kinase domain is the first priming site. Phosphoinositide-dependent protein kinase 1 (PDK1) phosphorylates the activation loop site of all PKC isoforms. Following that, the PKC is able to align and stabilize the two lobes of the kinase domain in preparation for catalysis (Fig. 1.3.1) [73-75]. Phosphorylation at the A-loop is constitutive for cPKC and nPKC but displays agonist dependence for aPKC. Interestingly, the activity of PDK1 towards cPKCs is independent of phosphoinositides [76], to which the PH domain of C-terminus of PDK1 binds, but it is controlled by the conformation of PKC itself [26]. Newly synthesized PKC is in an “open” conformation in which the pseudosubstrate is removed from the substrate-binding cavity, thus unmasking the activation loop site to allow phosphorylation by PDK1 (Fig. 1.3.1). Moreover, the replacement of the Thr at the A-loop of cPKC with neutral, non-phosphorylatable residues (Ala or Val) can prevent the subsequent phosphorylation on TM and HM sites [77, 78], indicating that phosphorylation of the A-loop is necessary to allow TM and HM motif phosphorylation. Such protein mutations in PKCs are highly susceptible to degradation [79]. Therefore, the PDK1 dependent PKC phosphorylation plays a critical role in controlling cellular levels of PKC.

Phosphorylation at the activation loop leads to phosphorylation at the second priming site within the V5 domain of the turn motif (Fig. 1.3.1) [64]. Structural analysis shows that phosphorylation of the TM anchors the C-terminal tail on the N-lobe of the kinase. Especially the phosphorylation of the Thr residue within the TM interacts with a cluster of basic residues in a pocket above the ATP-binding loop to stabilize the active conformation of the kinase that is then resistant to phosphatase activity [80]. The mammalian target of the rapamycin 2 complex (mTORC2) plays an important role in TM phosphorylation of some PKCs, such as cPKCs and PKC ϵ [81-83]. So far it is unclear whether mTORC2 directly phosphorylates PKC, or whether it controls the phosphorylation of this site indirectly, *e.g.*, by accompanying (chaperoning) or positioning freshly synthesized PKC for processing of phosphorylation, or by activating another upstream kinase for this site. Cells lacking mTORC2, however, have reduced expressing levels of PKC isoforms [15, 82], which is consistent with the essential role of priming phosphorylation in stabilizing PKCs.

Since no changes in phosphorylation levels of TM or expression levels of PKC δ / θ and aPKCs have been reported in mTORC2 negative cells [23], other signaling pathways or mechanisms of autophosphorylation may regulate these isoforms at this site. Interestingly, the TM of PKC δ has been reported to be an autophosphorylation site [82].

The mechanism of phosphorylation at the final priming site, the hydrophobic motif site (Fig. 1.3.1), seems to be isoform-specific. Kinetic analyses on purified proteins revealed that cPKC can be autophosphorylated at the hydrophobic motif by an intramolecular reaction, but this is difficult to resolve in living cells [84]. This site can also be phosphorylated *in vitro* by other kinases, including mTORC2 [82]. For nPKCs, interestingly, the phosphorylation of HM is sensitive to the mTOR inhibitor rapamycin [85], which indicates the possible involvement of the mTORC1 complex in the phosphorylation of these isoforms. Therefore it appears obviously that mTORC1, mTORC2, and other possible pathways have an impact on the HM phosphorylation of PKC isoforms and further regulate their function in diverse ways.

Our knowledge of these priming phosphorylations has been derived in large from studies of their function in cPKCs. Initial investigations assumed that other PKCs probably follow a similar pathway or mechanism to regulate all isoforms. Recent findings, however, have demonstrated that this is not always the case. Notable differences were reported for other PKC isoforms in terms of the signal transduction influencing the phosphorylation sites and the impact they have on isoform-specific function [15, 16, 23].

Table 1.1 Summary of phosphorylation of A-loop, TM and HM effects on catalytic activity of PKC isoforms. Modified from Cellular Signalling 23:753–762 [23].

PKC isoforms	A-loop	Turn motif	Hydrophobic motif
PKC α	Required for activity	Not required for activity	No convinced report
PKC β I	Not reported	Required for activity	Not reported
PKC β II	Required for activity	Required for activity	Not required for activity
PKC γ	Not reported	Not reported	Not reported
PKC δ	Not reported	No convinced report	Negative regulation of activity
PKC ϵ	Not reported	Not required for activity	Not reported
PKC θ	Required for activity	Not reported	Required for activity
PKC η	Not reported	Required for activity	Not reported
PKC ζ	Required for activity	Not required for activity	Not exist
PKC ι	Required for activity	Not reported	Not exist

1.3.2 Activation and translocation of PKC

The fully phosphorylated “mature” PKC localizes to the cytosol with the pseudosubstrate occupying the substrate-binding cavity and thus silencing the kinase activity. The dissociation of the pseudosubstrate from the catalytic cavity is the main step for PKC activation. Based on the specific structure of the regulatory domain of the particular PKC isoform, the detailed activation mechanism for each isoform is distinctive [20, 22].

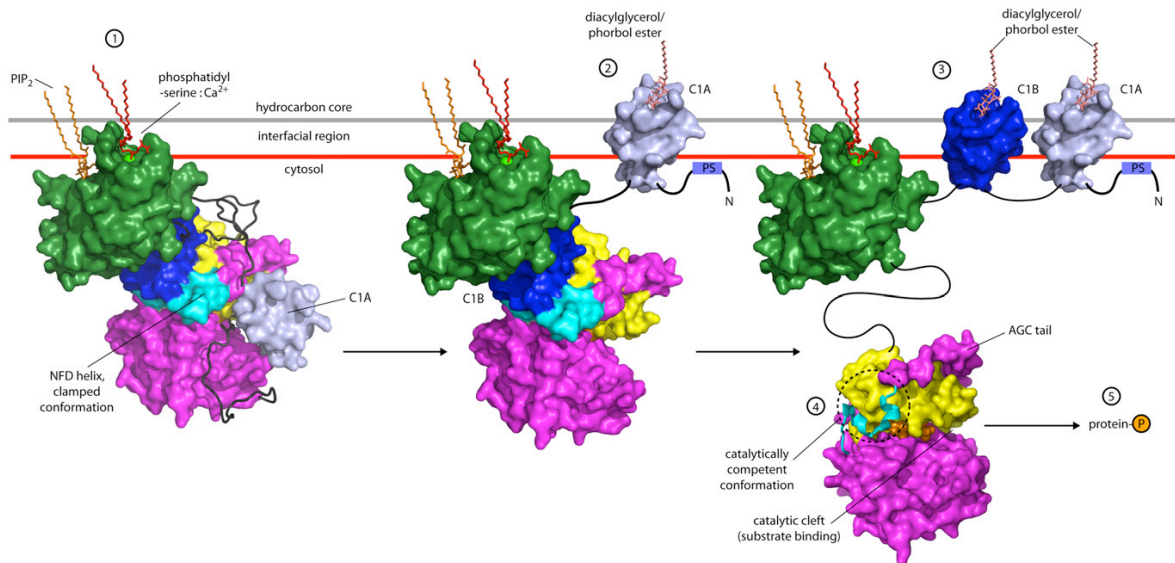


Fig. 1.3.2 Activation model of conventional PKC. (1) Upon Ca²⁺ release, cPKC isoforms translocate to the membrane, where Ca²⁺ bound C2 domain mediate bridging to the anionic phospholipids with an adjoining site on the C2 domain-binding PIP₂. (2) Subsequent binding of DAG to the C1A domain results in the removal of the pseudosubstrate from the catalytic cave. (3) Binding of a second molecule of DAG or PMA by the C1B domain results in unclamping of the kinase and (4) rearrangement of the NFD helix into the catalytically competent state, (5) resulting in phosphorylation of target proteins . Modified from Cell 144:55–66 [33]

For cPKCs, the main trigger for activation is intracellular Ca²⁺ [21, 86-89]. Intracellular Ca²⁺ is derived either from internal stores or from the external medium. In the case of the latter, Ca²⁺ influx is controlled by many different channels in the plasma membrane responding to various stimuli, such as membrane depolarization, agonist binding, or intracellular signaling. Ca²⁺ release from internal stores, mainly from the endoplasmic reticulum (ER) or the sarcoplasmic reticulum (SR), is evoked by Ca²⁺ itself or by signaling messengers, such as inositol-(1,4,5)-trisphosphate (InsP₃), which is generated from hydrolysis of PIP₂ by phospholipase (PLC). PLC isoforms can be activated by different mechanisms, *e.g.*, PLCβ activation by Gα_q protein through G protein coupled receptors and PLCγ activation by tyrosine kinase coupled receptors. InsP₃ then binds to InsP₃R in the ER membrane and evokes Ca²⁺ release from the ER. When intracellular Ca²⁺ increases, the C2 domain of cPKCs binds to Ca²⁺ via its specific Ca²⁺-binding loop. This binding triggers the

conformational changes not only in the C2 domain but also in the C1 domain and the pseudosubstrate. Due to the positive charges of Ca^{2+} , binding of the C2 domain and Ca^{2+} rapidly changes the surface charges of the C2 domain from negative to positive. Such a switch now allows the protein binding to the negatively charged phospholipids in the inner leaflet of the plasma membrane. The Ca^{2+} -induced cPKC plasma membrane targeting is quick but weak [87, 88] and the lifetime of membrane-bound cPKC is around 50 ms [90]. The interaction of Ca^{2+} and C2 domain alone is insufficient to fully activate cPKC, which needs more energy.

The natural product of PIP_2 hydrolysis by PLC is not only the diffusible InsP_3 but also membrane-delimited DAG. When cPKC is recruited to the plasma membrane, membrane embedded DAG binds to the C1A domain, which results in disengagement of the C1 domain and eventually forces the full extraction of the pseudosubstrate from the catalytic cavity. Simultaneously following the second binding of DAG to the C1B domain and rearrangement of NFD helix in the V5 domain, the cPKC obtains the competent catalytic ability to phosphorylate downstream signaling proteins [33]. Comparing to the phorbol esters, although the lifetime of DAG is limited, binding of the C1 domain and DAG still provide sufficient energy and time to activate cPKCs [43, 91, 92]. This open conformation is then free to bind to co-localized substrates. Once bound to its target, PKC phosphorylates Ser/Thr residues based on the primary sequences [93, 94] with an efficient enzyme activity, k_{cat}/K_m of PKC family ranging in $10^6 \text{ s}^{-1} \text{ M}^{-1}$ [95].

In contrast to cPKCs, the C2 domain of nPKCs is insensitive to Ca^{2+} due to the absence of Ca^{2+} coordinating residues. The intrinsic affinity of the C1 domain of nPKCs was reportedly sufficient to recognize DAG which may allow a direct recruitment to membranes by agonist-evoked levels of DAG [40, 41]. Lipid binding to the C1 domain therefore represents a crucial step in the allosteric activation of nPKCs and subsequent phosphorylation of nPKC substrates. However, the detailed activation mechanism of nPKC isoforms is still unclear.

In addition to the physiological C1-agonist DAG, other chemical compounds especially phorbol esters and their derivatives such as PMA display the potential to directly activate PKC isoforms. As described above, both the C1 domain of cPKCs and nPKCs have the capability to bind phorbol esters at the level of the plasma membrane. Such a translocation exhibits a slower dynamic than that of C2- Ca^{2+} interaction, but the binding between PMA and PKC is strong, which induces much longer residence time on the membrane (200 fold) than that of DAG-PKC binding [96], and also provides sufficient energy for allosteric activation of PKCs.

1.3.3 Inactivation of PKC

The short half-life of DAG is probably the key to terminate PKC signaling or to reverse the activation of PKCs, resulting in the membrane-recruited PKC to diffuse back to the cytoplasm. It has also been reported that dephosphorylation of activated PKC might be an important additional mechanism for inactivation [97]. After PKC's binding to the membrane, the conformation of the protein is open. This open conformation allows phosphatases easy access to phosphorylated residues. PKC's sensitivity toward dephosphorylation is thus increased almost two orders of magnitude [98]. Recently the PH domain leucine-rich repeat protein phosphatase (PHLPP) has been identified as one member of these phosphatases, which specifically affects the HM but no effects on TM of cPKCs and nPKCs [99]. Most recently, it has been revealed that in MEF cells type 2A phosphatase (PP2A)-induced dephosphorylation of the HM and TM motif of activated cPKCs requires the involvement of an adapter protein named Fas-associated protein with a death domain (FADD) [100]. It should be noted here, however, that although dephosphorylation serves as an important switch to turn off the activity of these enzymes, dephosphorylation does not necessarily predispose the enzyme to degradation [97]. Consistent with this, degradation of PKC can occur through an ubiquitin/proteasome pathway that does not involve dephosphorylation of the enzyme [101]. The precise mechanisms for inactivation and degradation of PKC isoforms remain to be further elucidated.

1.3.4 PKC and protein binding

In addition to the activation of PKC, in particular conventional and novel isoforms, by dynamic signaling of DAG or Ca^{2+} , PKC's activity is also regulated by a large number of scaffold or anchoring proteins. Among these, Mochly-Rosen and coworkers reported a series of structurally unrelated scaffold proteins associated to membranes, which were named receptors for activated C kinase (RACKs) [102-104]. Briefly, after activation, RACK proteins have the ability to recognize and bind individual PKC isoforms and to trap them in an activated conformation. Such a binding not only localizes PKCs but also has the potential to sustain PKC activity in the absence of second messenger binding. According to this theory, cells apparently express a unique set of RACKs with distinct subcellular localizations for each PKC isoform. Furthermore, PKC-RACK interactions are essential for isoform-specific cellular responses. To date, RACKs have only been reported for PKC β [27, 105, 106], δ [107], and ϵ [108, 109] isoforms, and in each case the respective RACK protein is known to serve other functions in addition to PKC binding (Table 1.2).

Table 1.2 RACK-PKC isoform protein-protein interaction.

PKC isoforms	RACK protein	RACK binding site
PKC β	RACK1	C2 domain / V5 domain
PKC δ	Annexin V	C2 domain
PKC ϵ	P32/gC1qBP, RACK2	C2 domain

A kinase anchoring proteins (AKAPs) may provide another example for scaffold proteins, which are signaling-organizing molecules that tether enzymes in subcellular complexes to control the phosphorylation or dephosphorylation of neighboring substrates [110]. AKAP79, one member of this family, was reported to anchor phospholipid-sensitive kinase and PKC on the membrane. Recently, it was reported that the binding of AKAP79 and PKC could not only synchronize the intracellular signaling of PKC, but also alter the pharmacological profiles of kinase inhibitors [111]. In addition, two putative 14-3-3-binding motifs have been mapped in the C1B domain of PKC γ (Fig. 1.2.2), indicating protein-protein interactions of PKCs to 14-3-3 proteins, a family of scaffold protein widely involved in signal transduction [112]. The peptides based on these sequences inhibit PKC γ binding to 14-3-3 *in vitro* and promote PKC γ translocation *in vivo* [113].

The cytoskeleton proteins are another category of molecules, which may bind to PKCs. Many cytoskeleton proteins, including tubulin, F-actin, vincentin, myofibrils, and membrane-cytoskeletal cross-linking proteins (MARCKS) [114-116], were found to bind to particular PKC isoforms in different cell lines or tissues by using immunocytochemistry or co-immunoprecipitation followed by Western blotting. For example, C1 domain of PKC ϵ binds F-actin (Fig. 1.2.2, [117]), C1B domain of PKC α interacts with fascin, an actin-bundling protein that contributes to cell adhesion and spreading on fibronectin [118], and C1A domain of PKC β II binds the centrosomal protein pericentrin to control microtubule organization, spindle assembly, and chromosome segregation during cell division [119]. Some of these cytoskeletal proteins have also been shown to be substrates for PKC [114, 115]. The question whether the interaction between PKC and the cytoskeleton is a simple binding or a functional phosphorylation requires further investigations.

1.4. Cytoskeleton and diffusion-driven PKC α distribution in Ca²⁺-induced plasma membrane translocation

It is well established that following Ca²⁺ increases cPKCs translocate to the plasma membrane via their C2 domain. The detailed mechanism, however, is still unclear and

multiple methods were employed to investigate this. Biochemists studied the C2 domain membrane association and dissociation *in vitro* and revealed very fast kinetics for both processes [90, 120]. The k_{on} rate for membrane association was around $10^{10} \text{ M}^{-1}\text{s}^{-1}$, while membrane dissociation (k_{off}) was still very fast (around 150 s^{-1}) [21, 120]. Compared to the Ca^{2+} dissociation from the C2 domain, $k_{off} 12 \text{ s}^{-1}$, they are in a comparable range [90], which indicates that Ca^{2+} unbinding and cPKC membrane dissociation are quasi-simultaneous. In contrast, the interaction of cPKC's C1 domain with the plasma membrane is characterized by much slower kinetics. In PKC β , for example, k_{on} and k_{off} were measured to be $10^9 \text{ M}^{-1}\text{s}^{-1}$ and 0.1 s^{-1} , respectively [41], which indicates a rather rapid association of cPKC isoforms to the plasma membrane, but a slow disassociation.

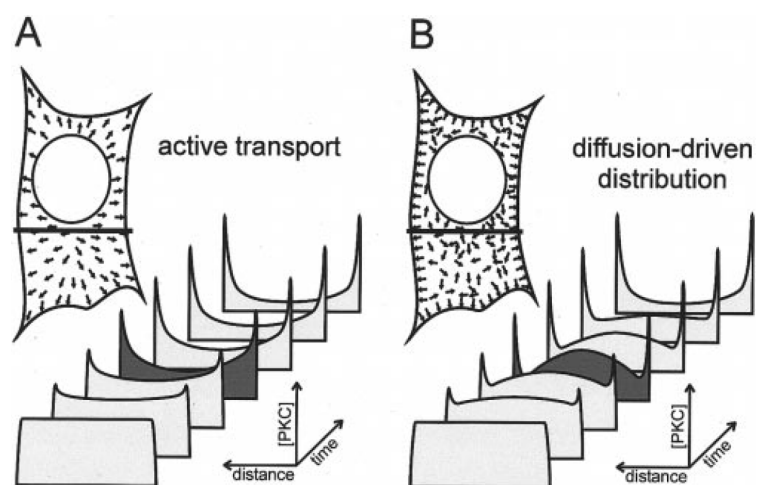


Fig. 1.4.1 Schematic diagram of two transport models of PKC. (A) Active transport model. Translocation of Ca^{2+} bound cPKCs to the plasma membrane follows a directional movement. The time-dependent distribution of PKC along the line labeled in the figure shows a minimum in the center of the cell until the equilibrium is achieved. (B) Diffusion-driven movement of cPKCs. Only in the proximity of the plasma membrane appears a highly efficient docking of PKCs, resulting in a directional movement that initially depletes the subplasmalemmal cytosol. Modified from FASEB J. 15:1634–1636 [87].

Michael Schaefer and colleagues revealed the existence of a transient subplasmalemmal depletion zone of cPKC during Ca^{2+} -induced cPKC plasma membrane translocation, which implied that the translocation of cPKC followed a diffusion-limited distribution model (Fig. 1.4.1 A) instead of an active transport model (Fig. 1.4.1 B) [87]. This model accurately explains the process of cPKC membrane translocation. In detail, only in the proximity of the plasma membrane the highly efficient association of cPKC to the plasma membrane via the Ca^{2+} bridge may result in a directional movement that initially depletes the subplasmalemmal cytosol, generating a gradient from the subplasmalemmal to the perinuclear cytosol. Later, diffusion equilibrates this gradient, which results in directed cPKC translocation from the cytosol to the plasma membrane.

According to Michael Schaefer's model, since the diffusion-driven distribution of PKC α crossing the cytosol is an essential step of Ca²⁺-induced PKC α plasma membrane translation, a further question arises, whether the cytoskeleton plays any role in such a process. Not only working as intracellular scaffolding, cytoskeletal filaments, consisting of actin filaments, microtubules, and intermediate filaments, engage in a variety of intracellular transport process, signal transduction, and cell movements [2, 121]. Briefly, the actin filaments form long and thin fibers beneath the plasma membrane providing mechanical strength to the cell, connecting transmembrane proteins to cytoplasmic proteins, and contributing to cell migration. The microtubules are straight and hollow cylinders whose wall is made up of α and β -tubulin, which are mostly involved in vesicular transport and cell division. The intermediate filaments are a family of related proteins with an average diameter of 10 nm, responding to mechanical stress. With respect to PKC proteins, the interaction between cytoskeleton components and PKCs have been reported from time to time (see chapter 1.3.4). Some reports showed that cytoskeletal components were even critical for PKC activation [122-124], Here I applied multiple approaches to deeply investigate the process of PKC α translation and test the involvement of the cytoskeleton.

1.5. Self-organized clustering of membrane-bound cPKC

Up to now when introducing PKCs we have only considered association and dissociation from the target membrane. cPKCs and nPKCs are believed to be only active when complexed with their respective activators, Ca²⁺ and/or lipids. It is well established that the PKC's kinase domain is notoriously slow with a turnover rate of only 10 phosphorylation events per second [125]. Therefore membrane residence time and target finding of PKC proteins appear of utmost importance for our understanding of how PKCs translate Ca²⁺ and lipid messages into phosphorylation events.

Ca²⁺ signals of much higher complexity, local Ca²⁺ signals, are established for almost 2 decades [126, 127] but very little is known on how the cells read-out such Ca²⁺ signals (sparks, puffs, quarks, blips). The very fast association and dissociation kinetics of cPKC render them almost an ideal read-out tool for such Ca²⁺ signals [88, 89].

In a previous study [88], we observed series of local translocation events (LTEs) of PKC α upon threshold stimulations of Ca²⁺ mobilization, 5-25 μ M ATP in this case. Many of the LTEs showed small amplitudes, brief lifetimes, and spatial restrictions following Ca²⁺ signal (Fig. 1.5.1 B). Interestingly, about 15% of LTEs displayed a distinctive spatiotemporal pattern (Fig. 1.5.1 A), in particular the lifetime of LTEs was prolonged to

more than 4 s, which was almost 5 fold longer than that of the Ca^{2+} puff, the underlying elementary Ca^{2+} signal with its limited amplitude and spatial spread. Such a phenomenon seems to challenge the classic theory of cPKC activation, exhibiting a dissociation between the Ca^{2+} signals and the membrane accumulation of cPKCs. We have to ask ourselves what kind of mechanism underlies it.

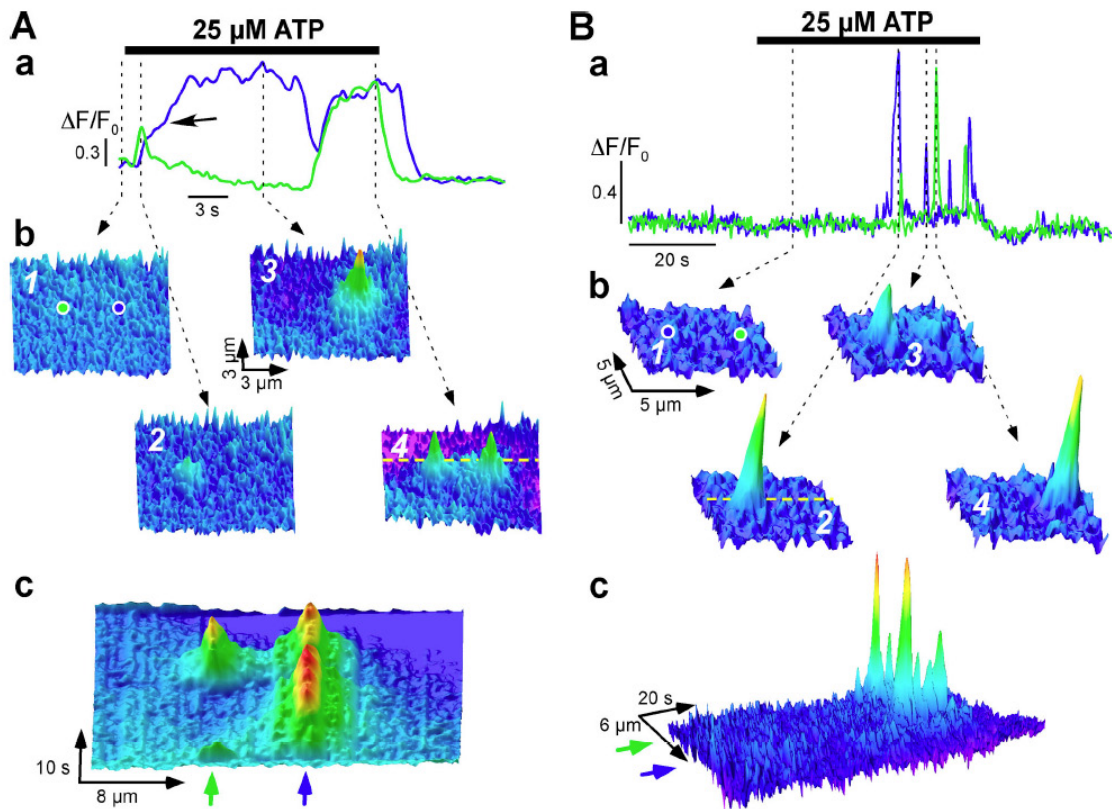


Fig. 1.5.1 Spatiotemporal variety of LTEs. Briefly, the long-lifetime of LTEs in PKC α -eYFP expressing cell after ATP stimulation shows in (A) and the short-lived LTEs shows in (B). (Aa and Ba) The blue and green plots over time shows the two LTE sites with the relative fluorescence signals respectively. (Ab and Bb) 3D surface plots of the fluorescence distribution at selected time points. The two ROI positions are indicated in (Ab 1 and Bb 1) respectively. (Ac and Bc) The 3D surface plots show the spatial dimension of LTEs by the 3D surface pseudo-linescan. The lines are marked in (Ab 4 and Bb 2) respectively. Taken from J. Cell Biol. 174:521–533.[88]

It is also important to understand this because such long-lived cPKC translocation could be a key to understand how cPKC decode local Ca^{2+} signals into phosphorylation events since such translocation of cPKC with a long lifetime would give the kinase enough time to target and phosphorylate their substrates.

In addition, I was interested in the specificity of this phenomena, whether this is a unique behavior of PKC α or it may occur during other cPKCs translocation. Even other C2

domain containing proteins, *e.g.*, cPLA, synaptotagmin, CAPRI, and so on, possessing the characteristic of Ca²⁺-dependent plasma membrane targeting [128-130] could also respond to local Ca²⁺ events.

1.6. C-domain toolkit of PKC decoding spatiotemporal signal

So far, many studies have reported that temporal differences of the cPKC and nPKC isoforms responses to complex Ca²⁺ and/or lipid signals in the velocity of translocation to the plasma membrane. Following activation of G_{αq}-coupled receptors or phorbol esters such as PMA, the plasma membrane has been identified as the major cellular target of PKCs [131-133]. Nevertheless, with respect to the similarity of consensus sequence for phosphorylation [16, 93, 94], how these different PKC isoforms decode the variety of incoming messengers into phosphorylation events appears to be instrumental for the understanding of many signaling mechanisms in cells.

In general, the specificity of phosphorylation events achieved by PKCs results from specific targeting rather than from substrate specificity [20, 22]. Presently, there are two conflicting models that try to explain how PKCs target specifically. One assumes that specific PKC targeting is a result of PKC binding to RACK proteins, which decide the final location of activated PKCs [103, 104, 108]. The other model suggests that PKC targeting is driven by signaling molecules, such as Ca²⁺ and lipid derivatives, which bind to the C1 and/or C2 domain of PKCs, particularly cPKCs, and trigger the translocation of PKC to the plasma membranes [22, 43, 86, 91].

With respect to PKC proteins themselves, *in vitro* studies have shown that the membrane targeting domain of PKCs has distinct preference for different membranes due to their phospholipid compositions [134-136]. Particularly the C1 domain of PKCs can distinguish DAGs based on their particular fatty acid composition [38, 86, 136]. It was also reported that unsaturated fatty acids alone may be sufficient for nPKC translocation to intracellular membranes [137], which highly indicates that specific lipids might determine or modulate PKCs targeting.

Using confocal microscopy of living cells, I aimed to address the following questions: (i) what are the translocation patterns of nPKCs (*e.g.*, PKC δ) in comparison to those of cPKCs (*e.g.*, PKC α) following the physiological activation of endogenous G-protein-coupled signaling pathways; (ii) which cellular membranes are targeted by cPKCs and nPKCs; (iii) which domains of PKC molecule account for its particular translocation

pattern; (iv) what are the underlying signaling cascades leading to the specific membrane targeting; (v) whether translocation leads to phosphorylation at the target membrane; (vi) and what are the physiological consequences of specific membrane targeting.

Chapter 2

MATERIAL AND METHODS

2.1 Material

2.1.1 Chemical compounds and solutions

Chemical compounds ATP, Bryostatin 1, 8-pCPT-2'-O-Me-cAMP, U37122, PMA, Ionomycin, Cytochalasin D (Cyto-D), and Nocodazole were purchased from Sigma-Aldrich (Munich, Germany). m-3M3FBS and Gö6983 were purchased from TOCRIS (Bristol, United Kingdom). ci-InsP₃/PM was purchased from SiChem (Hamburg, Germany). NP-EGTA/AM, Fura-2/AM, Fura-red/AM Fluo-4/AM, Indo-1/AM, and Pluronic[®] F127 were purchased from Life Technologies (Darmstadt, Germany).

Dulbecco's modified Eagle's medium (DMEM), Fetal bovine serum (FBS) and Pen-Strep (containing 10,000 U/ml penicillin and 10,000 µg/ml streptomycin) were purchased from Life Technologies (Darmstadt, Germany). Trypsin-EDTA (1x) was purchased from PAA (Cölbe, Germany). Transfection reagent NanoJuice[®] and Lipofectamine 2000[®] were purchased from EMD Millipore (Darmstadt, Germany) and Life Technologies (Darmstadt, Germany), respectively.

Tyrode solution consists of 135mM NaCl, 5.4 mM KCl, 2mM MgCl₂, 10mM glucose, and 10mM HEPES in pH 7.35. Modified Tyrode solution, containing 137 mM LiCl, 5.4 mM KCl, 2 mM MgCl₂ 10 mM EGTA, 10 mM glucose, and 10 mM EPES in pH 7.35 was applied in the assays specially indicated.

2.1.2 Enzymes and kits for molecular cloning

The restrict endonucleases, EcoRI, EcoRV, BglII, KpnI, MluI, XbaI, and XhoI, and T4 ligase were purchased from Fermentas (St Leon-Rot, Germany). The high fidelity DNA polymerase, Phusion[®] Hot Start II was purchased from Thermo Fisher (Bremen, Germany). The DH5 α competent cells were provided by Ms. Tanja Kuhn for plasmids transformation and amplification. The plasmid mini- and maxi-preparation kits and DNA gel extract kit, QIAquick[®] were purchased from Qiagen (Hilden, Germany).

2.1.3 Small interfering RNA

The human small interfering RNA (siRNA) structures, Epa1 siRNA (Catalog No. L-007676-00-0005), scrambled siRNA (Catalog No. D-001810-01-05), and transfection indicator, siGLO RED (Catalog no. D-001630-02-05), were purchased from Thermo Scientific (Bremen, Germany).

2.1.4 Primers

All DNA primers were synthesized by Life technologies[™] and diluted with RNase free water to 100 μ M stocked in -20°C.

2.1.5 DNA vectors and fluorescent labeled proteins

The plasmids, pcDNA3-PKC α _GFP (Fig. 2.1.1 A) and pcDNA3-PKC δ _GFP (Fig. 2.1.1 B), encoding human PKC α and PKC δ proteins fused with C-terminal eGFP, were kindly gifted from Prof. Michael Schaefer [133], which contain EcoRI recognized site in front of the initiation codon ATG of PKC and EcoRV/XhoI recognized site in front of the initiation codon of eGFP in the same ORF (Fig. 2.1.1). Other plasmids encoding PKC α fused with N-terminal eYFP, CFP or DsRed2 based on pcDNA3 were constructed by Dr. Gregor Reither with the same EcoRI and EcoRV/XhoI recognized set. Human PKC α is also fused to N-terminal TagRFP-T [138] based on a pCR259 vector (MP Biomedicals, Eschwege, Germany) by Dr. Anke Scholz with the EcoRI and EcoRV recognized set (Fig. 2.1.1 C). The mammalian bidirectional expression vector, pBI-CMV1, was purchased from Clontech (Mountain View, United State) (Fig. 2.3.3 A).

The fusion protein labeling the endoplasmic reticulum was construct from a sequence of calreticulin at the 5' end of DsRed2 and the KDEL ER-retention sequence at the 3' end of DsRed2, which was cloned from the commercial vector, pDsRed2-ER (Clontech, Mountain View, United State), and inserted to the pCR259 vector. The probe labeling Golgi was constructed with the N-terminal 81 amino acids of human beta 1,4-

galactosyltransferase, obtained from the commercial vector pECFP-Golgi (Clontech, Mountain View, United State), and fused with C-terminal mRFP into the pCR259 vector. The mitochondrial labeling protein was generated from subunit VIII of human cytochrome c oxidase, cloned from the commercial vector pDsRed1-Mito (Clontech, Mountain View, United State), and fused with C-terminal mRFP into the pCR259 vector. These plasmids were constructed by Dr. Sandra Ruppenthal.

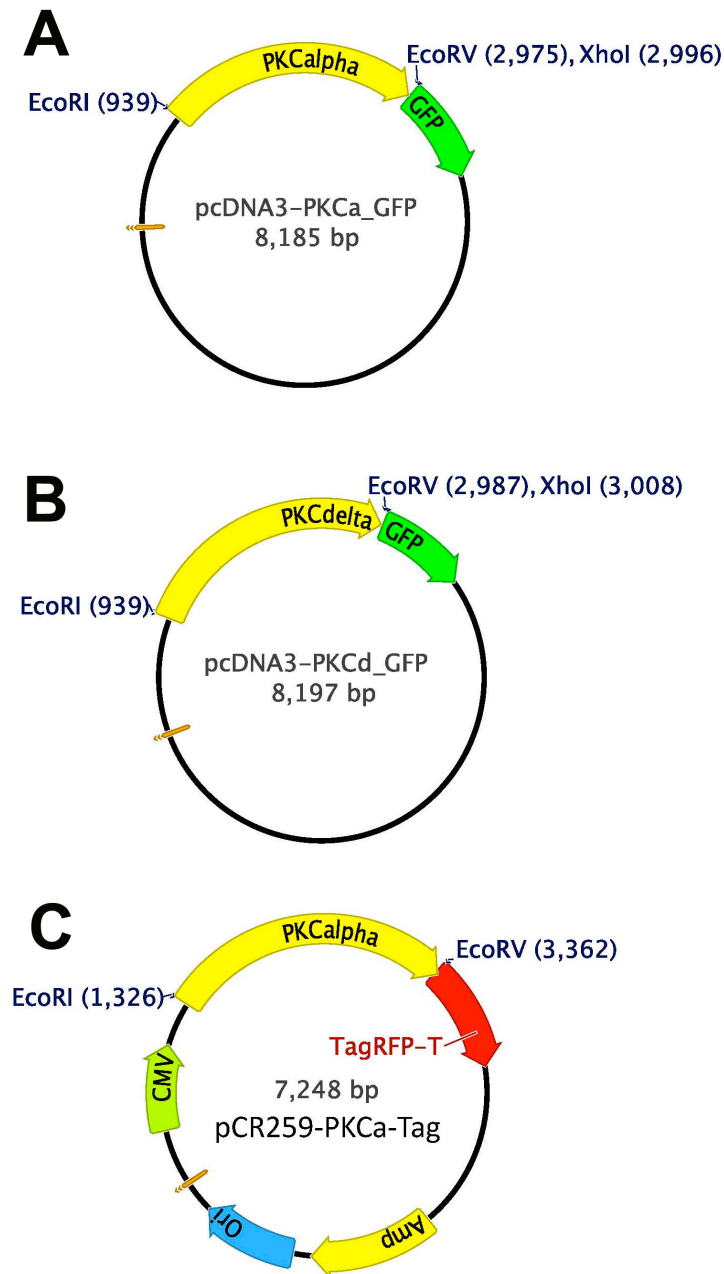


Fig. 2.1.1 Map of plasmids encoding fluorescent labeled PKC proteins. The sites recognized by restriction endonuclease are labeled. The open reading frames are indicated with respective colors.

The FRET based PKC activity probes, CKAR and PM-CKAR, were a kind gift of Prof. Alexandra Newton [139]. The plasmid mVenus-b(5) was supplied from Prof. Nica Borgese [140], which contained an ER-resident sequence, 20 amino acids of transmembrane domain of cytochrome b(5) with polar sequence. pCMV2-FLAG-RapGAP1 plasmid encoding human Rap1GAP protein was kindly provided by Prof. Lawrence Quilliam [141].

2. 2 Microscopy devices

2.2.1 Video-imaging system (TILL Photonics Imago)

The Imago microscope system was based on an inverted microscope (TE-2000, Nikon, Düsseldorf, Germany) equipped with a CCD camera, Imago-QE (TILL Photonics, Gräfelfing, Germany). A monochromator, Polychrome IV (TILL Photonics, Gräfelfing, Germany) was used to generate the desired excitation wavelengths, which were reflected by a suitable dichroic mirror and focused onto the cells with a 20x multi-immersion objective (NA 0.75, Plan Fluor, Nikon, Düsseldorf, Germany). The Digital Signal Processor (DSP)-driven Imaging Controlling Unit (ICU, TILL Photonics, Gräfelfing, Germany) controlled the camera and the monochromator and was operated by software TILLvisION v4.0 (TILL Photonics, Gräfelfing, Germany).

2.2.2 Confocal microscope (Leica TCS SP5)

The Leica TCS SP5 II (Leica Microsystems, Wetzlar, Germany) was based on an inverted epifluorescence microscope with a resonating x-scanner at a full speed of 8000 Hz. For excitation of eGFP, Fluo-4 with 488 nm and DsRed2, TagRFP-T with 514 nm spectrum, an Argon gas laser was employed. The laser line selection was controlled by a computer operated Acousto-Optic Tunable Filter (AOTF). The design of the confocal microscope allowed the selection of emission spectrum in a filterless mode by an Acousto-Optic Beam Splitter (AOBS) that substitutes the primary dichroic mirror. Photon detection was performed with a two-channel high sensitive SP prism spectrometer. The entire confocal system was controlled by Leica Application Suite software (ver. 2.4).

2.2.3 Kilobeam scanning confocal system (VisiTech-VTinfinity)

The VT infinity confocal microscopy was based on an inverted microscope (Eclipse TE 2000-U, Nikon, Düsseldorf, Germany) equipped with a kilobeam 2D-array scanner (VT Infinity, VisiTech International, Sunderland, United Kingdom), which enabled fast

acquisitions of two-dimensional images by guiding a bundle of excitation beams to the specimen via a galvanometer scanner and the emission beams through pinhole-arrays towards the detection device (Fig. 2.2.1). Different lasers (Cobolt, Solna, Sweden) supplied a selection of wavelengths and were controlled by an AOTF. A cooled EM-CCD-camera, iXon 887 (Andor Technologies, Belfast, United Kingdom), was employed for signal detection. The whole setup was integrated and controlled by VoxCellScan software (VisiTech International, Sunderland, United Kingdom).

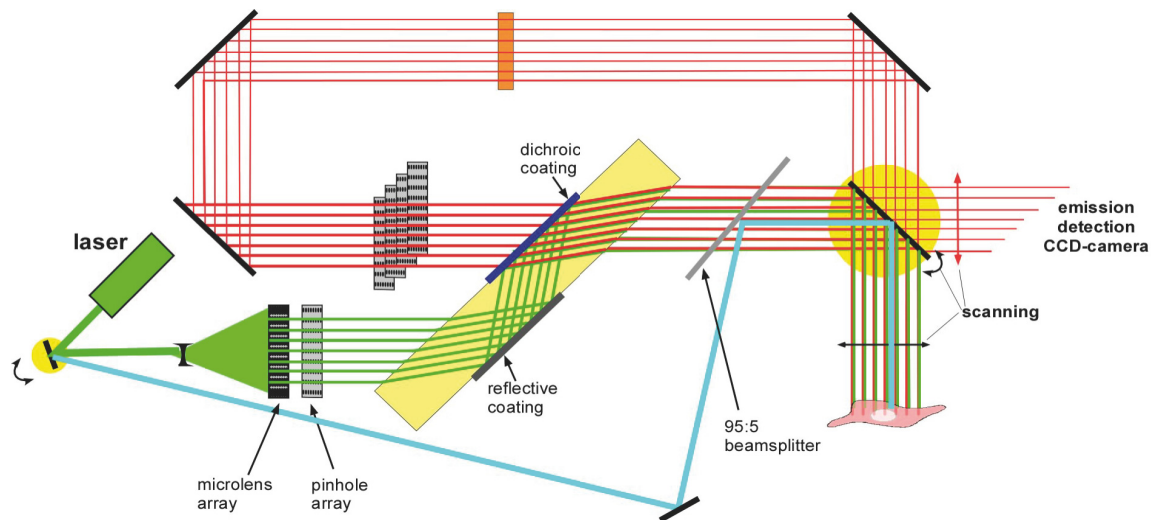


Fig. 2.2.1 Illustration of the kilobeam scanning confocal microscopy. The green lines indicate excitation laser light, the red lines show emission light, and the blue line illustrates the FRAP beam path. Adapted from Kaestner, L. Calcium signaling. Approaches and Findings in the Heart and Blood. (Springer: Heidelberg, 2013).

2.3 Methods

2.3.1 Recombination of the chimera constructions

In order to investigate the biological function of each regulatory domain of cPKCs and nPKCs, eight chimeras were constructed by mutually exchanging regulatory domains of PKC α and PKC δ , as shown in Fig. 2.3.1, and fused with the C-terminal fluorescent protein eGFP.

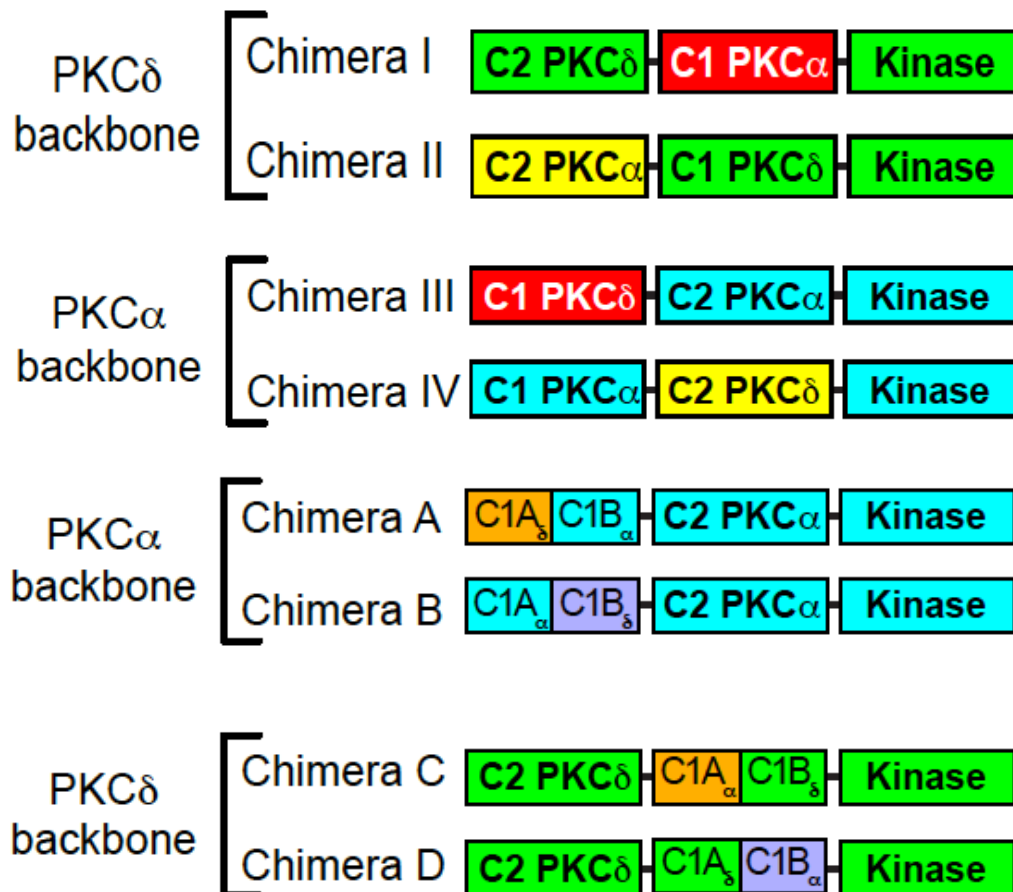


Fig. 2.3.1 Structure of chimeras. The original structures of PKC α domain are in cyan color, while the original structures of PKC δ domain are in green color.

The desired regulatory domains of PKC α and PKC δ were amplified individually by PCR from full-length wild-type PKC α and PKC δ . Briefly, in case of Chimera IV (ChimIV), the

PCR primer pairs, Forward- α x ChimIV-1, ChimIV-2 x ChimIV-3, and ChimIV-4 x Reverse-1 were used to generate three fragments of Chimera IV, including the 5' of PKC α with the C1 domain, the C2 domain of PKC δ and the 3' of PKC α with kinase domain. With the oligonucleotides, overlapping sequences were introduced in each of the fragments. During the second round of PCR amplification, the three fragments were used as template to amplify full-length Chimera IV with the pair of primers Forward- α , containing an EcoRI recognized site, and Reverse-1, containing a XhoI recognized site (Fig. 2.3.2). This two-step PCR is well discussed by Yokoyama and colleagues [142]. All other chimeras were generated in this way utilizing the respective pairs of primers listed in Table 2.1. In PCR process, high fidelity DNA polymerase was used and the annealing temperature of each PCR was set according to the lowest melting temperature of the primers. 1% agarose gel was used for DNA electrophoresis and the proper molecular size of PCR products were retrieved by a DNA gel extract kit following the manufacturer description. The purified chimera fragments were double-digested by restriction endonucleases, EcoRI and XhoI. With the EcoRI and XhoI sites the chimera fragments were inserted back into pcDNA3 together with eGFP as described above (Fig. 2.1.1). The correct construct of all chimeras was confirmed by DNA sequencing.

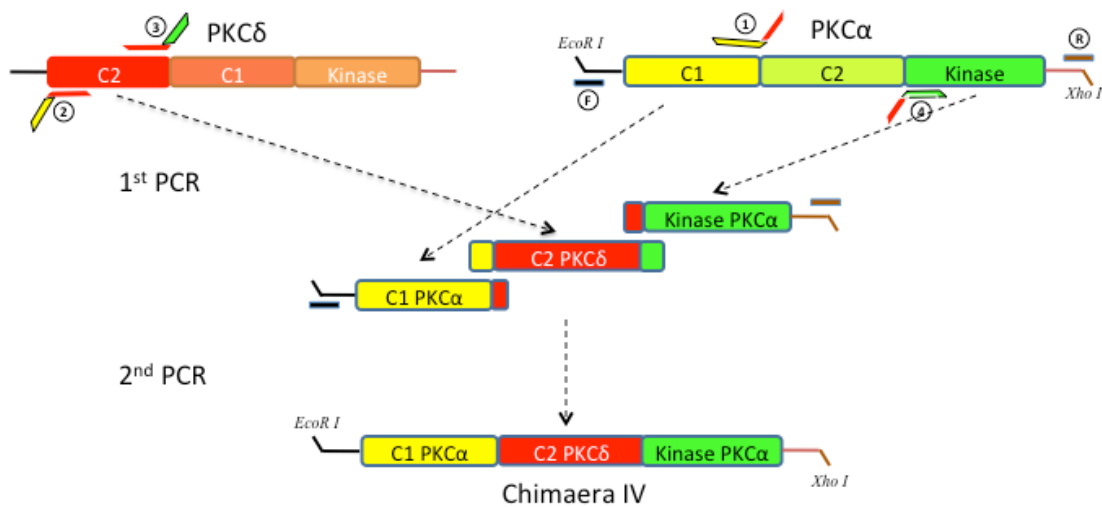


Fig. 2.3.2 Scheme of chimera construction. Briefly, KC δ C2 domain, PKC α C1 and kinase domain can be amplified by the indicated pair of primers with short linkers. Then the second round of PCR connect the separated domain fragments with the linker. The primers are listed in Tab. 2.1.

Table 2.1 The list of primers for PKC Chimeras construction

Name	Sequence 5'-3'
Forward-δ	TGGAATTCGCCCTTCCCACCAT
Forward-α	AGAATTCGCATGGCTGACGTTTTCCCG
Reverse-1	ATCTCGAGCGGCCGCCAGTGTG
ChimI-1	AGCGCGCGATGAATTTGTGGTTCTTGATGTAGTGGATTTTGGCC
ChimI-2	GGCCAAAATCCACTACATCAAGAACCACAAATTCATCGCGCGCT
ChimI-3	CCAAAAGCTTCTGGTTGATGCCGCAGAGGCTGGGGACATTGAT
ChimI-4	ATCAATGTCCCCAGCCTCTGCGGCATCAACCAGAAGCTTTTGG
ChimII-1	TAAATCCGCCCCCTTCTCTCGAACGGCGCCATGGTGGGAA
ChimII-2	TTCCCACCATGGCGCCGTTTCGAGAAGAGGGGGCGGATTTA
ChimII-3	TTGTTTGCAATCCACGTCTCTCCCCTTCCGGAATGGGTACG
ChimII-4	CGTACCCATTCCGGAAGGGGAGGACGTGGATTGCAAACAA
ChimIII-1	AGGTGGCGATAAACTCATGGTCCTTCACCTCGTGCACG
ChimIII-2	CGTGCACGAGGTGAAGGACCATGAGTTTATCGCCACCT
ChimIII-3	CTCAGTGTGATCCATTCCGCAGAGGTTGGCCACCTTC
ChimIII-4	GAAGGTGGCCAACCTCTGCGGAATGGATCACACTGAG
ChimIV-1	GAGTTGAAGGCGATGCGCAGAGTGTGATCCATTCCGCAGA
ChimIV-2	TCTGCGGAATGGATCACACTCTGCGCATCGCCTTCAACTC
ChimIV-3	TCCATGTTTCCTTCTCTCGTCCAGGAAATACTGAACAGACA
ChimIV-4	TGTCTGTTCAGTATTTCTCTGGACGAGGAAGGAAACATGGA
ChimA-1	The same as ChimIII-1
ChimA-2	The same as ChimIII-2
ChimA-3	CAAGATCATCGGCAGATGCCCGGGTGC GGATAAGGGAC
ChimA-4	GTCCCTTATCCGCACCCGGGCATCTGCCGATGATCTTG
ChimB-1	GCTGTTGGCCGCGGTGCCAGTACAAGAAA
ChimB-2	TTTCTTGTA CTGGCACCCGCGCCAACAGC
ChimB-3	The same as ChimIII-3
ChimB-4	The same as ChimIII-4
ChimC-1	The same as ChimI-1
ChimC-2	The same as ChimI-2
ChimC-3	GTTGGCCGCGGTGCCAGTACAAGAAAAAGTAACAAATTCATG
ChimC-4	CATGAATTTGTTACTTTTTCTTGTA CTGGCACCCGCGGCCAAC
ChimD-1	GTGTGGATTTTGA ACTTGTGCGGCATGTCGATGTTGAAG
ChimD-2	CTTCAACATCGACATGCCGCACAAGTTCAA AATCCACAC
ChimD-3	The same as ChimI-3
ChimD-4	The same as ChimI-4

2.3.2 PKC δ mutagenesis

In human PKC δ , sited-direct mutations were performed by a similar two-step PCR protocol as described above. Primers containing specific mutations were synthesized according to Table 2.2. In the first PCR, the forward primer, Forward- δ (listed in Tab. 2.1), paired with the reversed version of mutation oligo and the forward version of mutation oligo paired with the reverse primer, Reverse-1 (listed in Tab. 2.1), amplified the 5'-half and 3'-half PKC δ respectively. Taking advantage of the sequence overlapping around the mutation place, the two fragments working as template can be linked by the second round of PCR with the forward and reverse primers, Forward- δ and Reverse-1. Following the similar steps described above (chapter 2.3.1), the DNA fragment of single amino acid mutated PKC δ was inserted back to the pCDNA3 backbone fused with eGFP. All PKC δ mutants were confirmed by DNA sequencing.

Table 2.2 List of primers for PKC δ mutations

Mutant position	Sequence 5'-3'
W252K	TGCGGCAGCCTGCTCAAGGGACTGGTGAAG
K378R	GGAGAGTACTTTGCCATCAGGGCCCTCAAGAAGGATGTG
T507E	AGAGCCGGGCCAGCGAGTTCTGCGGCACCC

Due to the same open reading frame of PKC δ and PKC α with the same EcoRI and EcoRV restrict sites in the plasmids pCDNA3-PKC α -eGFP and pCR259-PKC α -Tag, it was convenient to change the included fluorescent protein from eGFP to TagRFP-T by double-digesting the fragment of wild type or mutated PKC δ from one vector and inserting it to another (Fig. 2.1.1).

2.3.3 Construct of PKC δ -eGFP and Rap1GAP co-expression vector

The mammalian bidirectional expression vector, pBI-CMV1 allows expression of two proteins of interest duo to its two constitutively active promoters that located just upstream of two independent multiple cloning sites (MCS) (Fig. 2.3.3 A). Using PCR technique, PKC δ -eGFP and Rap1GAP were amplified from plasmids pcDNA3-PKC δ _GFP and pCMV2-FLAG-RapGAP1 respectively by primers (Table 2.3) and inserted into pBI-CMV1 vector subsequently by pairs of restriction endonucleases, MluI and EcoRV for Rap1GAP at MCS 1, EcoRI and BglII for PKC δ -eGFP at MCS 2 (Fig. 2.3.3 B). The plasmid pBI-Rap1GAP-PKC δ -eGFP was confirmed by DNA sequencing.

Table 2.4 Primers for vector pBI-Rap1GAP-PKCd-eGFP

Name	Sequence 5'-3'
Rap-Forward	CTGACGCGTATGATTGAGAAGATGCAGG
Rap-Reverse	TATCGATCTAACAGCCCAGCTGGGG
PKCd-FW	TGGAATTCGCCCTTCCCACCAT
PKCd-RV	GGAGATCT CTAGCATTTAGGTGACAC

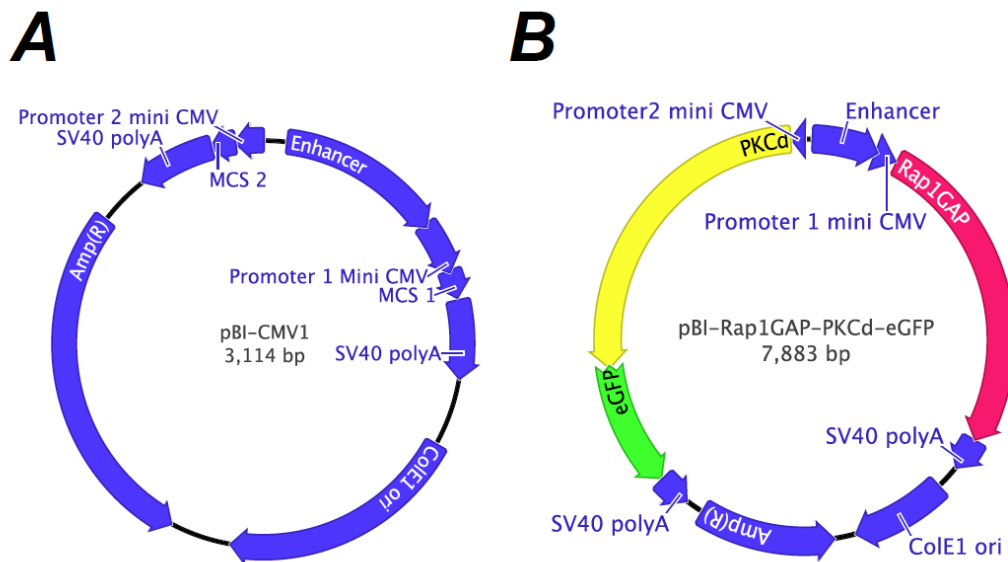


Fig. 2.3.3 Scheme of the bidirectional expression vectors. (A) The map of original pBI-CMV1 vector. (B) The map of plasmid pBI-Rap1GAP-PKCd-eGFP. The open reading frames of Rap1GAP, PKCd, and eGFP are indicated with red, yellow, and green respectively.

2.3.4 Generation of the ER localized CKAR

The ER targeted PKC specific activity probe (erCKAR) was constructed based on the plasmid pCDNA3-CKAR by fusing the ER targeting sequence, 20 amino acids of transmembrane domain of cytochrome b(5) with polar sequence, to the C-terminal of CKAR, which endow the fused protein specifically facing towards the cytoplasmic side of the ER rather than the ER luminal side [143, 144].

For this synthesis, I made use of KpnI and XbaI in the original plasmid pCDNA3_CKAR (Fig. 2.3.4), and amplified the part of the CKAR from the N-terminus of the FHA2 motif to the C-terminus of YFP, by employing the ER-Forward primer (Tab. 2.4) and the synthesized oligo linker, Linker-RV (Tab. 2.4), which consists of the C-terminus of CKAR and the N-terminus of the ER targeting sequence. The ER targeting sequence was amplified from N-terminus by the synthesized oligo linker, Linker-FW (Tab. 2.4), the reverse and complement of Linker-RV, to the C-terminus by the primer ER-Reverse with a XbaI site (Tab. 2.4). The second step of PCR linked the part of the CKAR and the ER

targeting sequence together by the primers ER-Forward and ER-Reverse. After double-digestion, the erCKAR fragment was inserted back into the pCDNA3_CKAR plasmid and named with pCDNA3_CKAR-ER (Fig. 2.3.4). The plasmid was confirmed by DNA sequence.

Table 2.4 Primers for DNA plasmid ER-CKAR

Name	Sequence 5'-3'
ER-Forward	CTGGTACCAAGGGTAATGGT
ER-Reverse	GATCTAGACCGGAATTCTCA
Linker-FW	GCATGGACGAGCTGTACAAGAAGCTGATCTCTGAGGAAGA
Linker-RV	TCTTCCTCAGAGATCAGCTTCTTGACAGCTCGTCCATGC

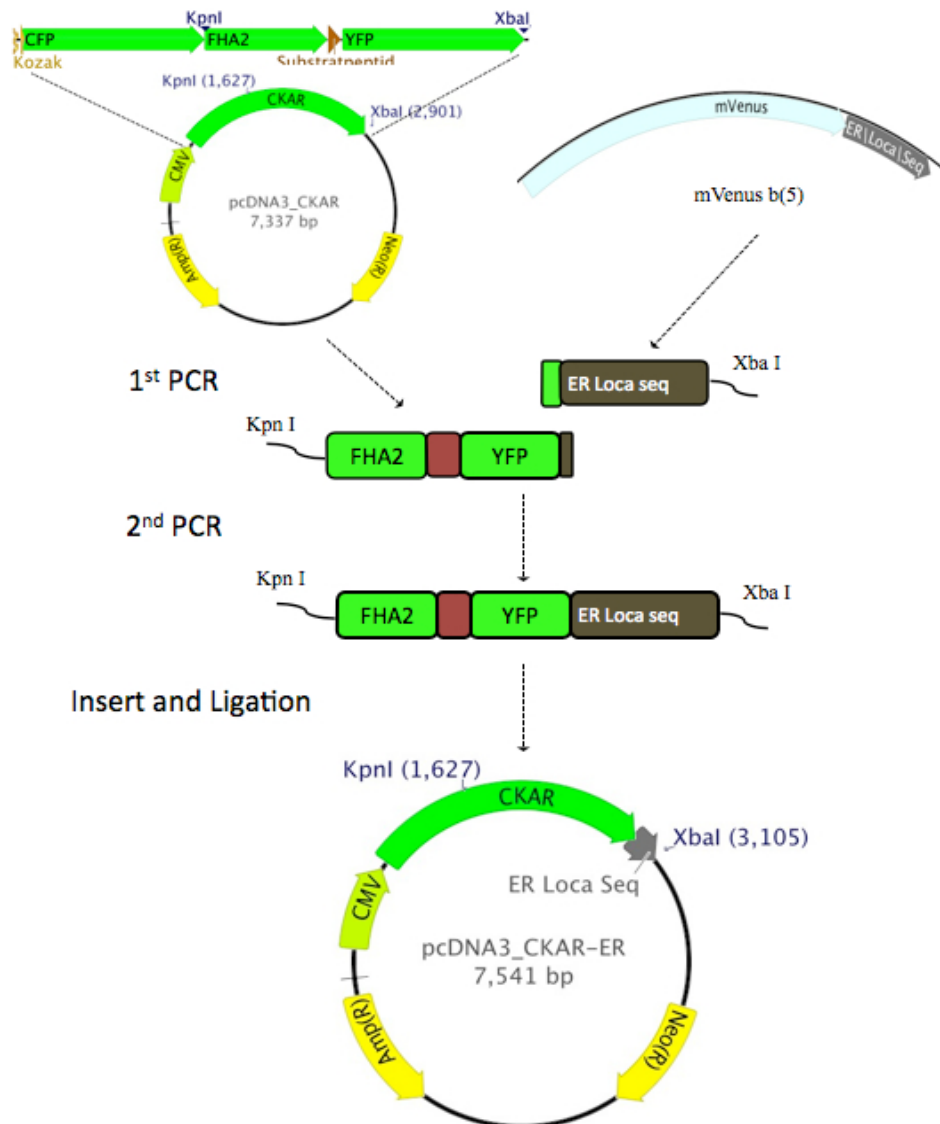


Fig. 2.3.4 Scheme of erCKAR generation. Briefly, the ER location sequence and FHA2-YFP fragment were amplified from mVenus b(5) plasmid and pcDNA3_CKAR plasmid with a linker, respectively. The second

round of PCR links the two fragments with a designed pair of primers. Finally the fragment inserts back with the ER location sequence.

2.3.5 Cell culture and transfection

The human embryonic kidney 293 (HEK293) cell line was maintained in DMEM with 5% (v/v) FBS, 100 U/ml penicillin and 100 µg/ml streptomycin at 37°C in 5% CO₂ in an air humidified incubator. Before the day of transfection, cells were plated on 20 mm diameter glass coverslips in a 12-well plate at about 30% confluence.

For the DNA plasmid transfection, NanoJuice[®] was applied, which comprised two chemical reagents, Core transfection reagent and Booster. Main steps of operation are listed;

- 1) Preparing a master mix for all desired wells and mixing it thoroughly;
For each well of a 12-well plate: 50 µl DMEM (without antibiotics)
0.5 µl Core transfection reagent
1 µl Booster
- 2) Incubation of the reagents and medium mixture at room temperature for 5 min;
- 3) Preparing plasmid tubes for different DNA or DNA combinations,
1 µg of total amount of DNA plasmid per well;
- 4) Adding the reagents and medium mixture to the plasmid tube and mixing gently;
- 5) After incubation at room temperature for 20 min, 50 µl of mixture per well was dropped to the cells evenly;
- 6) Cells were maintained in the incubator at 37°C and 5% CO₂ for 48 h.

In DNA plasmids and the siRNA co-transfection assay, Lipofectamine 2000[®] was utilized. Main steps of operation are listed;

- 1) Preparing a master mix for all cells and mixing it thoroughly;
- 2) For each well of a 12-well plate: 50 µl DMEM (without antibiotics)
2 µl Lipofectamine 2000[®]
- 3) Incubation of the reagents and medium mixture at room temperature for 5 min;
- 4) Dilution of plasmid and siRNA with DMEM (without antibiotics), 1 µg of DNA plasmid, 5 µl siRNA (20 nmol), and 2 µl siGlo (0.1 nmol) in 50 µl DMEM per well;
- 5) Incubation of the mixture of reagents and siRNA at room temperature for 20 min;
- 6) Removing the complete medium from cell culturing wells and gently adding the transfection mixture;
- 7) After incubation at 37°C and 5% CO₂ for 6 h, replacing the HEK293 cell complete medium and keeping in incubator for another 72 h.

2.3.6 Immunocytofluorescence labeling of actin filaments

When HEK293 cells reached about 40% confluence, they were fixed in 4% paraformaldehyde (in PBS) for 10 min. After a wash step with PBS, the fixed cells were permeabilized with 0.1% Triton X-100 (in PBS) for 10 min. After a PBS wash step, 5% BSA in PBS was used for blocking unspecific binding for 20 min at room temperature. For actin filament staining, 0.5 μM ATTO-647N phalloidin (Atto-Tec, Siegen, Germany) was employed in 1% BSA of PBS at room temperature for 2 h. After washed with PBS for 3 times, the cells were mounted in ProLong Gold Antifade reagent and visualized by confocal microscopy.

High-resolution images were acquired by the TCS SP5 II confocal microscope with a Plan Apo 63x oil immersion objective (Leica, Wetzlar, Germany). The excitation was achieved at 635 nm and fluorescent emission was collected in the spectral range of 648 to 750 nm.

2.3.7 Confocal imaging of living cells on Leica TCS SP5

Coverslips with HEK293 cells were mounted in custom-made chambers and bathed in Tyrode solution. The chamber was mounted on the stage of the microscope. The bath solution was rapidly changed by means of pipetting and liquid suction. The volume of the reservoir was about 400 μl . Confocal images were recorded with the TCS SP5 II microscopy using a 63 \times , NA 1.4, Plan-Apo oil immersion objective (Leica, Wetzlar, Germany). Excitation was achieved with appropriate excitation wavelengths, 488 nm for eGFP or 561 nm for mRFP, DsRed2, and TagRFP-T. The respective emission was captured at 495-550 nm for eGFP and 600-750 nm for mRFP, DsRed2, and TagRFP-T. 1024x1024 pixels images were recorded at 0.2 frames per second (fps). When necessary, Fura-red/AM, a cell membrane-permeable Ca^{2+} indicator with excitation at 450-500 nm and emission at around 660 nm, was employed to monitor Ca^{2+} transient with PKC α -eGFP translocation simultaneously. Fura-red/AM was stored in a stock solution at 1 mM in DMSO containing 20% Pluronic F-127 and finally diluted to 1 μM with Tyrode as working concentration. It need to note that fluorescence intensity of Fura-Red excited at 488 nm decreases once the indicator binds Ca^{2+} . Experiments were performed at room temperature (20-22°C).

2.3.8 Intracellular Ca^{2+} flash photolysis assay

NP-EGTA/AM, a cell-permeable photo-labile Ca^{2+} chelator, was stored in a stock solution at 1 mM in DMSO containing 20% Pluronic F-127 and finally diluted to a working concentration of 7.5 μM with Tyrode. NP-EGTA exhibits not only a high selectivity for Ca^{2+} , bur also a dramatic increase of its K_d for Ca^{2+} (from 80 nM to 1 mM) after illumination with UV light. Cells were incubated with NP-EGTA/AM for 40 min and

allowed 10 min for de-esterification. The VT infinity confocal microscope was employed for image recording through an oil immersion objective (40× NA 1.3 S-Fluor Nikon, Düsseldorf, Germany). The desired laser wavelength was selected for excitation of the particular fluorescent probe respectively, 491 nm for eGFP, 512 nm for YFP, and 561 nm for DsRed2. The fluorescence emission was collected by a 515 nm long-pass filter. Images (256x256 pixels) were recorded at 10 fps with 2x2 binning. Ca²⁺ photolysis was achieved by a bright UV flash (TILL Photonics, Gräfelfing, Germany) via a 400 nm long-pass dichroic mirror.

2.3.9 Intracellular InsP₃ flash photolysis assay

Membrane permeable caged InsP₃, ci-InsP₃/PM was stored in a stock solution at 1 mM in DMSO. Fluo-4/AM was also stored in a stock solution at 1 mM in DMSO containing 20% Pluronic F-127. The cells were loaded with 1 μM Fluo4/AM and 0.5 μM ci-InsP₃/PM for 40 min with an additional 10 min for de-esterification. During the experiment, cells were pretreated with the required compound for 15 min and bathed in normally Ca²⁺-free Tyrode solution, containing LiCl instead of NaCl. The VT infinity confocal microscope was used for Ca²⁺ imaging via a 40×, NA 1.3, S-Fluor, oil immersion objective (Nikon, Düsseldorf, Germany). Fluo-4 was excited with the 491 nm laser and emission was collected through a 515 nm long-pass filter. Images (120x128 pixels) were recorded at 2 fps with 4x4 binning. Intracellular InsP₃ uncaging was performed with a bright UV flash delivered by a 400 nm long-pass dichroic mirror. The graded intensity of the UV flash was achieved by multiple number of flashes in a short period of time (< 20 ms) but with a constant energy of each single flash. The trigger of UV flash and the image acquisition were automatically controlled by the software.

2.3.10 Fura-2 based Calcium imaging

The ratiometric Ca²⁺ indicator Fura-2/AM was dissolved in DMSO containing 20% Pluronic F-127 as a 1 mM stock solution and finally diluted to 1 μM with Tyrode. The cells were incubated in the dye solution for 30 min and deesterification was allowed for 10 min. A video-imaging microscope (the TILL Photonics Imago system) was used for image recording. The monochromator (Polychrome IV, Till Photonics, Germany) was applied for alternating excitation of Fura-2 (340 nm and 380 nm) while the emitted fluorescence was collected through a 515 nm long pass filter and an oil immersion objective (20x NA 0.75 Pan-Fluor, Nikon, Düsseldorf, Germany) onto the CCD camera (Imago-QE, TILL Photonics, Germany). Image acquisition was performed with 160x132 pixels at 10 fps at 4x4 binning. ATP stimulation was performed by means of a solenoid-driven custom-made perfusion system, which provided a laminar flow of about 200 μm in which all cells were

contained. A change of solution was achieved rapidly by opening and closing of appropriated solenoids.

2.3.11 Förster resonance energy transfer (FRET)

Experiments were performed on the TILL Photonics Imago video-imaging microscope with cells expressing FRET probes. A monochromator, Polychrome IV, was used for excitation CFP of 430 nm and YFP of 512 nm. The excitation light was reflected via a CFP/YFP double dichroic mirror through an oil immersion objective (20x NA 0.75 Pan-Fluor, Nikon). The emitted fluorescence was separated into two channels, 475/24 nm for CFP-channel and 535/30 nm by an image splitter with a CFP/YFP FRET filter-set (OptoSplit II, Cairn Research, Kent, United Kingdom) and simultaneously recorded with a single CCD. Images (160x240 pixels) were acquired at 0.1 fps with 2x2 binning. During the experiment, the extracellular solution was quickly changed by means of a pipette and liquid suction. To redress the spectral excitation and emission cross-talking, cells expressing YFP and CFP respectively were measured in the condition described above to obtain the acceptor relative fluorescent signal α and donor crosstalk fraction β .

Where desired, the FRET measurements were also combined with recordings of intracellular Ca^{2+} in CFP and YFP co-expressing cells. The Ca^{2+} dye Indo-1/AM was stocked in DMSO containing 20% Pluronic F-127 at 1 mM and finally diluted to 2 μM with Tyrode prior to the experiment. The cells were incubated with Indo-1/AM for 40 min and deesterification was allowed for 10 min. Three alternating excitation wavelengths, 350 nm for Indo-1, 430 nm for CFP, and 512 nm for YFP, were applied on specimen and fluorescence was collected from the same CFP/YFP FRET filterset. The Indo-1 signal was collected from two channels, 475/24 nm and 535/30 nm simultaneously, in which the signal from the 535/30 nm channel worked as a reference. The other setting rendered the same as described above.

2.3.12 Image analysis

The acquired images were stored using OMERO software (OME, Dundee, UK) and further analyzed using custom-build macros in ImageJ (W. Rasband, NIH, USA). The fluorescence over time data in regions of interest (ROI) were transferred into IGOR software (Wavemetrics, USA) and further processed using custom-written macros. When necessary, images were de-noised using a wavelet-based algorithm that was recently introduced [142, 145] and built into an ImageJ plug-in. Considering inhomogeneous distribution of the fluorophores, self-ratio images were calculated where necessary. For this purpose, I divided subsequent images of a video by a mean image obtained after averaging

the first 10-20 images of the video [88]. Color-coded 2D images were constructed in ImageJ from 16-bit or 8-bit grey scale images by applying the appropriate look-up tables. Image correlation analysis was based on Pearson's coefficient approach using the ImageJ plug-in, JACoP (F.P. Cordelieres, Institut Curie, France).

To avoid interference from cell movement, bleaching and spectral excitation and emission cross talk, I calculated the apparent FRET efficiency instead of the simple CFP/YFP fluorescence ratios according to a method published previously [146] using the following formalism:

$$Ef_{DA} \frac{\varepsilon_D}{\varepsilon_A} = \frac{F_{CFP_{ex}YFP_{ch}}^{YC} - \alpha F_{YFP_{ex}YFP_{ch}}^{YC} - \beta F_{CFP_{ex}CFP_{ch}}^{YC}}{\alpha F_{YFP_{ex}YFP_{ch}}^{YC}}, \text{ with}$$

h F^{YC} being the fluorescence signal of the FRET sensor and CFP_{ex} and YFP_{ex} referring to the excitation wavelength applied and CFP_{ch} and YFP_{ch} to the emission channels recorded,

$$\alpha = \frac{F_{CFP_{ex}YFP_{ch}}^{YFP}}{F_{YFP_{ex}YFP_{ch}}^{YFP}},$$

where the acceptor relative fluorescence signal α ,

$$\beta = \frac{F_{CFP_{ex}YFP_{ch}}^{CFP}}{F_{CFP_{ex}CFP_{ch}}^{CFP}},$$

crossstalk fraction β , were obtain by measurement described in chapter 2.3.11.

2.3.13 Statistical analysis

When necessary, the values are given as mean values \pm S.E.M (standard error of the mean). At the beginning of each statistical analysis the distribution of the values was tested. When the values showed a normal distribution, the unpaired two-tailed t test was applied using the software Prism 5 (GraphPad Software Inc., USA). The effects were regarded as significant only when p value < 0.05 . The effects were also presented in the bar graphs, one asterisk standing for $p < 0.05$, two asterisks for $p \leq 0.01$, three asterisks for $p \leq 0.001$, and N.S. for $p \geq 0.05$. The n-numbers were accumulated from more than 3 independent experiment and presented in each figure.

Chapter 3

RESULTS

3.1 Mechanisms of PKC α translocation

3.1.1 Ca²⁺-induced redistribution of PKC α to plasma membrane

PKC α activity is evoked primarily by a translocation from the cytosol to the plasma membrane directly following intracellular Ca²⁺ increases [88]. Therefore the intracellular Ca²⁺ rise is an important step of PKC α activation. Here I utilized the UV-flash to photolyze NP-EGTA caged Ca²⁺ in living cells, which . After loading the cell with 7.5 μ M NP-EGTA/AM, a membrane-permeable Ca²⁺ chelator, and Fluo-4/AM, a membrane-permeable Ca²⁺ dye, HEK293 cells were stimulated with 100 μ M ATP for 30 s (Fig3.1.1, upper middle) allowing to preload NP-EGTA with Ca²⁺. The UV-flash was uncaging Ca²⁺ rapidly and increased the intracellular Ca²⁺ concentration within milli-seconds (Fig. 3.1.1, upper right). The traces show changes of Ca²⁺ at the regions indicated. While the red color showed Ca²⁺ recordings within the illuminated region, the blue trace was obtained from a cell outside the illuminated area (yellow dashed region). As shown by the images and traces, the photolysis approach allows us to restrict UV-excitation to a small part of the field of view, increasing Ca²⁺ inside the illuminated region but without effects on cells outside this region (Fig. 3.1.1 upper right, the yellow ring), which provides the advantage to record cells under control conditions in parallel. Thus, with characteristics of rapid response, high Ca²⁺ reaction, and spatial restriction of the illuminated region, the UV photolysis of caged Ca²⁺ is proved to be an efficient approach for further studies.

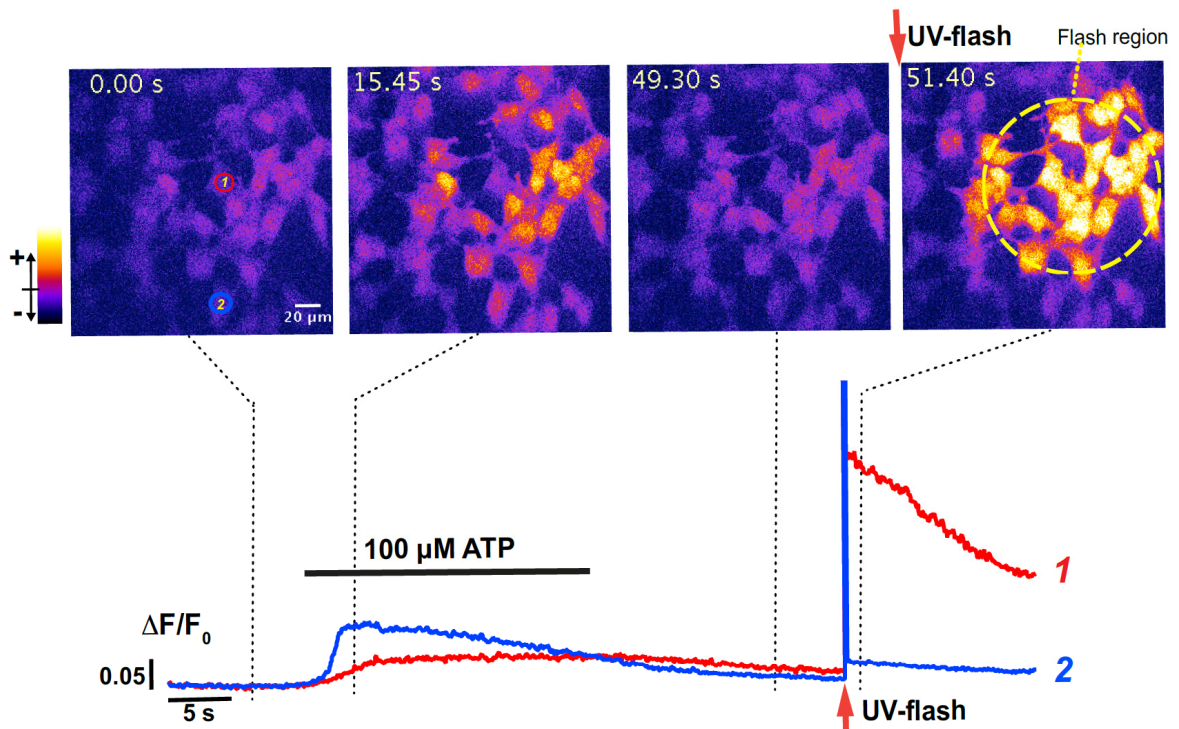


Fig. 3.1.1 Photolysis of caged Ca^{2+} in living cells. The fluorescent images (the upper row) show NP-EGTA and Fluo-4 loaded HEK293 cells at the indicated times before and after UV-flash. The yellow dash ring indicates the flash area (rightmost image). The traces illustrate plots of intracellular fluorescence over time at the region of interest, which are indicated in the upper left image. All data are representative of at least 30 cells in 3 independent experiments.

For the following studies, the human $\text{PKC}\alpha$ fused to eGFP was transiently expressed in HEK293 cells (Fig. 3.1.2 A). After NP-EGTA loading, the $\text{PKC}\alpha$ -eGFP expressing cells were used in the Ca^{2+} photolysis assay. Following Ca^{2+} uncaging, the fluorescence at the plasma membrane rapidly increased, while the fluorescence in the cytosol of cells was decreasing (Fig. 3.1.2 A), indicating the redistribution of $\text{PKC}\alpha$ -eGFP after the Ca^{2+} increase. The construction of a pseudo line scan clearly presented this dynamic process (Fig. 3.1.2 B). Interestingly, the detailed line scan analysis (Fig. 3.1.2 B) revealed that immediately after the UV flash, plasma membrane fluorescence increased rapidly while nearby cytosolic regions depicted an initial $\text{PKC}\alpha$ depletion. Here, central cytosolic regions did not show any changes at this time point. Only later after the UV flash, there was a $\text{PKC}\alpha$ -depletion wave engulfing the entire cytosol. During this process the plasma membrane fluorescence accumulation continued. In order to appreciate this process, I compared fluorescence intensity from plasma membrane (red trace in Fig. 3.1.2 C) and from an adjacent cytosolic region (blue traces in Fig. 3.1.2 C). The rapid and antiparallel time course of the plasma membrane and cytosolic fluorescence is obvious.

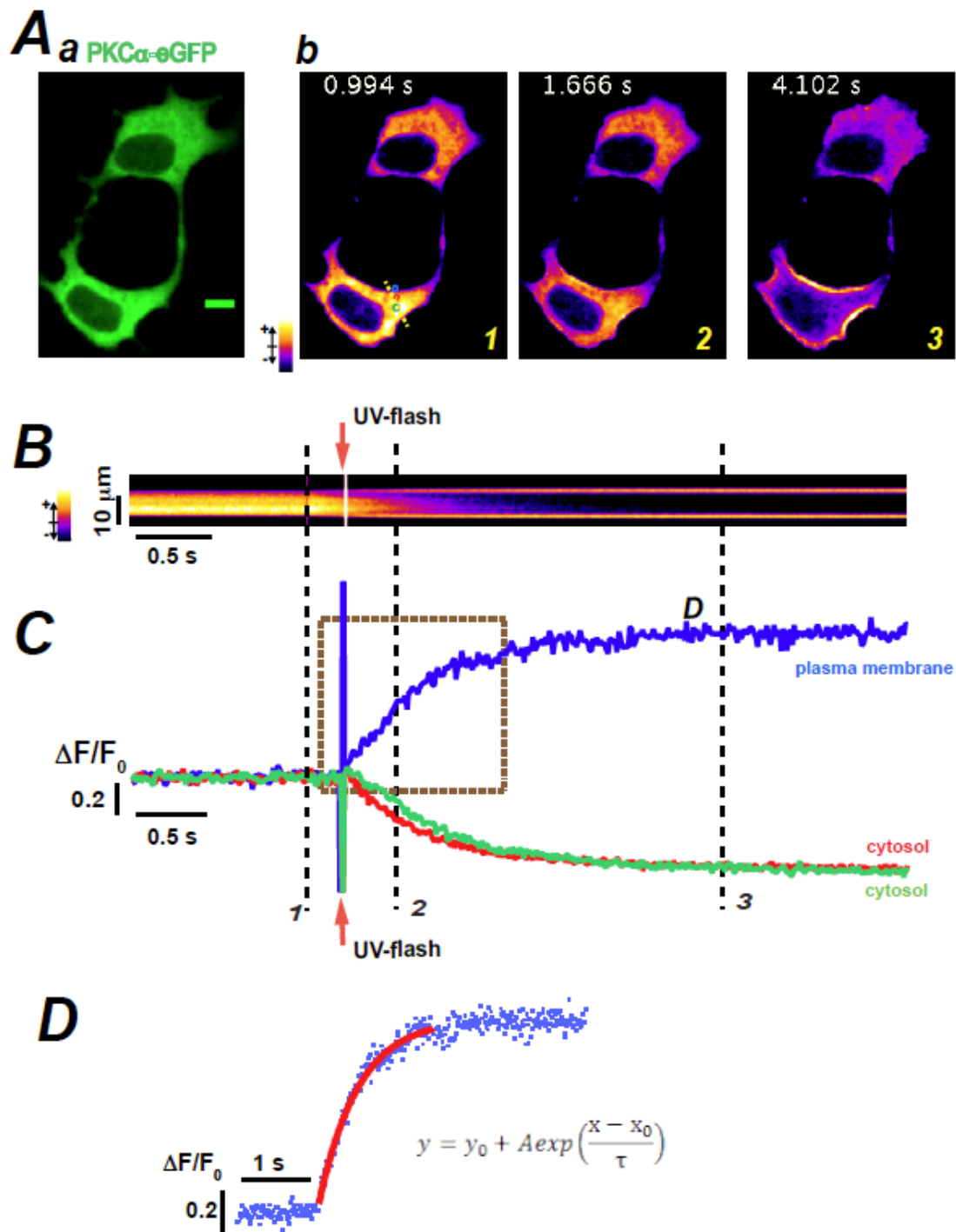


Fig. 3.1.2 Quantitative analysis of PKC α -eGFP translocation. (Aa) PKC α -eGFP distribution in HEK293 cells at the resting state. (Ab) The relative fluorescent image of PKC α -eGFP upon UV-flash in NP-EGTA loaded HEK293 cells at the time points indicated. Scale bar is 10 μ m. (B) The pseudo line scan at the labeled position (yellow dash line in the panel Ab1). (C) Plots of fluorescence over time at the plasma membrane (blue) and the cytosol (green and red) from the regions of interest, indicated with blue green, and red circles in the panel Ab1, close to the yellow dash line. The numbers at the traces correspond to the three images in panel Ab. (D) The magnified plot from upstroke trace indicated with the dash box in C was fitted with an exponential decay function (red line).

Such a representation allowed me to characterize the plasma membrane accumulation quantitatively as depicted in Fig. 3.1.2 D. Here, I fitted the membrane accumulation by a mono-exponential equation. The most important parameter that could be extracted was the time constant of this process, tau (τ), characterizing the speed of accumulation, that appeared rather independent of the expression level and represented the following processes (i) Ca^{2+} binding to the C2 domain and (ii) binding and accumulation of PKC α at the plasma membrane. As mentioned above, subplasma membrane cytosolic regions were quickly depleted from PKC α molecules and further accumulation was thus majorly determined by diffusion of PKC α from deeper cytosolic compartments.

Considering the important role of the DAG-C1 domain interaction in PKC-membrane targeting and the possibility of DAG production from Ca^{2+} -activated Phospholipase C γ (PLC γ), I further verified that PKC α translocation was only C2 domain dependent. A single amino acid mutation, D256N, located in the C2 domain of PKC α and critical for Ca^{2+} binding [51] was introduced. In Ca^{2+} photolysis experiments, no plasma membrane translocation could be observed in PKC α (D256N)-eGFP expressing HEK293 cells (Fig. 3.1.3), although the mutated PKC α still translocated to the plasma membrane following the treatment with phorbol ester, PMA, (Fig. 3.1.3, right most image). Taking together, I confirmed that the Ca^{2+} -C2 domain complex plays a predominant role for Ca^{2+} -induced PKC α translocation.

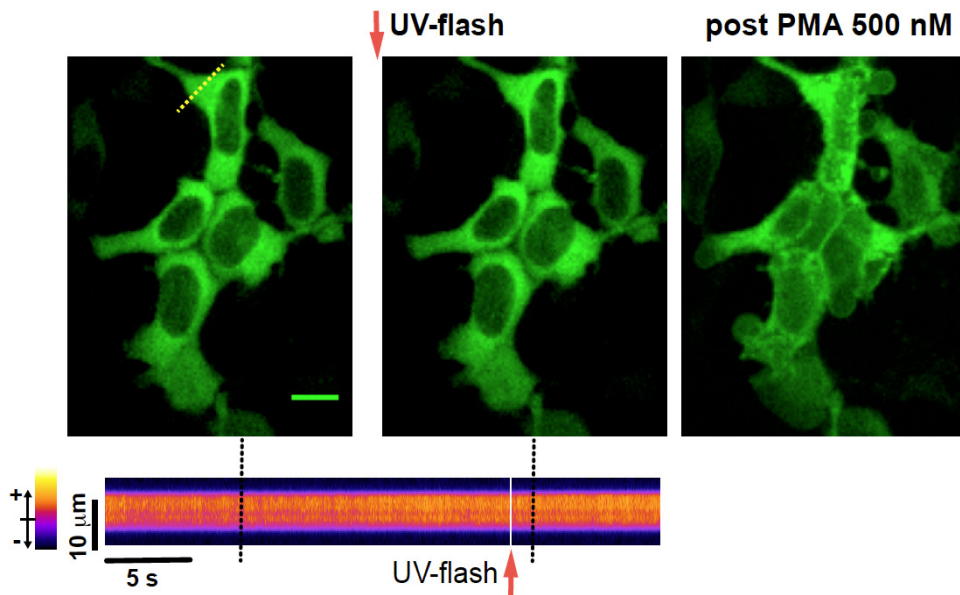


Fig. 3.1.3 The C2 domain of PKC α is essential for Ca^{2+} -induced PKC α translocation. After loading with NP-EGTA, PKC α (D256N)-eGFP expressed HEK293 cells (left picture) received a UV-flash (middle picture), and eventually 500 nM PMA for 20 min (right picture). Pseudo line scan (taken from dashed line in the left image, $t=0$ s) indicates no membrane translocation of PKC α (D256N) upon UV-flash. The black dash lines indicate the time of images.

3.1.2 Dynamics of PKC α translocation

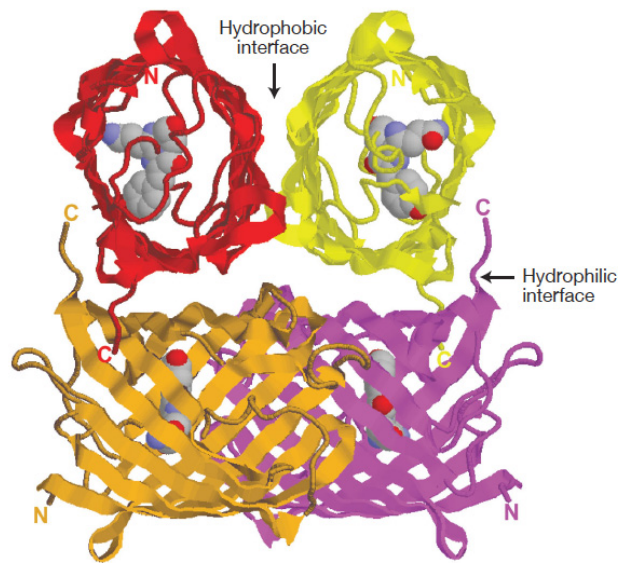


Fig. 3.1.4 DsRed2 tetramer structure. Monomers of DsRed2 are shown in different colors. N- and C-terminus of monomer are labeled in respective colors. Carbon, nitrogen and oxygen atoms are gray, blue and red, respectively. Modified from Nat Biotechnol 22:289–296 [147].

To investigate the sensitivity and reliability of the assay for analyzing the kinetics of PKC α translocation, I took advantage of the property of some fluorescent proteins to form oligomerized complex, *e.g.*, DsRed2. Due to the hydrophobic interaction between single DsRed2 proteins, four DsRed2 form a tetramer with each fused host protein at both N or C-terminal locations as depicted in Fig. 3.1.4. Thus, four PKC α aggregate together through DsRed2 oligomerization from different angles. Taking advantage of PKC α -DsRed2 tetramer, I further investigated the kinetic process of PKC α fused to the monomer and tetramer fluorescent proteins. Interestingly, following UV photolysis of intracellular Ca²⁺, PKC α -DsRed2 shows slow plasma membrane translocation when compares to the monomer form, PKC α -eYFP (Fig. 3.1.5 A, upper images). The traces from the plasma membrane and the cytosol illustrate such a difference (Fig. 3.1.5 A, lower lines). The statistical analysis of the τ values of the monomer and tetramer forms of PKC α -FP confirmed that the τ value of the tetramer (2.09 ± 0.192) is almost three times larger than that of the monomer (0.75 ± 0.060) (Fig. 3.1.5 C), which is comparable to the reported ratio (3.8 ± 0.4) of the hydrodynamic radius of the DsRed2 tetramer to that of the monomer [148]. Therefore the results strongly indicate that during Ca²⁺-induced PKC α plasma membrane translocation, the diffusion process is a main contribution to cytosolic PKC α transport.

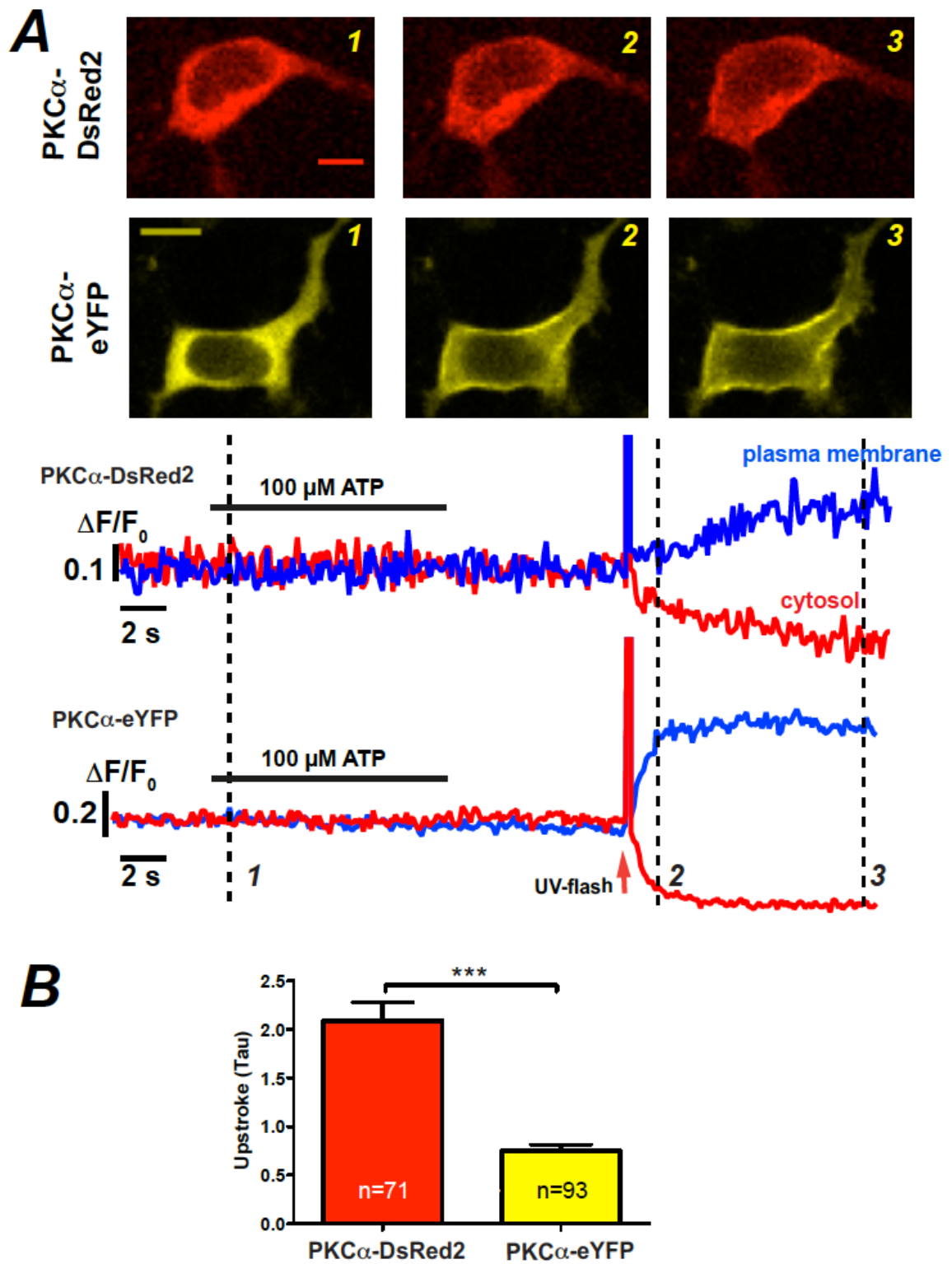


Fig. 3.1.5 Dynamic process of PKC α monomer and tetramer translocation. (A) The distribution of PKC α -DsRed2 and PKC α -eYFP in NP-EGTA loaded HEK293 cells at selected time points in the upper images and plots of the relative fluorescence over time at the plasma membrane (blue) and the cytosol (red). Bar is 10 μ m. (B) The diagram shows statistical analysis of upstroke τ value on PKC α -DsRed2 and PKC α -eYFP expressing cells.

3.1.3 PKC α translocation and the cytoskeleton

As described above, numerous reports have suggested that the distribution and localization of PKC α depends on the localization and the properties of the cytoskeleton [104, 122-124, 149]. I thus wondered to what degree the polymerization state of the cytoskeleton might affect the translocation properties of PKC α in living cells. For this purpose, I initially established experimental conditions that allowed me to study translocation in the presence or in the absence of a functional cytoskeleton. In this study, I concentrated on actin filaments and microtubules. For both components of the cellular cytoskeleton there are two well-known substances that can reliably influence the polymerization state of the filaments; (i) Cyto-D for the actin filaments and (ii) nocodazole for the microtubules. In preliminary experiments, I established that Cyto-D at a concentration of 4 μ M (for 1 h) and nocodazole at 5 μ M (for 2 h) substantially reduced the ordered arrangement of their respective cytoskeleton components, actin filaments and microtubules, as shown in Fig. 3.1.6. To study the influence of the cytoskeleton on PKC α translocation, I used such conditions to substantially reduce filamentous structures in living cells.

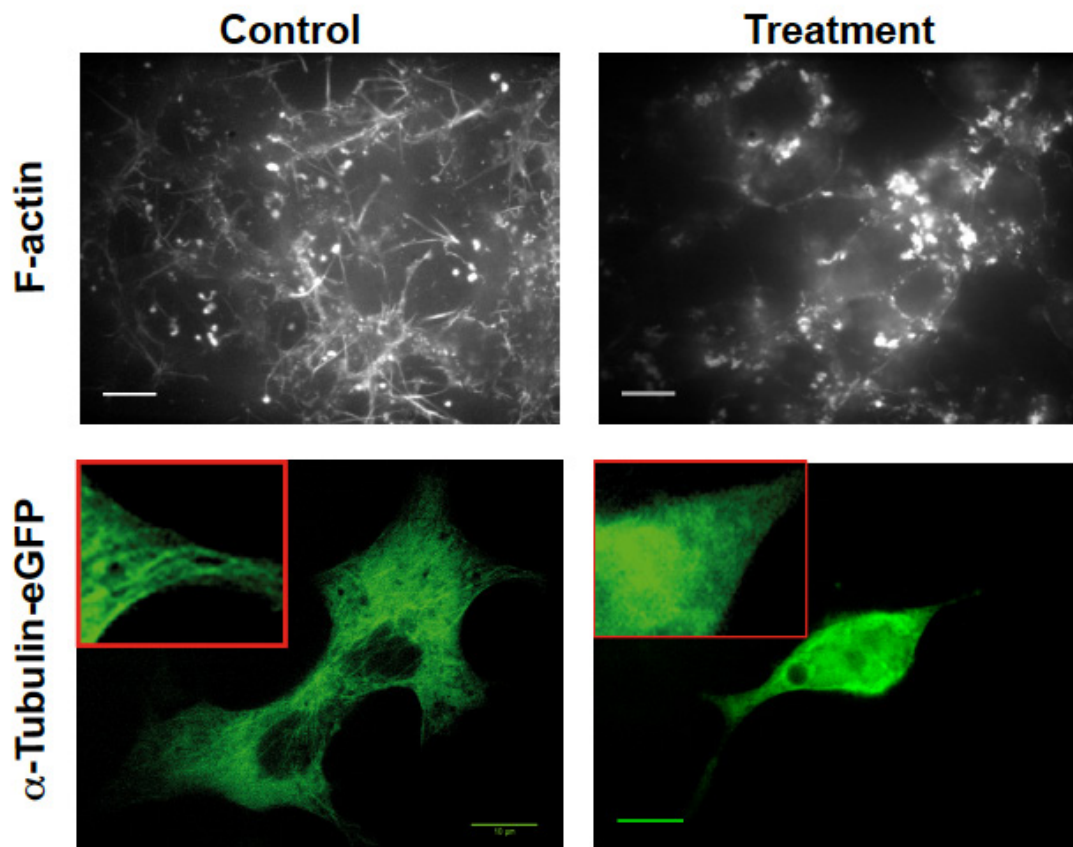


Fig. 3.1.6 Effects of Cyto-D and nocodazole on the cytoskeleton. Confocal images of phalloidin stained actin filaments in control HEK293 cells (upper left) and Cyto-D treated HEK293 cells (upper right). Confocal images of α -tubulin-eGFP expressing HEK293 cells with or without nocodazole treatment (lower row). Bar is 10 μ m. Similar results were obtained from more than 30 cells in 3 independent experiments.

Another important set of control experiments was to test whether depolymerization of the cytoskeleton with either Cyto-D or nocodazole could change the property of Ca^{2+} uncaging by UV-flash photolysis. After loading with NP-EGTA/AM and Fluo-4/AM and pre-stimulating with 100 μM ATP, the Cyto-D or nocodazole pretreated cells were illuminated with a UV-flash, similar to Fig. 3.1.1. The amplification of Ca^{2+} uncaging were analyzed in the control group, the Cyto-D treated group, and the nocodazole treated group. The statistical result shows no significant difference between any of the groups as depicted in Fig. 3.1.7, indicating that both compounds didn't affect Ca^{2+} transients triggered by photolysis.

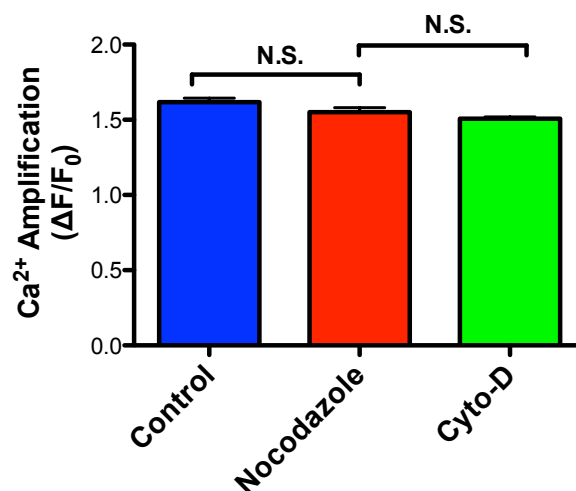


Fig. 3.1.7 Effects of Cyto-D and nocodazole on intracellular Ca^{2+} photolysis. The diagram shows statistical analysis of Ca^{2+} photolysis in three groups. Two-tail t-test, $n \approx 90$ in each group.

Using Cyto-D and nocodazole at the conditions stated above, I tested the effect of cytoskeletal organization on Ca^{2+} -induced $\text{PKC}\alpha$ translocation to the plasma membrane. The left panels in Fig. 3.1.8 A depict exemplified confocal images from $\text{PKC}\alpha$ -eYFP expressing cells before (labeled 1) and following UV flash photolysis of caged- Ca^{2+} (labeled 2). The time course of the membrane (blue) and cytosolic (red) fluorescence is illustrated in the graphs in the right part of panel A of Fig. 3.1.8. These data indicate that depolymerization of actin filaments or microtubules has no significant effects on $\text{PKC}\alpha$ translocation kinetics. In order to quantify this notion I analyzed a large population of cells and characterized the membrane association by determining the upstroke time constant of the membrane fluorescence (blue traces). The results of such an analysis are depicted in Fig. 3.1.8 B and clearly support the notion that $\text{PKC}\alpha$ translocation properties are independent of the polymerization state of actin filaments and microtubules.

To summarize the results obtained above, I can draw the conclusion that the distribution of cytosolic $\text{PKC}\alpha$ to subplasmalemmal in Ca^{2+} -induced plasma membrane translocation is

driven by diffusion and it is independent of the main component of cytoskeleton components, actin filaments and microtubules.

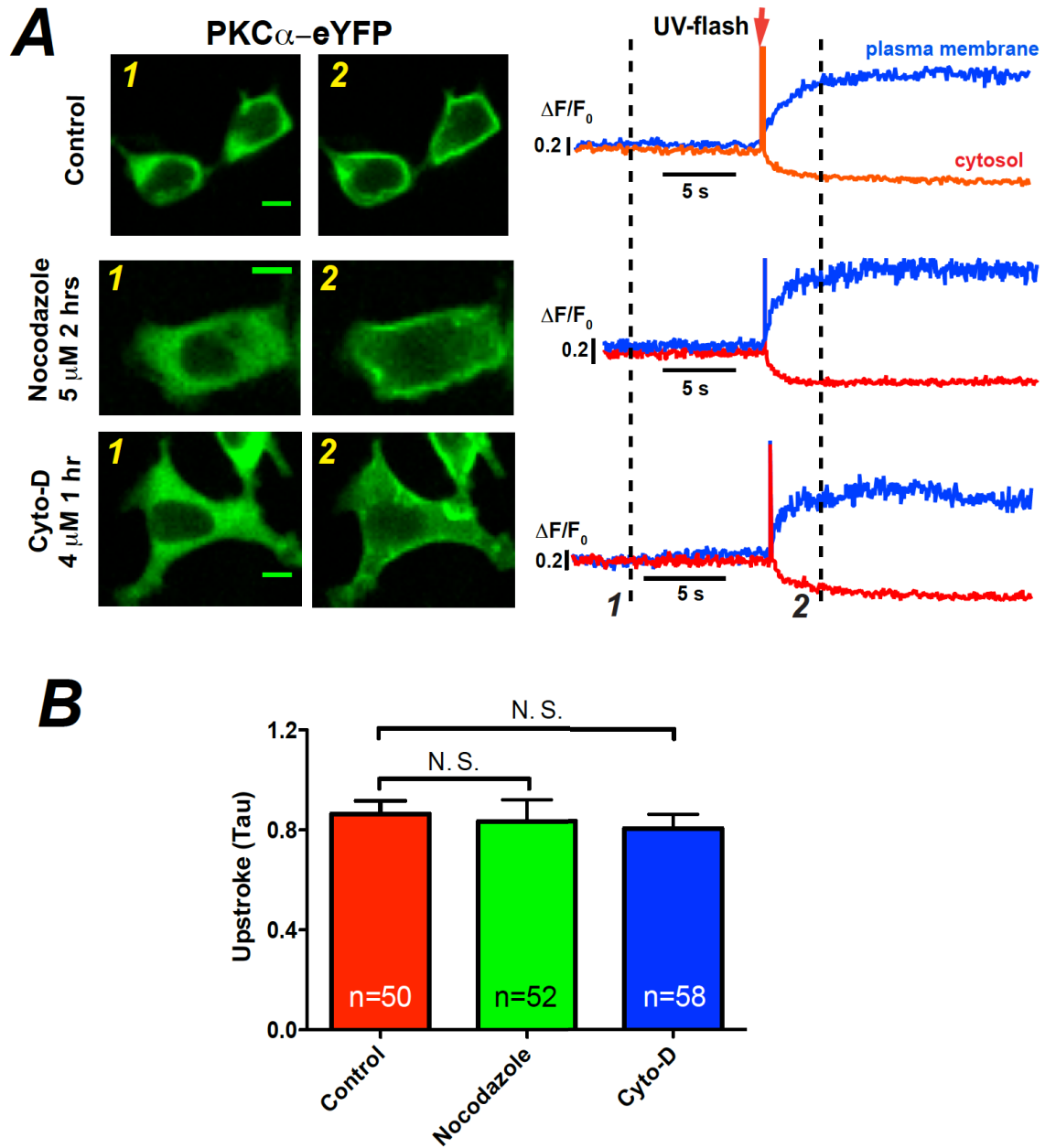


Fig. 3.1.8 PKC α translocation independent of the depolymerization status of actin filaments or microtubules. (A) shows the distribution of PKC α -eYFP at given time points in NP-EGTA loaded HEK293 cells after indicated treatment. The plots of relative fluorescence over time at the plasma membrane (blue) and the cytosol (red) correspond to the left images. Scale bars represent 10 μ m. (B) The statistical analysis of the upstroke time constant τ in three experimental conditions. A two-tailed t-test was performed to test for significance.

3.2 Self-organized clustering of membrane-bound cPKC

3.2.1 Transient interaction of plasma membrane-bound cPKC upon ATP stimuli

It has been reported that cPKCs working as an intracellular Ca^{2+} signal read-out, responded to global Ca^{2+} signal fast [88, 89]. Application of 100 μM ATP on PKC α -eGFP expressing and Fura-red loaded HEK293 cells, global Ca^{2+} transient was immediately evoked as depicted by the images and the black trace in Fig. 3.2.1 A, following with a recruitments of PKC α to the plasma membrane as depicted by the green traces in Fig. 3.2.1. It should be note that fluorescence intensity of Fura-Red decreases when the indicator binds Ca^{2+} at 488 nm excitation. Concomitant with the membrane recruitment, the cytosolic fluorescence levels transiently dropped as depicted in Fig. 3.2.1 A, the red trace. Furthermore, application of 100 μM ATP in PKC α -CFP and PKC α -eYFP co-expressing HEK293 cells, interestingly, I found that the amount of FRET (blue trace in Fig. 3.2.1 B) changed in parallel with membrane accumulation (green trace in Fig. 3.2.1 B) when calculating the apparent FRET efficiency (see Material and Methods 2.3.12). Even though in this case video-imaging system (see Material and Methods 2.2.1) was used to investigate intramolecular interactions, ATP-induced PKC α translocation on the plasma membrane still could be identified readily with such a magnitude. This finding shows that when the recruitment of PKC α to the plasma membrane occurs, intramolecular FRET substantially increases, indicating that during ATP-evoked Ca^{2+} oscillations, an oscillatory intramolecular, intimate interaction between PKC α molecules occurs.

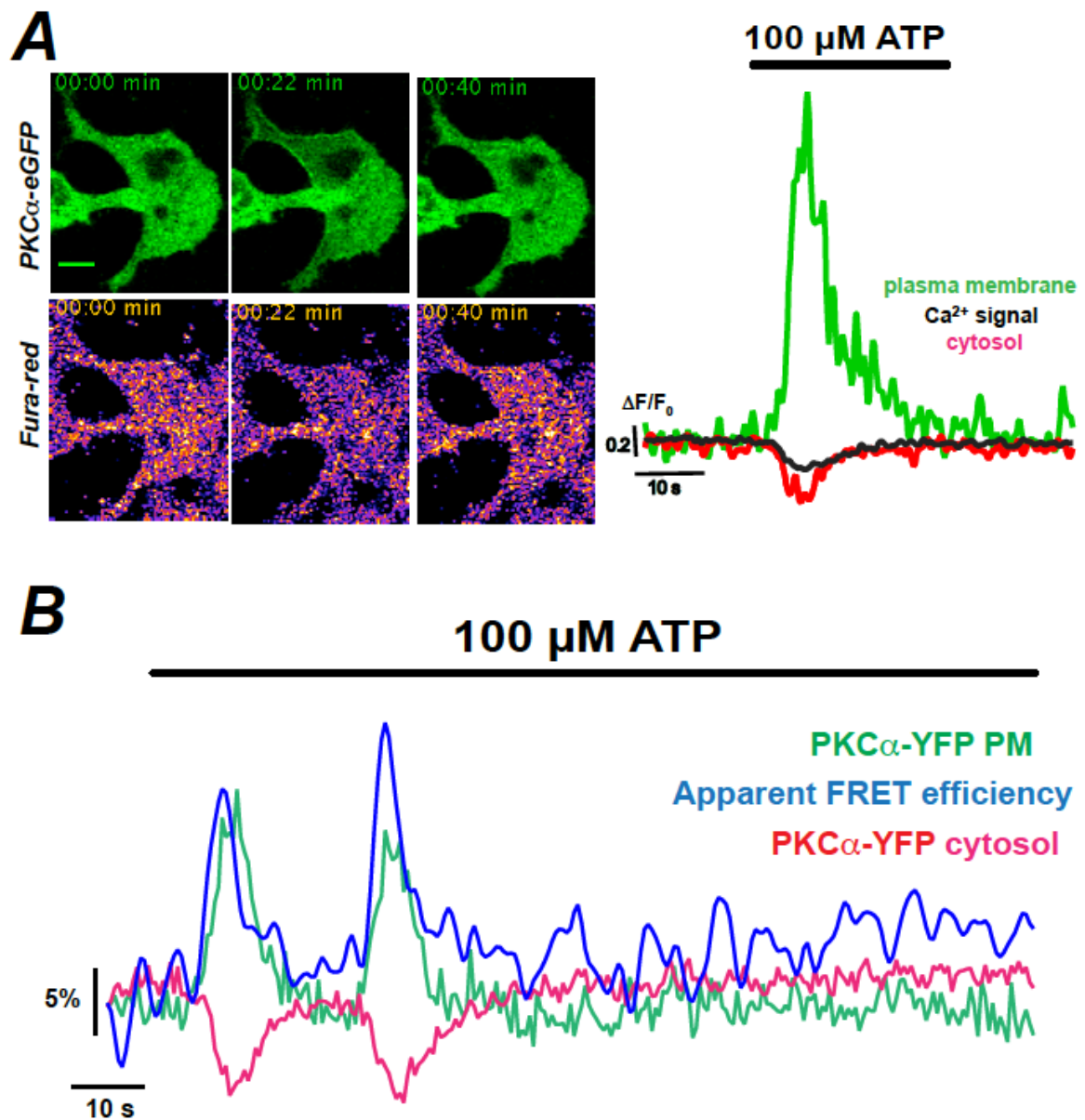


Fig. 3.2.1 Transient interaction of plasma membrane-bound cPKC upon ATP stimuli. (A) The distribution of PKC α -eGFP and fluorescence intensity of Fura-red in HEK293 cell upon ATP stimuli on the given time (left panel). The plots over time against relative fluorescence intensity at plasma membrane (green), cytosol (red), and intracellular Ca²⁺ (black) correspond to the left images. The scale bar corresponds to 10 μ m. (B) The plots over time show the apparent FRET efficiency (blue) and relative fluorescence intensity at the plasma membrane (green) and in the cytosol (red) upon ATP stimulation in PKC α -CFP and PKC α -eYFP co-expressed HEK293 cells.

3.2.2 Persistent interaction of membrane-bound cPKC following Ca²⁺ influx

Since application of ATP stimulates G α_q -coupled receptors that induce formation of the second messengers, *i.e.* DAG at the plasma membrane and diffusible InsP₃ (evoking Ca²⁺ release), it remains unclear whether this intimate interaction between the membrane

localized PKC α molecules is driven by Ca $^{2+}$ alone or whether DAG binding may indeed be required for such intramolecular interactions. I thus simplified the experimental design by limiting plasma membrane recruitment to that occurring in a Ca $^{2+}$ -dependent manner. For this purpose I permeabilized PKC α -CFP and PKC α -eYFP co-expressing HEK293 cells with the Ca $^{2+}$ ionophore, ionomycin [53, 150], and varied the extracellular Ca $^{2+}$ concentration in order to manipulate intracellular Ca $^{2+}$ concentration.

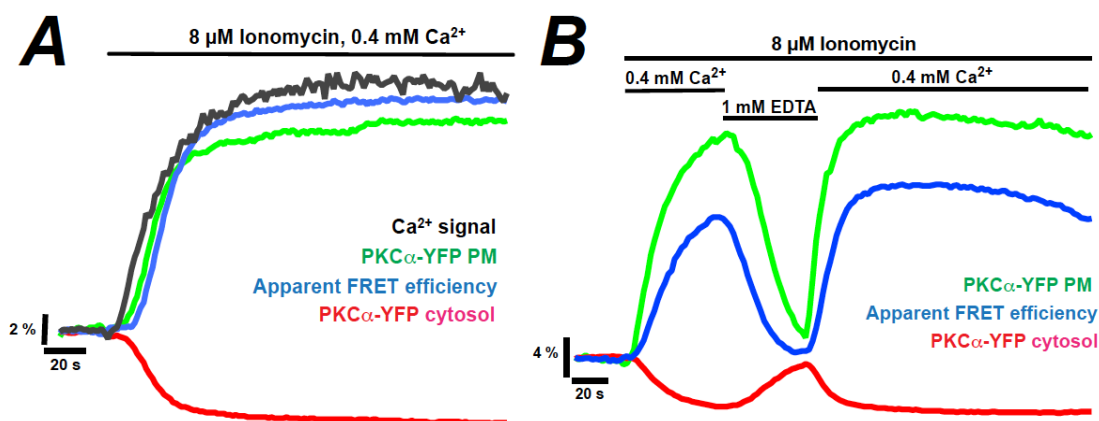


Fig. 3.2.2 Consistent FRET signals with PKC α -membrane binding. (A) The plots over time show a constant apparent FRET efficiency (blue), intracellular Ca $^{2+}$ flux (black) and relative fluorescence intensity on plasma membrane (green) and in the cytosol (red) within PKC α -CFP and PKC α -eYFP co-expressed HEK293 cell following constant 400 μ M Ca $^{2+}$ and 8 μ M ionomycin stimulation. (B) The plots over time show the fluctuation of apparent FRET efficiency (blue) and relative fluorescence intensity on plasma membrane (green) and in the cytosol (red) in PKC α -CFP and PKC α -eYFP co-expressed HEK293 cell following indicated Ca $^{2+}$ or EDTA stimulation in the presence of 8 μ M ionomycin.

Figure 3.2.2 depicts typical results of such an experiment. In Figure 3.2.2 A the HEK293 cells were additionally loaded with the Ca $^{2+}$ sensitive fluorescent probe Indo-1, allowing simultaneous Ca $^{2+}$ recordings. Interestingly, solely increasing the intracellular Ca $^{2+}$ concentration appears sufficient to induce a robust FRET signal between the PKC α molecules on the membrane. Please note that for this particular example although I have chosen HEK293 cells that allowed clear identification of the plasma membrane after translocation even with video-imaging system, fluorescence traces of cytosol and plasma membrane were not determined confocally.

In the next set of experiments, I addressed the questions of reversibility and reproducibility or refractoriness of the FRET process. For this purpose I rapidly switched between Ca $^{2+}$ -containing and Ca $^{2+}$ -free (1 mM EDTA) solutions as illustrated in the typical example shown in Figure 3.2.B. It's clearly illustrated that the FRET process is readily reversible, reduction of the apparent FRET occurred immediately after reducing the intracellular Ca $^{2+}$ concentration (and PKC α dissociation from the plasma membrane). Moreover rapid re-addition of Ca $^{2+}$ results in a quick reoccurrence of FRET. These data support my notion

that Ca^{2+} itself is sufficient to cause PKC-PKC interaction and the occurrence of intermolecular FRET.

One of the important questions remains, whether the FRET signal I recorded is indeed specific PKC-PKC interaction or merely resulted from unspecific CFP-YFP interactions due to molecular crowding [151, 152].

3.2.3 Self-organized formation of membrane-bound cPKC

I gained more insight into this question after analyzing the Ca^{2+} dependency of the PKC-PKC interaction process. Fig. 3.2.3 depicts results from experiments in which I used two different extracellular Ca^{2+} concentrations, a moderately lower and a substantially higher one (see Fig. 3.2.3 A&B). While the lower Ca^{2+} gained the same results as described before, the higher Ca^{2+} concentration (around 25 μM) caused a surprising result. The initial rapid upstroke of the apparent FRET signal (blue trace in Fig. 3.2.3 B) was followed by a spontaneous FRET decrease despite a continuous rise in the Ca^{2+} concentration (red traces in Fig. 3.2.3 A&B). The analysis of a greater population of HEK293 cells (Fig. 3.2.3 C) revealed that lower Ca^{2+} concentrations did not show substantial decay (green bar in Fig. 3.2.3 Ca), while at higher Ca^{2+} concentrations the decay time constant was reduced by almost 2 orders of magnitude (red bar in Fig. 3.2.3 Ca). Concomitant with this, the difference between the peak FRET change and the plateau was significantly larger at high Ca^{2+} (see bars in Fig. 3.2.3 Cb). In order to test whether this spontaneous FRET decay at higher Ca^{2+} concentration might be due to an unexpected dissociation of PKC molecules from the membrane, I analyzed Ca^{2+} signal, apparent FRET efficiency, and fluorescence intensity from cytosolic and plasma membrane PKC α simultaneously and found that a decrease of the plasma membrane PKC content was not the reason for the observed decay in FRET efficiency (see Fig. 3.2.3 D). Even though PKC α levels on the membrane were constant or even slightly increasing, the apparent FRET signal peaked and spontaneously decayed (blue trace in Fig. 3.2.3 D).

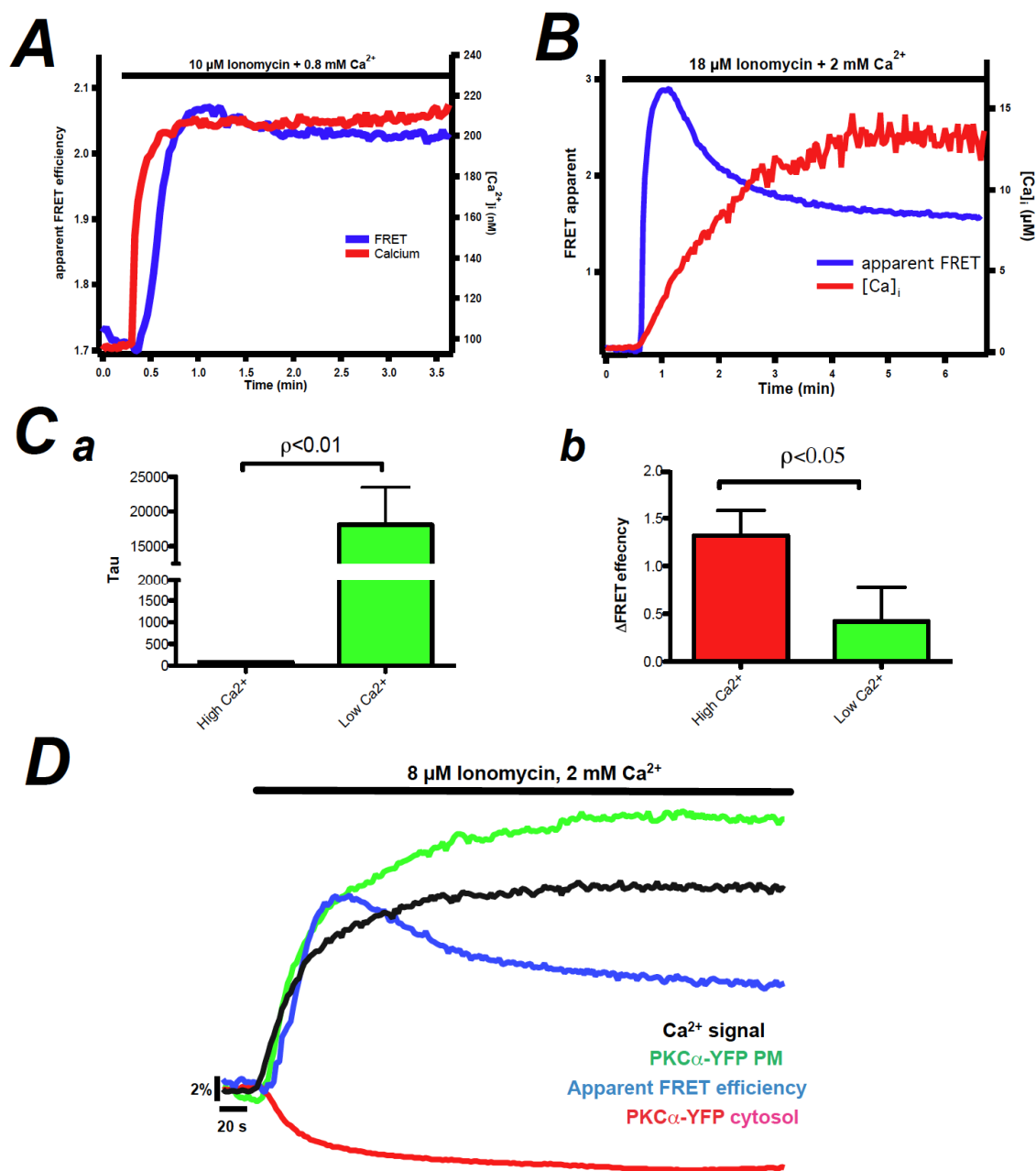


Fig. 3.2.3 Spontaneous decay of the FRET signal within a constant PKC α membrane binding. (A) The plots over time show a constant apparent FRET efficiency (blue) and intracellular Ca^{2+} (red) in PKC α -CFP and PKC α -eYFP co-expressing HEK293 cell following constant stimulation with 800 μM extracellular Ca^{2+} and 10 μM ionomycin. (B) The plots over time show a dynamic change of apparent FRET efficiency (blue) and intracellular Ca^{2+} (red) in PKC α -CFP and PKC α -eYFP co-expressing HEK293 cell following constant 2 mM extracellular Ca^{2+} and 10 μM ionomycin treatment. (C) The bar graphs depict the corresponding statistical analysis of the decay time constant (Tau) (a) and the difference between the peak and plateau of the FRET signal (b) in high (B) and low (A) Ca^{2+} concentration. $n=37-46$ from 4 experiments. (D) The plots over time show a constant intracellular Ca^{2+} flux (black) and relative fluorescence intensity on plasma membrane (green) and in the cytosol (red) within PKC α -CFP and PKC α -eYFP co-expressing HEK293 cells but with a spontaneously decaying FRET signal (blue) with a persistent 2 mM Ca^{2+} and 8 μM ionomycin stimulation.

3.3 C-domain toolkit of PKC decoding spatiotemporal signal

3.3.1 PKC α and PKC δ target distinctive compartments of cell

Due to their lipid-sensitive C1 domains, members of the cPKC and nPKC isoforms can be activated by PMA, a widely used member of phorbol esters. By expressing PKC α , a member of the cPKC subfamily, or PKC δ , a member of the nPKC subfamily, alone, or co-expressing PKC δ -eGFP and PKC α -TagRFP-T together in HEK293 cells, I investigated translocation patterns of these PKC isoforms following PMA stimulation (Fig. 3.3.1). My data show that PMA always recruits both isoforms to the plasma membrane and PKC δ also to the nuclear envelop due to its nuclear location under resting conditions. I was particularly puzzled by the plasma membrane targeting of both isoforms and asked myself how these PKC subfamilies would achieve substrate specificity if they both targeted the same membrane. I therefore tested the translocation patterns of these two isoforms following physiological stimulation with ATP.

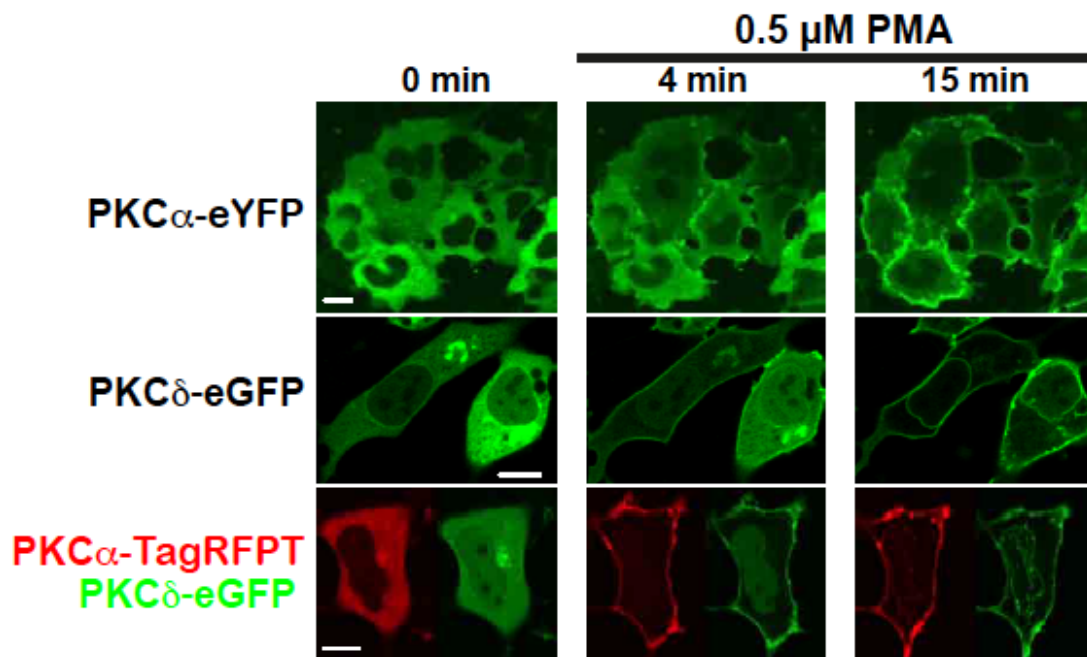


Fig. 3.3.1 PMA-induced PKC translocation. HEK293 cells expressing PKC α -eYFP (upper row), PKC δ -eGFP (middle row) alone, or co-expressing PKC α -TagRFP-T and PKC δ -eGFP (lower row) were treated with 0.5 μ M PMA (at least 22 cells from 3 experiments). Scale bars correspond to 10 μ m.

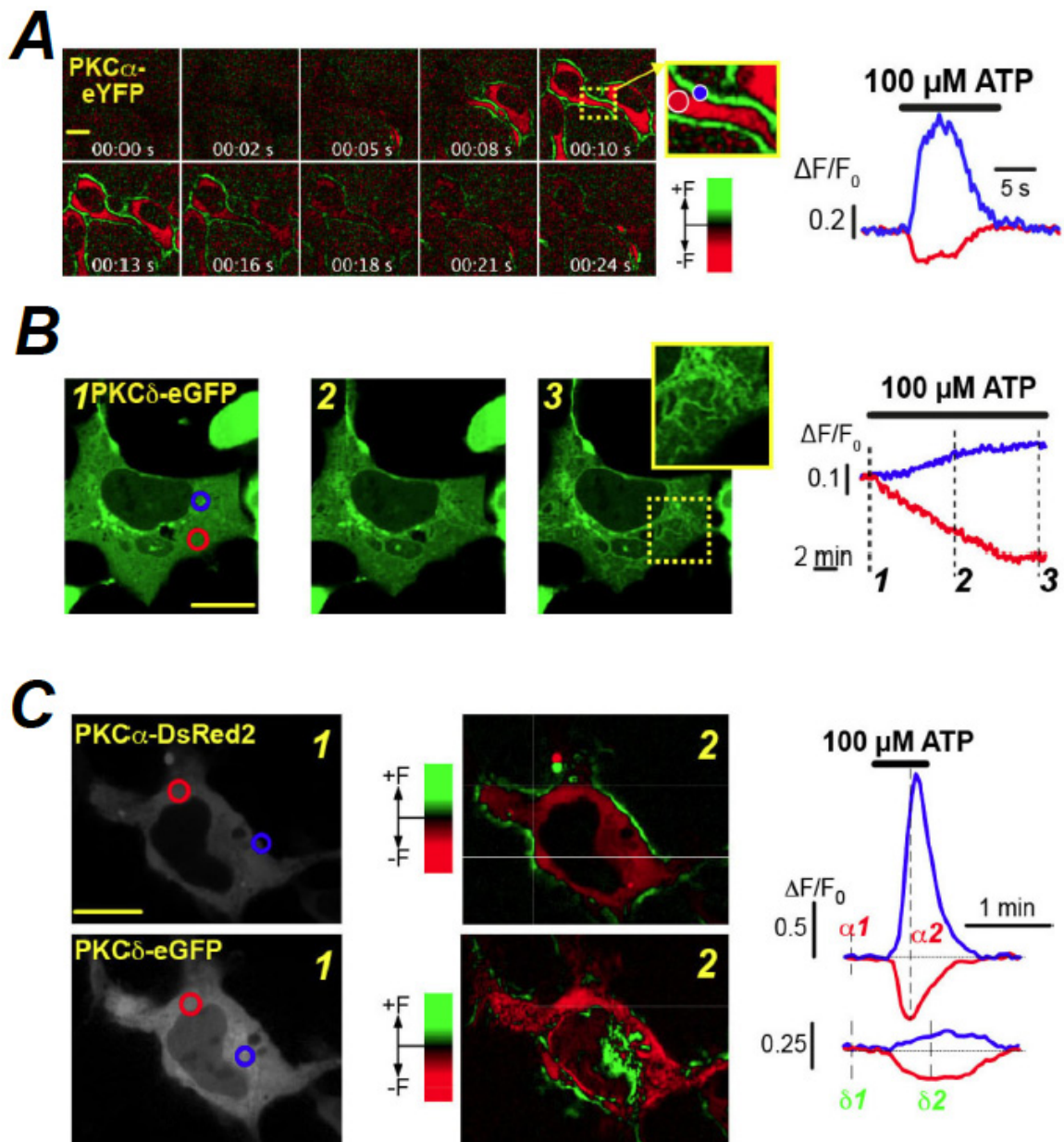


Fig. 3.3.2 PKC α and PKC δ are differentially targeted following ATP stimulation. (A) Representative images (left) and plots of the relative fluorescence over time (right). Blue denotes the plasma membrane, and red corresponds to the cytosolic fluorescence (see magnified image). (B) Representative images (left) and plots of the relative fluorescence over time (right) for two regions of interest. Blue denotes the ER membrane, and red corresponds to the cytosolic fluorescence (image 1). (C) Representative images (left) and relative plots of fluorescence over time for two regions of interests. The left column of the images displays the resting distribution of the PKC constructs while the right column illustrates the increases (green) or decreases (red) of the fluorescence relative to the resting condition. The numbers denote the two time points. For the traces, blue denotes the plasma membrane (PKC α) or ER membrane (PKC δ) and red cytosolic fluorescence (for both PKCs). Similar data were obtained in 56 cells from 18 independent experiments. Scale bars correspond to 10 μ m.

Following ATP stimulation, PKC α responded by rapidly translocating to the plasma membrane (Fig. 3.3.2 A). In contrast to that, the PKC δ -eGFP displayed a rather different behavior following ATP stimulation. With a slow time course PKC δ accumulated on intracellular membranes. To verify such differential translocation patterns, I co-transfected PKC α -DsRed2 and PKC δ -eGFP in the same HEK293 cells and investigated redistribution of these PKC isoforms following ATP stimulation (Fig. 3.3.2.C). Similar to my finding in HEK293 cells expressing either of these two isoforms, ATP stimulation of double expressing HEK293 cells also displayed a rapid plasma membrane accumulation for PKC α and a slower recruitment to intracellular membranes for PKC δ . It appears noteworthy to mention that in several hundred of HEK293 cells analyzed under such an experimental condition I never observed a single events of PKC δ translocation to plasma membrane.

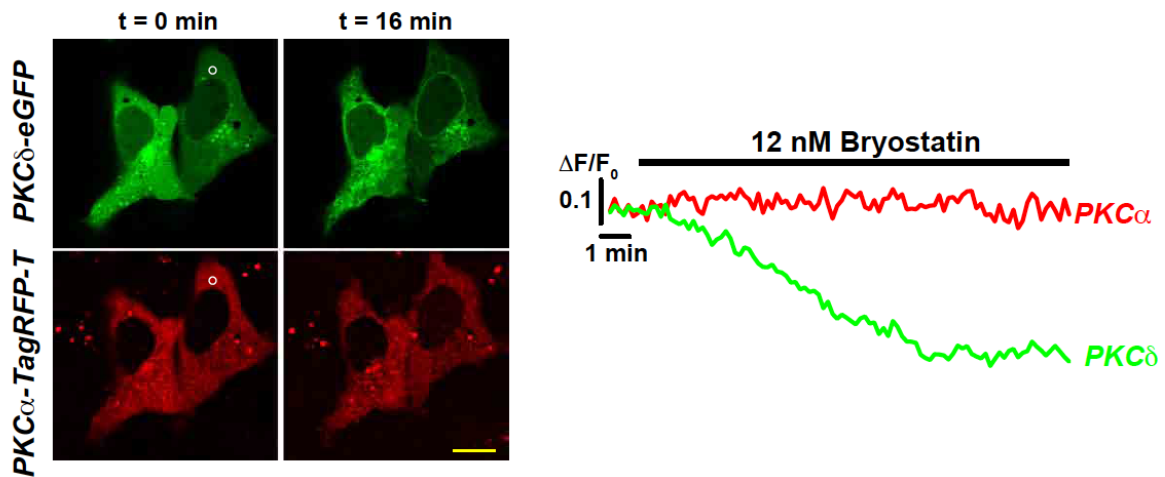


Fig. 3.3.3 Bryostatin 1 specifically recruits PKC δ to intracellular membrane. Left images denote the fluorescence distribution of PKC δ (upper row) and PKC α (lower row) at the time points given. The traces depict plots of the intracellular fluorescence over time for PKC α (red) and PKC δ (green). Regions of interests are indicated in the images and the scale bar depicts 10 μ m.

To confirm such a differential translocation of the PKC isoforms, I used an alternative compound to activate PKC, Bryostatin 1 [153, 154]. Using a concentration of 12 nM, Bryostatin 1 selectively and specifically resulted in translocation of PKC δ (green traces in Fig. 3.3.3), while in the same cell PKC α did not redistribute at all (Fig. 3.3.3 red trace). Thus Bryostatin 1 appears as an alternative and selective tool for evoking PKC δ translocation.

3.3.2 PKC δ targets the ER-membrane following ATP stimulation

To identify the subcellular target membrane of PKC δ , I co-transfected PKC δ -eGFP and specific markers of the major three intracellular membrane systems: the endoplasmic reticulum (ER, Fig. 3.3.4 A), mitochondria (Fig. 3.3.4 B), and Golgi (Fig. 3.3.4 C) respectively. The quantitative analysis of the protein distributions was supported by the generation of co-localization plots before (upper rows in Fig. 3.3.4) and following 10 min of ATP stimulation (lower rows in Fig. 3.3.4). While mitochondrial labeling did not reveal co-localization in either condition (Fig. Fig. 3.3.4 B) and Golgi-labeling only depicted a weak co-localization with very little changes after stimulation (Fig. 3.3.4 C), the co-localization plots illustrated in Fig. 3.3.4 A (right panels, yellow dash lines) strongly suggested the ER-membrane as the main target of ATP-evoked translocation of PKC δ -eGFP. It appears noteworthy to mention here, that although the fluorescence plots in Fig. 3.3.4 A, right depicted a recruitment of PKC δ -eGFP (y-axis) to the ER (increase in steepness, dashed line), the co-localization was not zero under resting conditions, *i.e.* before ATP application (yellow dash line). Such co-localization indicates that a significant portion of PKC δ could be pre-recruited to the ER membrane already under resting conditions.

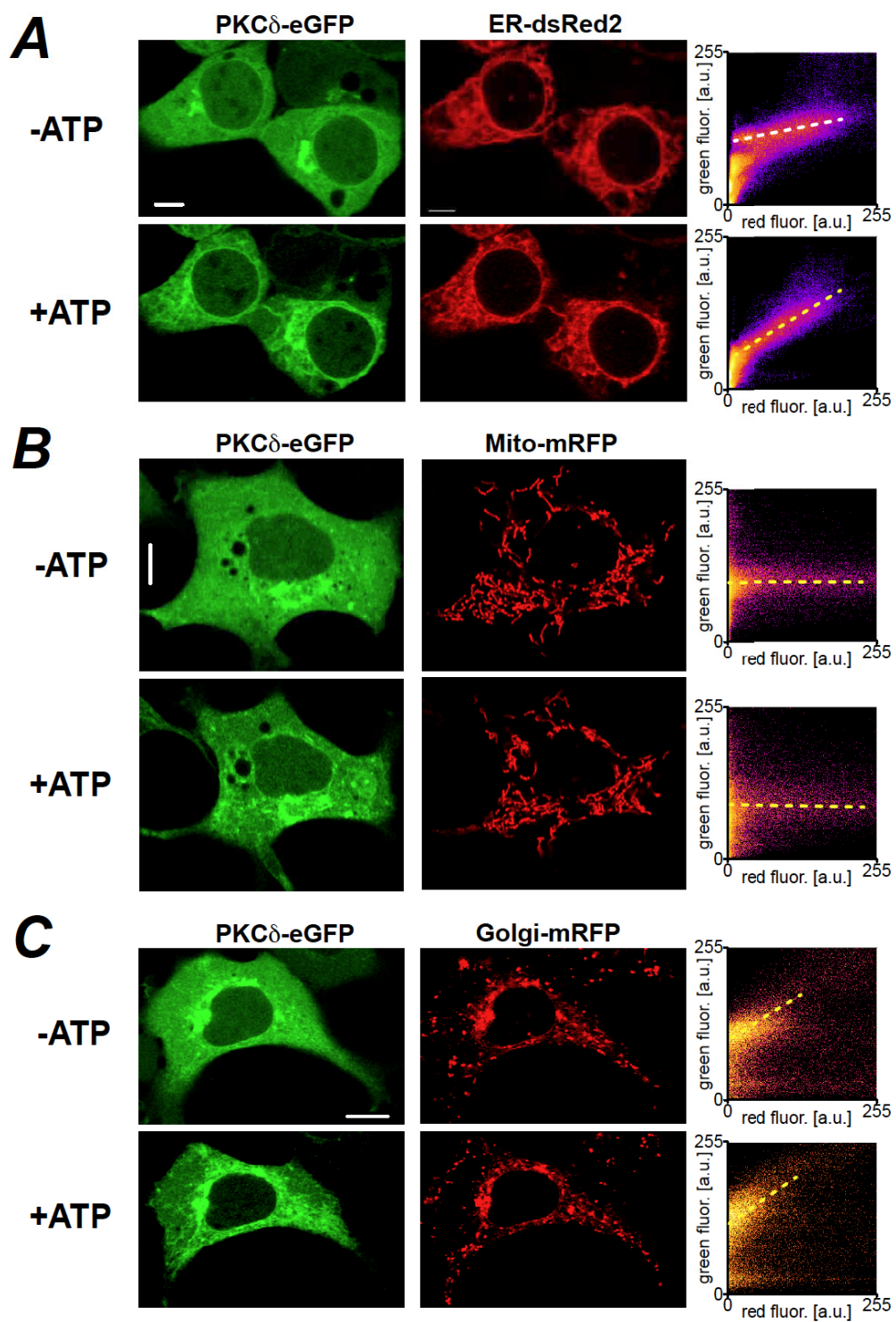


Fig. 3.3.4 PKC δ targets the ER membrane following ATP stimulation. HEK293 cells were co-transfected with PKC δ -eGFP and different organelle markers, (A) ER-DsRed2, (B) Mito-mRFP and (C) Golgi-mRFP and stimulated with 100 μ M ATP. For each condition, the left columns display PKC δ fluorescence, the middle columns correspond to organelle fluorescence, the right columns represent the co-localization analysis and the upper and lower row of images were taken before and during ATP stimulation, respectively. Typical examples for 20-30 cells from 3 different experiments. Scale bars depict 10 μ m.

3.3.3 ER recruitment of PKC δ is mediated by a cAMP-Epac-PLC ϵ signal pathway

In the following, I addressed the putative signaling pathway resulting in PKC δ recruitment to the ER. Purinergic receptors are well known to couple to G α_q proteins that stimulate the PLC β -InsP $_3$ signaling cascade resulting in plasma membrane limited DAG production. It appeared therefore rather unlikely that the G α_q -coupled cascade would be responsible for translocation of PKC δ to the ER membrane. To elucidate upstream signaling of PKC δ targeting, I initially addressed the question whether DAG production at the ER would indeed be the trigger for PKC δ redistribution. To achieve that I utilized the pan-specific PLC activator m-3M3FBS and found that general PLC activation was sufficient to cause ER-targeting of PKC δ (Fig. 3.3.5 A). In support of this, inhibiting PLCs by pre-incubation with U73122 followed by application of m-3M3FBS indeed suppressed PKC δ translocation (Fig. 3.3.5 B). These data are supportive of the notion that ER-delimited DAG production by a PLC is the underlying mechanism for PKC δ recruitment.

A key finding that fostered the compilation of the signaling cascade was the fact that following their stimulation some members of the P2Y receptors family were not only able to couple to G α_q but simultaneously also to G α_s stimulating the production of cAMP and evoking downstream events. At this time the literature did not reveal any possible link between cAMP and PKC signaling, I still pursued this route and tested whether increases of cAMP were sufficient to trigger ER-targeting of PKC δ . The Epac protein, a guanine nucleotide exchange factor (GEF), can read out cAMP signals and in addition is able to reportedly activate PLC ϵ [155, 156]. I thought of making use of specific cAMP analogues that were (i) membrane permeable and (ii) did not preferentially activate PKA in order to exclude any effects from PKA. The cAMP analogue, 8-pCPT-2'-O-Me-cAMP, known to be inefficient in PKA activation but rather potent in stimulation of Epac [157, 158] made this approach rather promising.

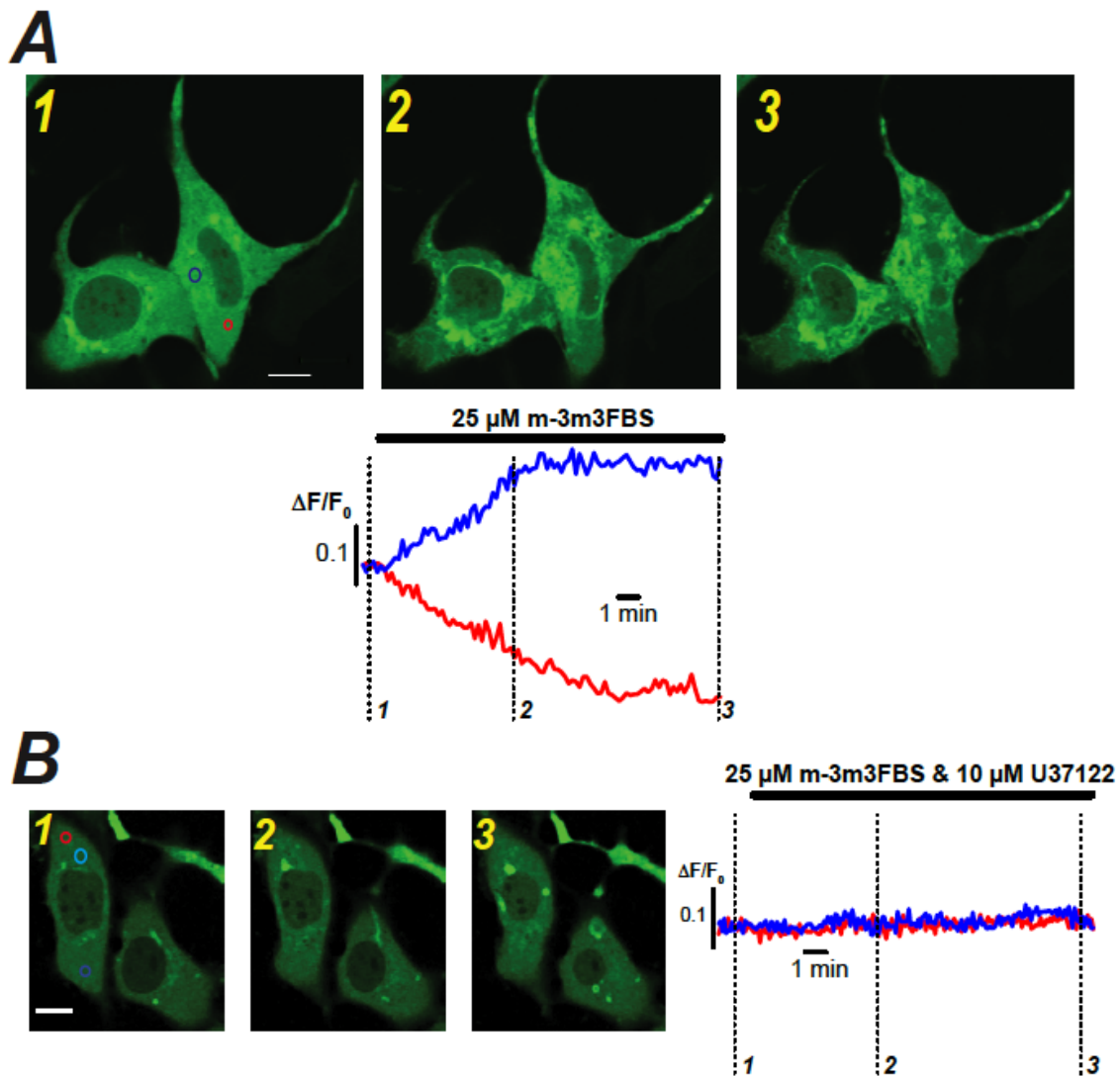


Fig. 3.3.5 PLC is engaged in the targeting of PKC δ to the ER. (A) The upper images display the distribution of PKC δ -eGFP in HEK293 cells upon m-3M3FBS at the time point denoted by the numbers. The blue traces denote the fluorescence at the ER membrane, and the red traces represent cytosolic fluorescence. (B) The left images denote the fluorescence distribution of PKC δ -eGFP in HEK293 cells upon m-3M3FBS and U37122 at the time points given. The traces depict plots of the intracellular fluorescence over time on the ER membrane (blue) and in the cytosol (red). Regions of interests are indicated in the first images and the scale bar represents 10 μ m. Similar data were obtained in 20-30 cells from 5 independent experiments.

Fig. 3.3.6 A illustrates a typical result of an experiment in which I stimulated HEK293 cells expressing PKC δ -eGFP with 8-pCPT-2'-O-Me-cAMP. From the data it becomes clear that application of the cAMP analogue causes a robust recruitment of PKC δ to the ER. To exclude possible unwanted side effects of 8-pCPT-2'-O-Me-cAMP and to confirm its specificity in activation of EPAC, I applied specific Epac-siRNA to abrogate Epac expression [159]. For this purpose I co-transfected specific anti-Epac siRNA and PKC δ -eGFP in HEK293 cells for 72 h and retested them with 100 μ M ATP.

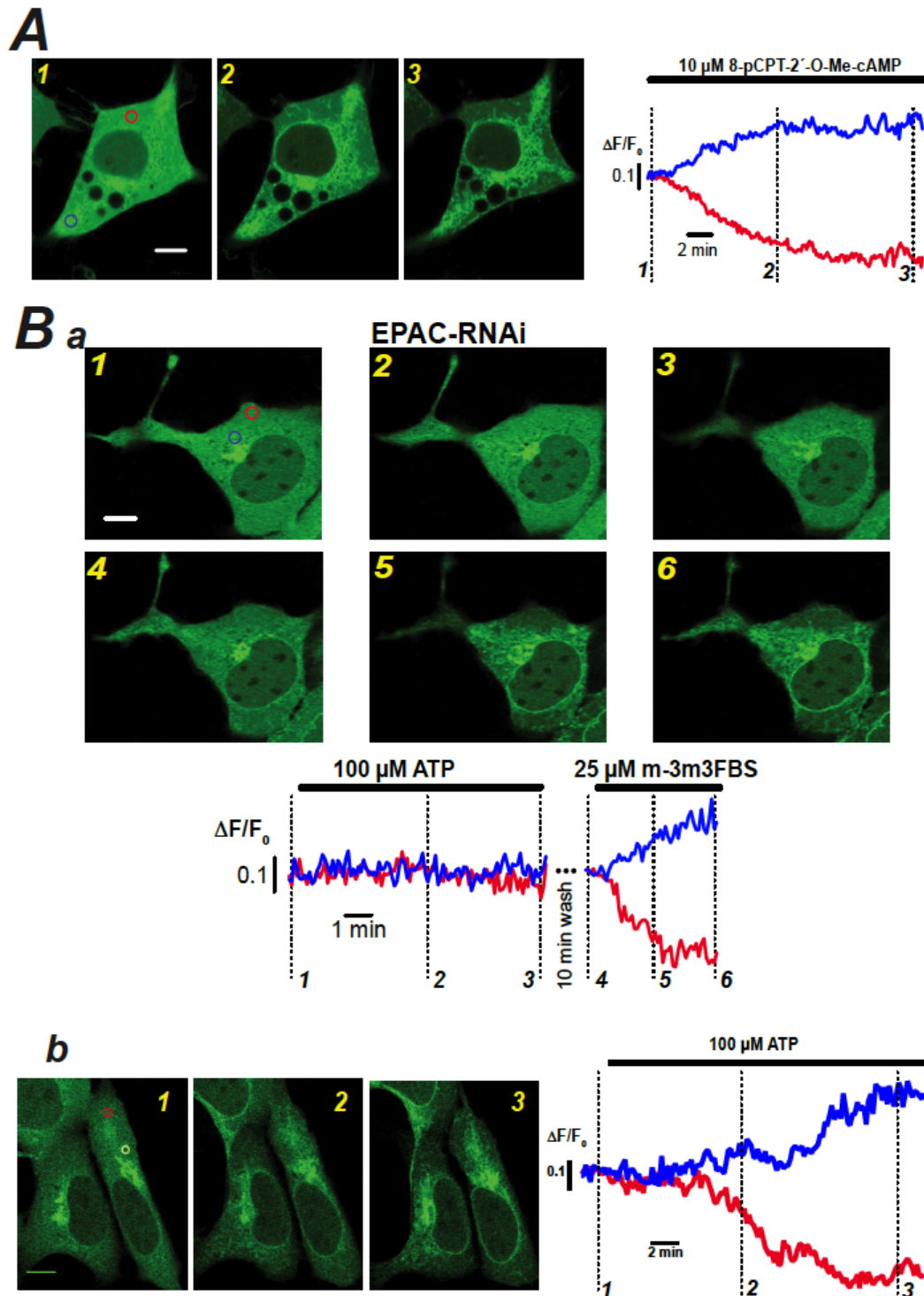


Fig. 3.3.6 The involvement of cAMP-Epac in PKC δ ER recruitment. (A) The left images display the distribution of PKC δ -eGFP in HEK293 cells upon membrane-permeable cAMP analogue at the time point denoted by the numbers. The blue traces denote the fluorescence at the ER membrane, and the red traces represent cytosolic fluorescence. (B) The images show distribution of PKC δ -eGFP in Epac1 down-regulated HEK293 cells (a) and control HEK293 cells (b) upon indicated stimuli at the time point denoted by the numbers. The traces depict plots of the corresponding intracellular fluorescence over time for the ER membrane (blue) and cytosol (red). Typical examples for 23-28 cells from 4 independent experiments. Scale bars depict 10 μ m.

Fig. 3.3.6 B depicts a typical result of such experiments. In contrast to naive cells in which ATP caused ER translocation in 100% of all cells analyzed, it failed to target PKC δ to the ER in all cells expressing PKC δ -eGFP and Epac-siRNA. Interestingly, application of m-3M3FBS to the same cell stimulated PKC δ recruitment to the ER (Fig. 3.3.6 Ba) indicating that PLC responsibility for DAG production at the ER membrane was still intact. When using scrambled control siRNA for Epac all cells expressing PKC δ -eGFP showed the translocation of PKC δ to the ER when stimulated with 100 μ M ATP. Such data supports my notion that Epac a readout protein for cAMP increases plays an essential role in the process of PKC δ ER translocation. Therefore, in the following I addressed the possible links between Epac and PLC activation at the ER membrane.

Another thorough search in the literature revealed that for other cell types, the small Ras-like GTPase, Rap protein not only can be activated by Epac [160-162], but is also able to stimulate distinct PLC isoforms, such as the ER resident PLC ϵ [155, 163, 164]. To test whether Rap protein might indeed be the missing link in my signaling pathway, I needed to figure out how to specifically activate or inactivate Rap proteins. I thought of applying the natural regulator of GTPase activity, the GTPase activating protein (GAP), RapGAP. Thus, when over-expressing RapGAP in HEK293 cells the hydrolytic activity of Rap should be substantially unregulated and should thus substantially decrease the lifetime of the GTP-bound active Rap protein. Such an augmented GTP turnover should consequently down-regulate or functionally inhibit signaling transduction through Rap [160, 165, 166]. To easily identify RapGAP expressing HEK293 cells, the mammalian bidirectional expression vector pBI-Rap1GAP-PKC δ -eGFP was applied so that all cells expressing PKC δ -eGFP (green colour) also expressed Rap1GAP. As shown in Fig. 3.3.7 A, cells co-expressing PKC δ -eGFP and RapGAP were unresponsive to ATP stimulation (Fig. 3.3.7A 1-3 and traces below), while application of m-3M3FBS was still potent to cause PKC δ redistribution (Fig. 3.3.7A 4-6 and traces below). HEK293 cells transfected with PKC δ -eGFP and the backbone plasmid for RapGAP displayed the normal sensitivity towards ATP (Fig. 3.3.7 B).

All the results presented in this chapter strongly support the existence of a cAMP-Epac-Rap-PLC ϵ signaling pathway that is responsible for ER-membrane limited DAG production and PKC δ recruitment.

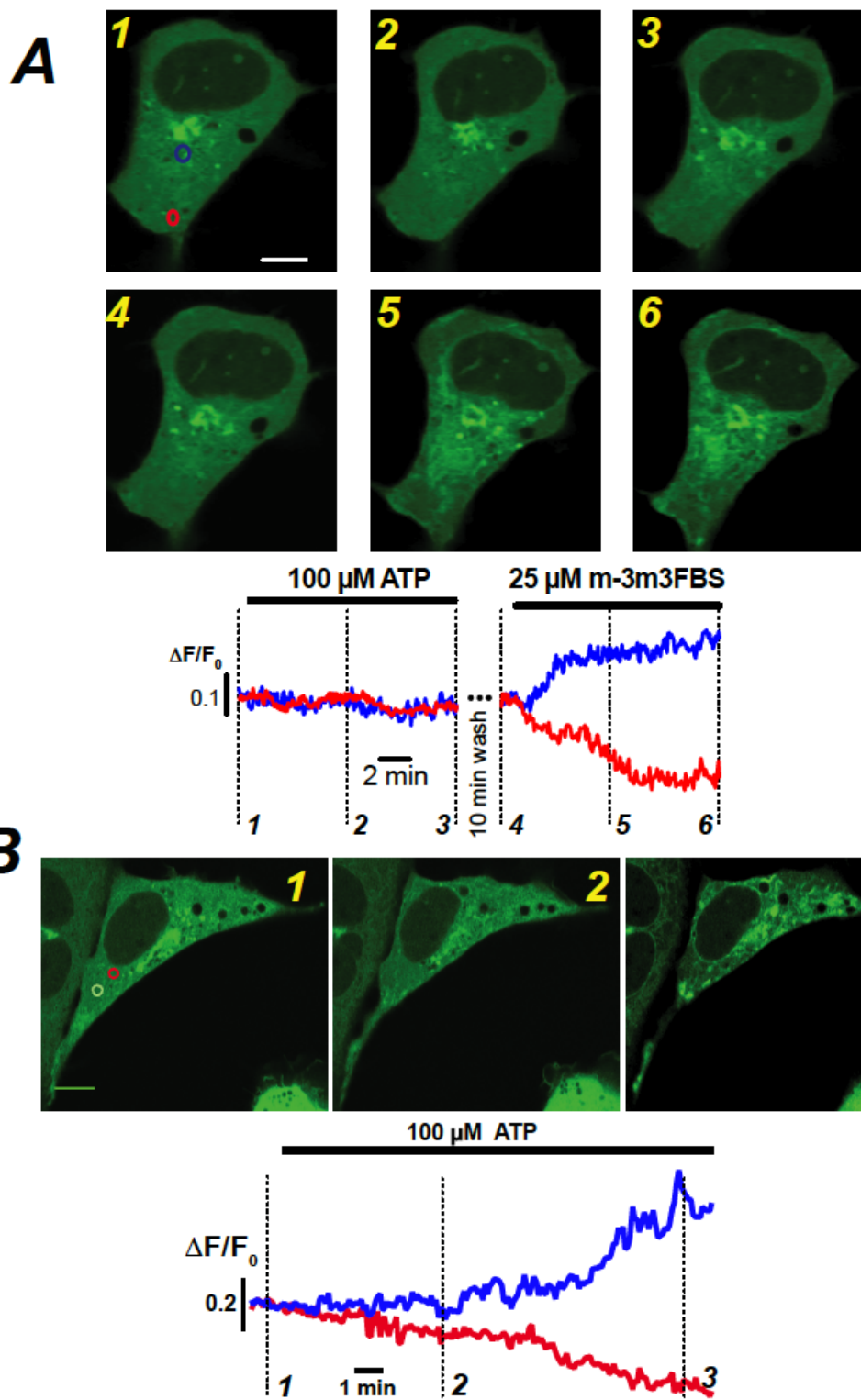


Fig. 3.3.7 Inhibitory effects of Rap1GAP protein on ATP-induced PKC δ recruitment to the ER. The images show the distribution of PKC δ -eGFP in Rap1GAP over-expressed HEK293 cells (A) and control HEK293 cells (B) upon indicated stimuli at the time point denoted by the numbers. The traces depict plots of the corresponding intracellular fluorescence over time for the ER membrane (blue) and cytosol (red). Similar data were obtained in 20 cells from 4 independent experiments. Scale bars depict 10 μ m.

3.3.4 The C1 and C2 domain of PKC α and PKC δ can signal independently of one another

Recruitment of PKC isoforms to their targets relies on their regulatory domains, protein binding domains, or their interaction with receptors of activated PKCs (RACKs). To explore the various possibilities, I envisaged a novel approach: design of artificial chimeras by swapping the C1 and C2 domains of PKC α and PKC δ . This design presumed that targeting via the C1 and C2 domains would indeed be sufficient to explain the different translocation pattern of PKC α and PKC δ based on lipid-protein interactions. To test this, I constructed and expressed 4 chimeras (Chimera I-IV) fused to eGFP. To characterize the translocation patterns of each chimera, I setup 3 different live-cell assays using (i) physiological stimulation with ATP, (ii) Ca²⁺ uncaging by photolysis, and (iii) stimulation with phorbol esters.

A very interesting set of data was acquired from Chimera III, whose structure is illustrated in Fig. 3.3.8, C1 domain of PKC δ in a PKC α backbone. Immediately following ATP administration, Chimera III rapidly translocated between the cytosol (Fig. 3.3.8 Ac red trace) and the plasma membrane (Fig. 3.3.8 Ac blue trace), reproducing the behavior expected from a Ca²⁺-sensitive PKC. After a more detailed analysis of the image series, I found that in addition to this rapid shuttling, Chimera III also displayed a slower, longer lasting accumulation at the membrane of the ER. This behavior was never seen from wt-PKC α and could thus be clearly linked to the inclusion of the PKC δ -C1 domain, because wt-PKC δ protein accumulated at the ER membrane as detailed in chapter 3.3.1. The two additional assays reported the expected behavior for a PKC α backbone with intact C2 and C1 domains. Rapid increases of intracellular Ca²⁺ by flash photolysis of caged-Ca²⁺ (Fig. 3.3.8 B) or application of PMA (Fig. 3.3.8 C) recruited the Chimera III to the plasma membrane.

A very similar behavior was observed for Chimera II, which based on a PKC δ backbone with the C2 domain of PKC α . Following ATP stimulation, Chimera II also rapidly and transiently translocated to the plasma membrane while simultaneous ER accumulation was detected (Fig. 3.3.9 A). Results from the caged-Ca²⁺ photolysis assay (Fig. 3.3.9 B) illustrated that for Chimera II sole increases of Ca²⁺ were sufficient for plasma membrane recruitment. Moreover, application of PMA resulted in a long lasting plasma membrane and nuclear envelope accumulation of Chimera II as depicted in Fig. 3.3.9 C.

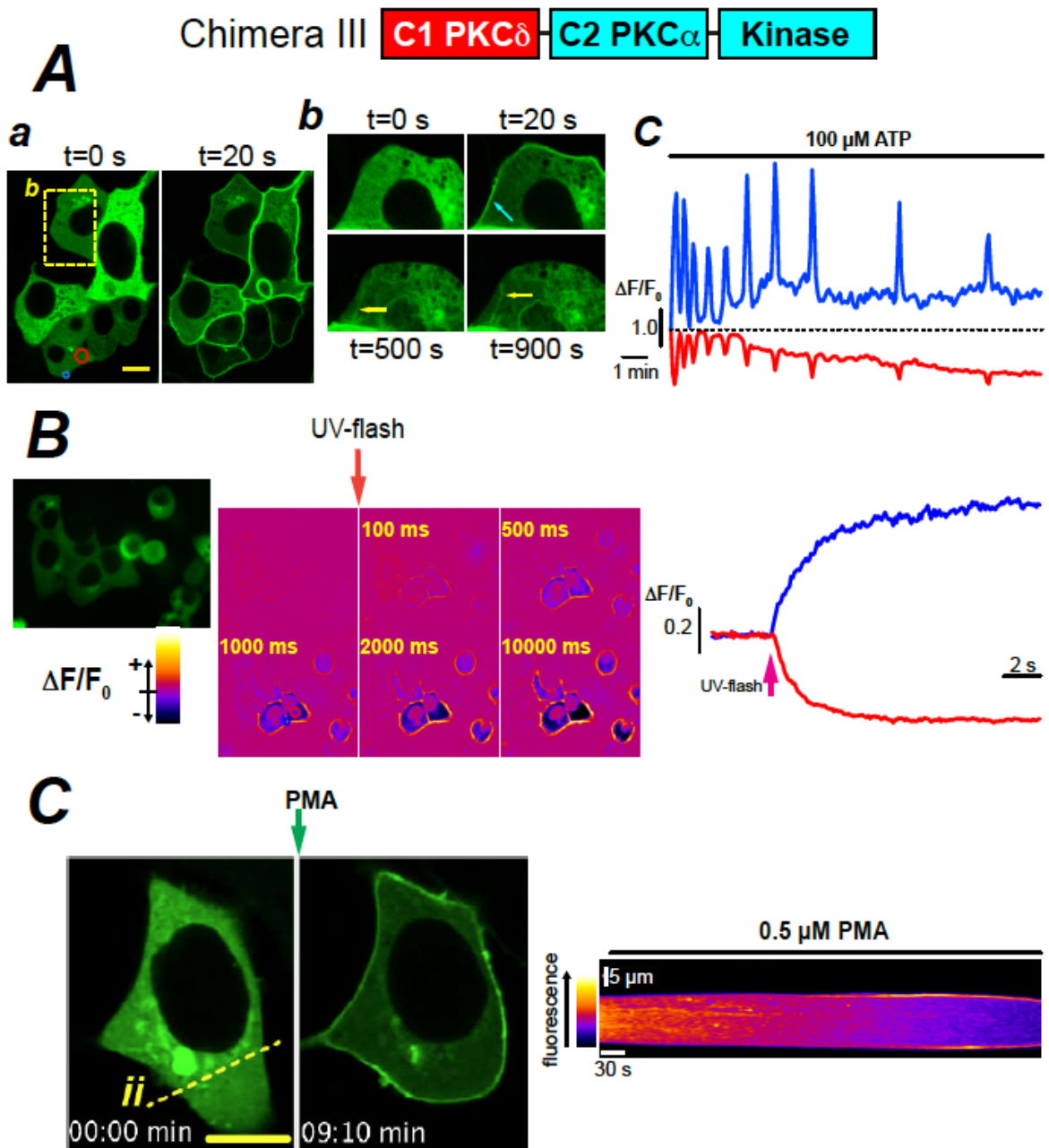


Fig. 3.3.8 Intracellular distribution of Chimera III following different stimulation regimes. The domain composition of Chimera III structure is shown on the top. (A) Translocation of Chimera III with ATP stimulation illustrated both plasma membrane (light blue arrow) and ER (yellow arrow) accumulation. (a) and (b) depict representative fluorescence distributions for the time points given. (c) Traces of the fluorescence over time for the plasma membrane (blue) and in the cytosol (red). Region of interests are denoted in (a). (B) The fluorescence distribution of Chimera III at rest is displayed on the left. The middle panel shows relative fluorescence images of the distribution of Chimera III at the time points given. The blue arrow indicates the time point of the UV flash. The right traces of the fluorescence over time are taken from regions of interest on the plasma membrane (blue) and in the cytosol (red). (C) The fluorescent distribution of the Chimera III following PMA stimulation at the time points given. A pseudo line scan was derived from the line marked by the yellow dash line. The green arrow indicates the time of PMA application. Scale bars correspond to 10 μ m.

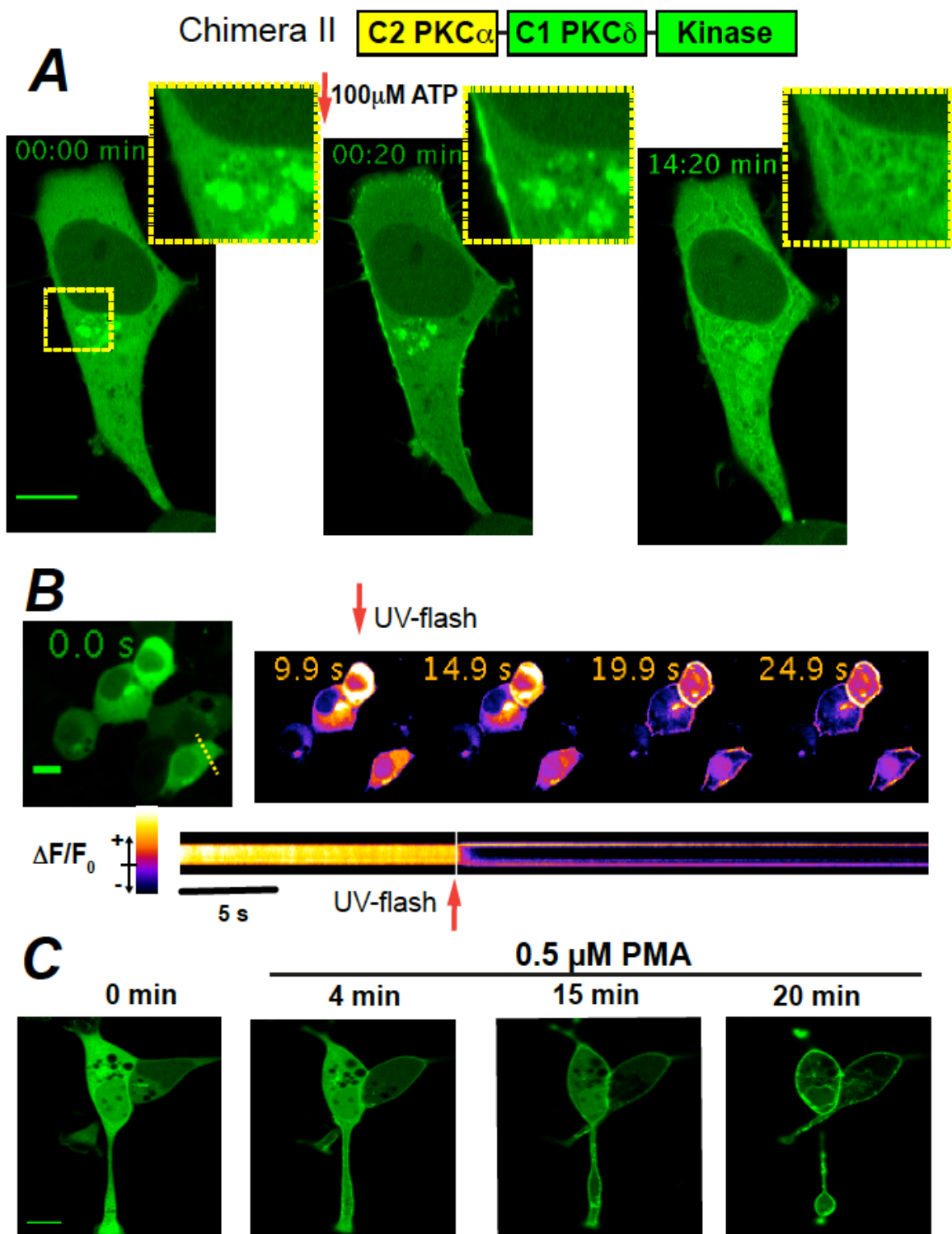


Fig. 3.3.9 Translocation of Chimera II following various stimulation regimes in HEK293 cells. The domain structure of the Chimera II is shown on the top. (A) Translocation patterns of Chimera II with ATP stimulation in HEK293 cells. The magnified images of the dashed boxes are shown on the upper row. The red arrow indicates the time point of ATP application. (B) Fluorescence distribution of Chimera II at rest is depicted in the leftmost image. The relative fluorescence images show the distribution of Chimera II at the time points given. The lower panel depicts a pseudo line-scan along the desired yellow line in the resting image. The red arrow marks the time point of the UV flash. (C) The redistribution of Chimera II following PMA application in HEK293 cells at the given time points. Scale bars depict 10 μ m.

Chimera I based on the PKC δ backbone with the C1 domain of PKC α . No translocation events was observed either after ATP stimulation or in the Ca²⁺ photolysis assay, although Chimera I still translocated onto plasma membrane and nuclear envelop during PMA treatment (Fig. 3.3.10 A). For Chimera IV, which based on the backbone of PKC α but with a C2 domain of PKC δ , a similar behavior as Chimera I was observed: a lack of response to ATP and Ca²⁺, only PMA-induced translocation to the plasma membrane could be achieved (Fig. 3.3.10 B).

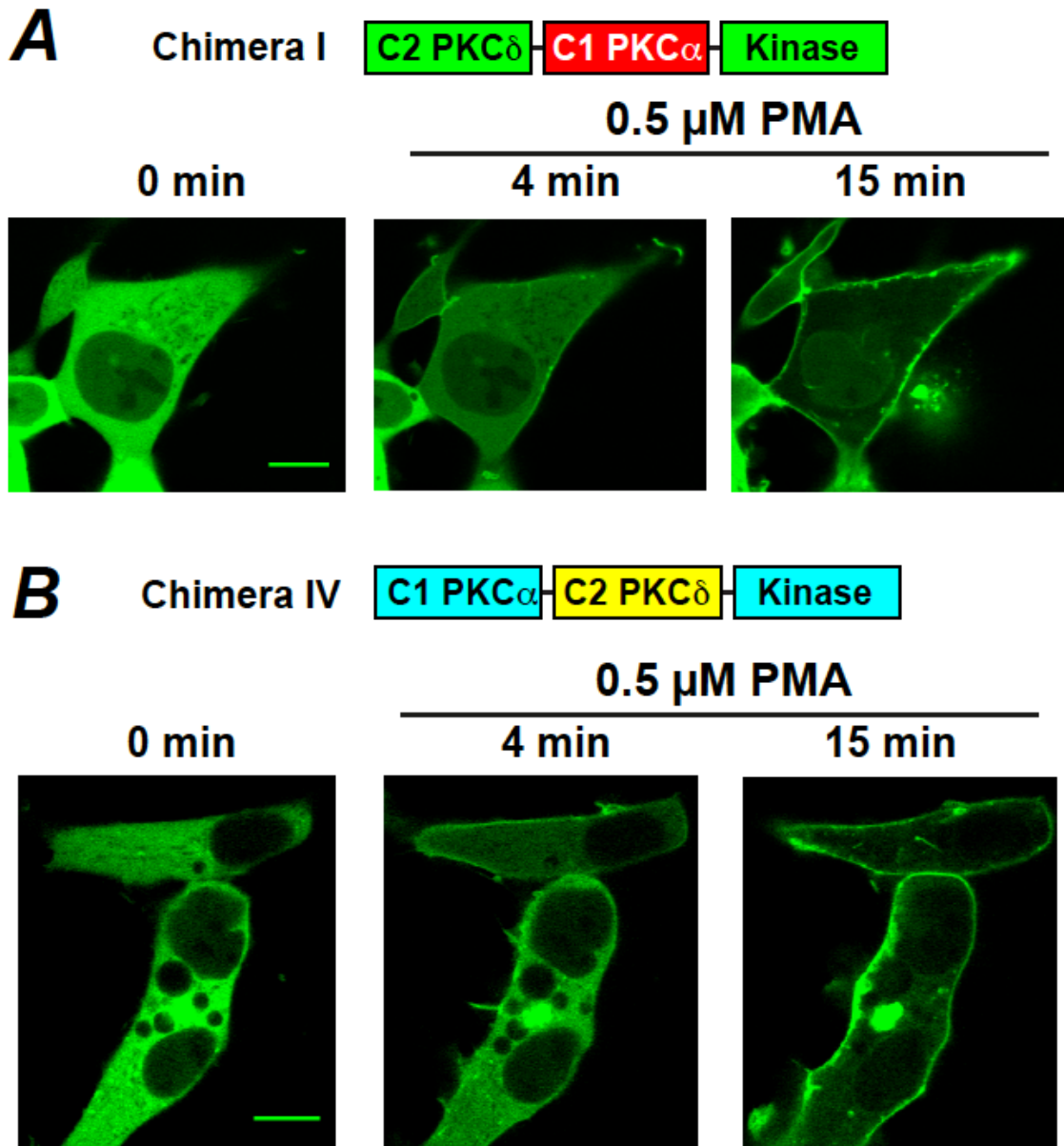


Fig. 3.3.10 Distribution of Chimeras I and IV following PMA stimulation. The images display the distribution of Chimera I (A) and Chimera IV (B) upon PMA in HEK293 cells at the pointed time. The domain structures of Chimera I and IV are depicted on the top of panels (A) and (B), respectively. Scale bars represent 10 μ m.

Table 3.3.1 Summary of the translocation pattern of Chimera I-IV

Name	Domain Structure			ATP	Ca ²⁺ photolysis	PMA
	C1	C2	Backbone			
Chimera I	α	δ	PKC δ	No response	No response	Plasma membrane & nuclear envelope
Chimera II	δ	α	PKC δ	Plasma membrane & ER	Plasma membrane	Plasma membrane & nuclear envelope
Chimera III	δ	α	PKC α	Plasma membrane & ER	Plasma membrane	Plasma membrane
Chimera IV	α	δ	PKC α	No response	No response	Plasma membrane

Table 3.3.1 summarizes the results obtained for all chimeras. PMA stimulation caused translocation of all chimeras to the plasma membrane (see also Fig. 2.3.1). Interestingly, those chimeras based on the PKC δ backbone also displays translocation to the nuclear envelope because the PKC δ backbone contains a NLS and is thus also expressed in the nucleoplasm [167]. Chimeras I and IV contain PKC δ -C2 and PKC α -C1 domains and both are incapable of translocating at all following ATP stimulation. Remarkably, ATP stimulation evokes the chimeras comprising PKC α -C2 and PKC δ -C1 domains to display translocation profiles inherited from both C-domains: a rapid and transient phase of plasma membrane binding and a slower but more persistent phase of ER accumulation (Fig. 3.3.8 A and 3.3.9 A). It appears reasonable to assume that the former behavior relies on the presence of the PKC α -C2 domain, while recruitment to the ER is a feature attributed to the PKC δ -C1 domain. From these data, I conclude that the C1 and C2 domains might behave as independent members of a signaling toolbox for designing the desired recruitment patterns of PKCs. In such a scenario, the intact Ca²⁺ binding with C2 domain of PKC α would always support Ca²⁺ sensitivity, regardless of the other molecular environment, while the contribution of the C1 domain appears to be much more complex. Despite the presence of PKC α -C1 in the Chimera I and IV, I never observed any plasma membrane recruitment, although DAG was produced at the plasma membrane following extended ATP stimulation [88]. Only when the PKC δ -C1 domain was present I observed ER-targeting (Chimera II and III).

3.3.5 The C1B domain of PKC δ is responsible for ER recognition

The molecular structure of the C1 domain of PKC α and PKC δ are complex, comprising C1A and C1B subdomains, each with its characteristic lipid binding profile. To investigate which one of these two domains is responsible for the ATP-evoked ER recruitment, I constructed four additional chimeras (Chimera A-D) in which I exchanged the C1A and C1B domains of PKC α and PKC δ between the backbones of the two isoforms (Fig. 2.3.1). After expressing these chimeras with fused fluorescent protein in HEK293 cells, I stimulated the cells with 100 μ M ATP and analyzed their translocation patterns. The exchange of the C1A domains of PKC α and PKC δ in the reciprocal backbone did not alter the behavior of the chimeras, Chimera A still translocated to the plasma membrane only and Chimera C was still recruited to the ER membrane (Fig. 3.3.11 A&C). Interestingly, the presence of the C1B domain of PKC δ in the PKC α backbone (Chimera B) resulted in a transient and rapid plasma membrane recruitment and a more persistent and slower ER translocation (Fig. 3.3.11 B), while insertion of the C1B domain from PKC α into the PKC δ backbone suppressed any translocation events under ATP stimulation. All these results are summarized in Table 3.3.2.

Table 3.3.2 Summary of translocation pattern from Chimera A-D

Name	Domain Structure			ATP
	C1A	C1B	Backbone	
Chimera A	δ	α	PKC α	Plasma membrane
Chimera B	α	δ	PKC α	Plasma membrane & ER
Chimera C	α	δ	PKC δ	ER
Chimera D	δ	α	PKC δ	No response

To further substantiate my hypothesis that the C1B domain of PKC δ determines the ER translocation, I designed a PKC δ construct with a single amino acid mutation, W252K in the C1B domain of PKC δ that reduced the binding affinity of DAG *in vitro* [40]. When the PKC δ W252K expressed in HEK293 cells, the PLC activator, m-3M3FBS, was unable to induce its ER translocation (Fig. 3.3.12 A). To confirm the functional integrity of the PKC δ C1B binding pocket, I challenged the cells with PMA and found the expected aggregation on the plasma membrane (Fig. 3.3.12 B).

Gathering all of these data, I conclude that the C1B domain of PKC δ determined its ER-targeted translocation.

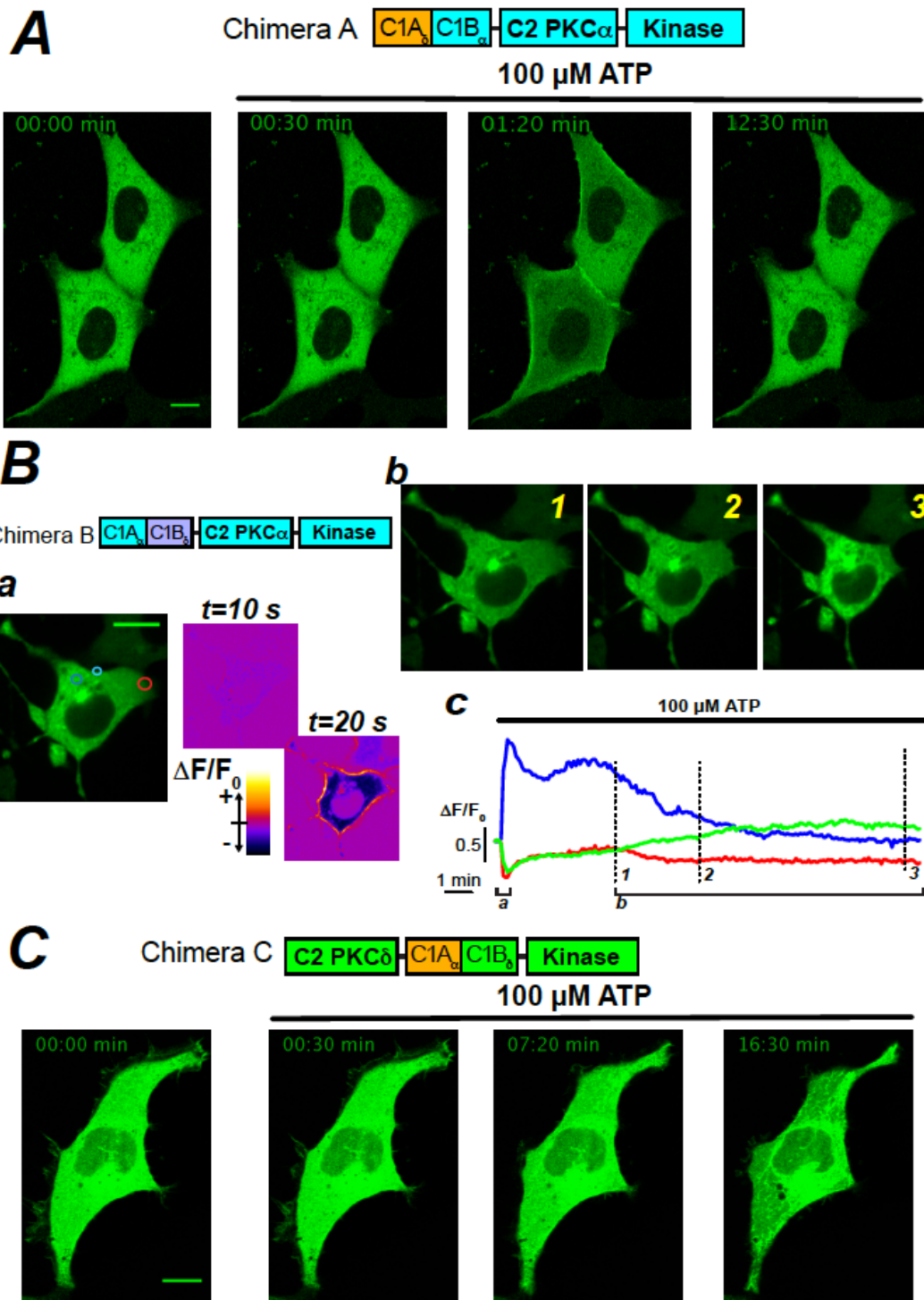


Fig. 3.3.11 The C1B domain of PKC δ is responsible for ER targeting. (A) The domain structure of Chimera A and its distribution during ATP stimuli at the time points given. (B) The domain structure of Chimera B and its distribution during ATP stimulation. (a) The left image depicts the resting distribution; the right images show the relative fluorescence changes at the time points given. (b) ER recruitment at later time points (numbers in b correspond to numbers in c). (c) Plots of the relative fluorescence over time on regions of the interest indicated in (a). Blue denotes the plasma membrane, green corresponds to the ER membrane and red represents cytosolic fluorescence. (C) The domain structure of Chimera C and its distribution upon ATP stimulation in a HEK293 cell at the time point given. Scale bars depict 10 μ m.

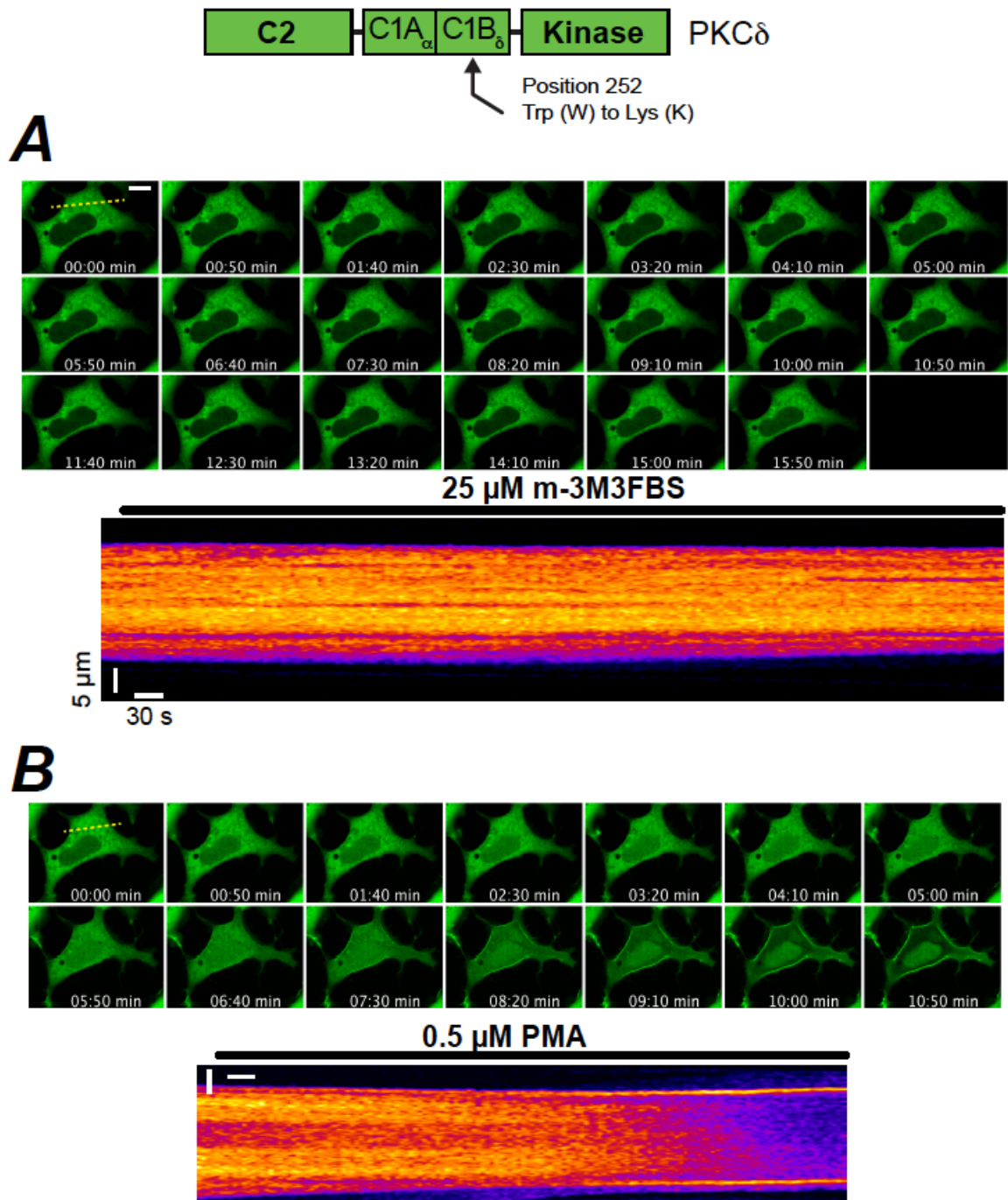


Fig. 3.3.12 Effects of mutation in PKC δ C1B domain on the ER translocation. (A) The upper rows display examples of images of the PKC δ^{W252K} distribution at the time points indicated. The lower panels depict pseudo line scans constructed from the dashed lines at t=0 min. The scale bars depict 10 μ m. (B) PMA stimulation was performed 10 min after m-3M3FBS washout in the same cell. Similar data were obtained in an additional 22 cells from 9 experiments. The scheme of the mutation position in the C1B domain of PKC δ is shown on the top of the figure.

3.3.6 PKC phosphorylation at subcellular compartments

The next step was to investigate whether translocation of the PKC isoforms indeed led to activation of the kinase activity on their respective target membranes. With respect to the spatio-temporal properties of phosphorylation by PKC, the FRET based phosphorylation sensor CKAR (C kinase activity reporter), provided a feasible method to investigate the activity of PKC in living cells [139, 168]. In order to study localized phosphorylation activity, plasma membrane targeted CKAR (pmCKAR) and ER-targeted CKAR (erCKAR) was expressed in HEK293 cells and their location was confirmed by confocal imaging (Fig. 3.3.13 A). ER targeting was achieved with the tail-anchor of cytochrome b(5), which ensured that the phosphorylation sensor was facing to the cytosol. It should be noted here that decreases of the apparent FRET efficiency indicated increases of phosphorylation in the FRET probe. In the following, I tested the kinase activity at the plasma membrane (green traces in Fig. 3.3.13 B) and ER (red traces in Fig. 3.3.13 B) respectively by two experimental regimes: PMA (Fig. 3.3.13 B, left) and Bryostatins 1 (Fig. 3.3.13 B, right panel) stimulation. Interestingly, while PMA stimulation only results in a plasma membrane delimited phosphorylation increase (left panel in Fig. 3.3.13 B), Bryostatins 1 causes phosphorylation confined to the ER (right panel in Fig. 3.3.13 B). In both cases the phosphorylation increase can be abrogated by the application of the pan specific PKC inhibitor Gö6983 [169, 170], supporting the notion that the CKAR probe preferentially detects PKC-dependent phosphorylation. These data show that the differential targeting of PKC isoforms to distinct cellular membranes also results in opening of the molecule, release of the autoinhibitory domain, and activation of the kinase domain. In chapter 3.3.1 and 3.3.3, I have described ATP-dependent ER recruitment of PKC δ and introduced the signaling mechanism leading to PKC δ recruitment. Now I wanted to test whether such regimes indeed also cause increased phosphorylation at the ER membrane, *i.e.* whether such translocations also translate into kinase activity of the PKC δ molecule. For this purpose I transfected HEK293 cells with erCKAR and stimulated them with various agonists recruiting PKC δ to the ER membrane (see Fig. 3.3.2 & 3.3.6). Interestingly, both ATP and the Epac specific cAMP analogue, 8-pCPT-2'-O-Me-cAMP caused robust increases of phosphorylation at the ER membrane as depicted in Fig. 3.3.13 C. Because there is no specific inhibitor of PKC δ , I thought of a different approach to support my notion that the stimulation regimes illustrated in Fig. 3.3.13 C indeed resulted from PKC δ

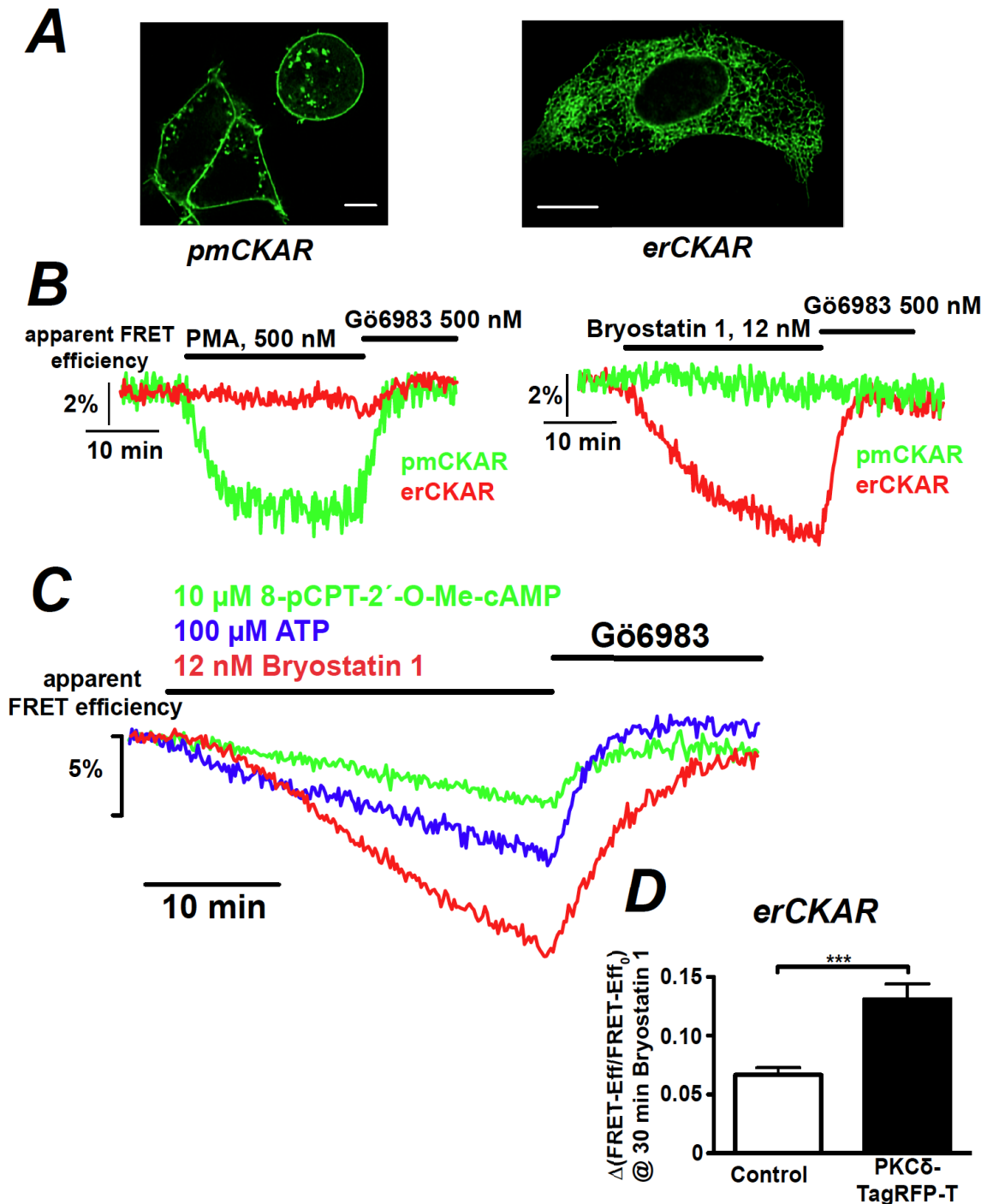


Fig. 3.3.13 Directed PKC translocation is associated with kinase activity at the target membrane. (A) Subcellular distribution of PKC phosphorylation sensors *pmCKAR* (left) and *erCKAR* (right). Scale bars depict 10 μ m. (B) *pmCKAR* and *erCKAR* were expressed in HEK293 cells and stimulated with PMA (left panel) and Bryostatin 1 (right panel). Green traces denote the apparent FRET efficiency detected by *pmCKAR* while the red one indicates signals from *erCKAR*. Note that FRET decreases indicate phosphorylation activity increases. (C) HEK293 cells expressing *erCKAR* were challenged with different agonists recruiting PKC δ to the ER membrane. (D) Over-expression of PKC δ -TagRFP-T increases Bryostatin 1-induced increases of ER phosphorylation activity. Statistical analysis shows the apparent FRET changes 30 min after the onset of the Bryostatin 1 stimulation in control (white bar) and in cells expressing the PKC δ constructs (black bar). $n=26-28$ in each group from 4 independent experiments.

recruitment to the ER membrane. In theory, other nPKCs expressed in the HEK293 cells and could also provide the necessary kinase activity. For this purpose I over-expressed fluorescent-labeled PKC δ and tested the effects of PKC δ over-expression on the ER-confined kinase activity following stimulation with Bryostatin 1 (Fig. 3.3.13 D). Interestingly, ER-limited phosphorylation was almost doubled in the PKC δ over-expressing cells strongly indicating that PKC δ 's ER accumulation indeed translates into increases of phosphorylation around the ER membrane.

3.3.7 Recruitment of PKC δ to the ER reduced InsP $_3$ -sensitivity of the InsP $_3$ R

The last series of experiments addressed the question about the possible physiological relevance of ER-targeted PKC δ recruitment and which putative phosphorylation targets might be involved. Because global Ca $^{2+}$ signals are regarded as a very sensitive and integrative function of the cell, I investigated whether PKC δ recruitment to the ER might modulate global Ca $^{2+}$ signaling in HEK293 cells and how it may happen. Stimulation of naïve HEK293 cells with 50 μ M ATP resulted in Ca $^{2+}$ oscillations (Fig. 3.3.14 A, left panel green line), while stimulation Bryostatin 1 pre-incubated HEK293 cells with ATP showed much shorter lifetime of Ca $^{2+}$ oscillations (Fig. 3.3.14 A, left panel). I quantified the lifetime of these global Ca $^{2+}$ signals by fitting the relaxation phase of the Ca $^{2+}$ transient with a mono-exponential decay function (dashed lines in Fig. 3.3.14 A, left panel). The further statistical analysis of the decay time constant of these global Ca $^{2+}$ signals show that the Bryostatin 1 treated cells generate Ca $^{2+}$ signal with a significantly faster relaxation period.

Several aspects of intracellular Ca $^{2+}$ handling might be modulated after PKC δ activation that can explain the observed changes in the Ca $^{2+}$ transients. (i) Ca $^{2+}$ -ON mechanisms, such as ER-Ca $^{2+}$ release by the InsP $_3$ R or (ii) Ca $^{2+}$ -OFF mechanisms such as intracellular Ca $^{2+}$ buffering, plasma membrane Ca $^{2+}$ efflux or SERCA-mediated ER Ca $^{2+}$ uptake. To test whether cellular Ca $^{2+}$ removal mechanisms might be altered, I set up an experiment in which I inhibited the InsP $_3$ R by higher concentrations of caffeine [171] and suppressed plasma membrane Na $^+$ /Ca $^{2+}$ exchanger activity by substituting extracellular Na $^+$ with Li $^+$ [172]. Thereafter I specifically increased intracellular Ca $^{2+}$ by UV flash photolysis of caged-Ca $^{2+}$ and analyzed the resulting Ca $^{2+}$ transient as depicted in Fig. 3.3.14 B, left panel. Before (green traces and bar) and following pre-stimulation of HEK293 cells with Bryostatin 1 (red traces in bar) the decay time constants of the mono-exponential Ca $^{2+}$ decay were indistinguishable and statistically not different. Thus I concluded that putative alterations of Ca $^{2+}$ removal processes are not affected by the pre-stimulation protocol. Thus I wondered whether ER-mediated Ca $^{2+}$ release might be dampened following Bryostatin 1

pre-incubation. To test this hypothesis, I compared naive and pre-stimulated HEK293 cells while inducing ER- Ca^{2+} release by a robust UV flash after loading the cells with a membrane permeable caged InsP_3 (Fig. 3.3.14 C). Interestingly, the peak Ca^{2+} concentrations reached during flash photolysis were the same in both populations, but when I analyzed the decay time constant of the global Ca^{2+} transient I found that after pre-stimulation of the cells with Bryostatin 1, relaxation was significantly faster. How can this be envisaged?

An earlier report described consensus sequences in the InsP_3R for putative PKC phosphorylation and the authors speculated that such phosphorylation might modulate the InsP_3R 's sensitivity towards its natural agonist InsP_3 [173, 174]. Would indeed be a decreased sensitivity sufficient to explain my results? Following UV flash photolysis of caged- InsP_3 the InsP_3 concentration most likely rapidly decreased due to the intrinsically high metabolization rate for InsP_3 . Thus the observed faster decay in InsP_3 -induced global Ca^{2+} transients could indeed be explained by a decreased sensitivity of the InsP_3R .

To test effects of PKC phosphorylation on InsP_3R in living cells, I set up a graded InsP_3 photolysis assay in living HEK293 cells with the modified Tyrode solution, which intended to avoid the interference from the $\text{Na}^+/\text{Ca}^{2+}$ exchanger in the plasma membrane. By adjusting the flash energy, I established that 1/4 of the full UV-flash energy was just above the threshold for inducing global Ca^{2+} transients while the full energy generated a super-maximal InsP_3 increase and thus inducing a robust Ca^{2+} response. While two successive flashes with 25% and 100% energy triggered two robust responses in control conditions (Fig. 3.3.15 A, green trace), pre-stimulation with Bryostatin 1 reduced the first Ca^{2+} response by more than 70% (Fig. 3.3.15 A, red trace). The reduction was reversed by simultaneous pre-incubation with Bryostatin 1 and the PKC inhibitor Gö6983 (Fig. 3.3.15 A, blue trace). The amplitude of the first peak and the ratio of two responses, which may correct for the Fluo-4 loading difference between cells, were quantitatively analyzed and the statistical results presented in Fig. 3.3.15 B. All of these data demonstrate that Bryostatin 1 dramatically affects the sensitivity of InsP_3R towards InsP_3 .

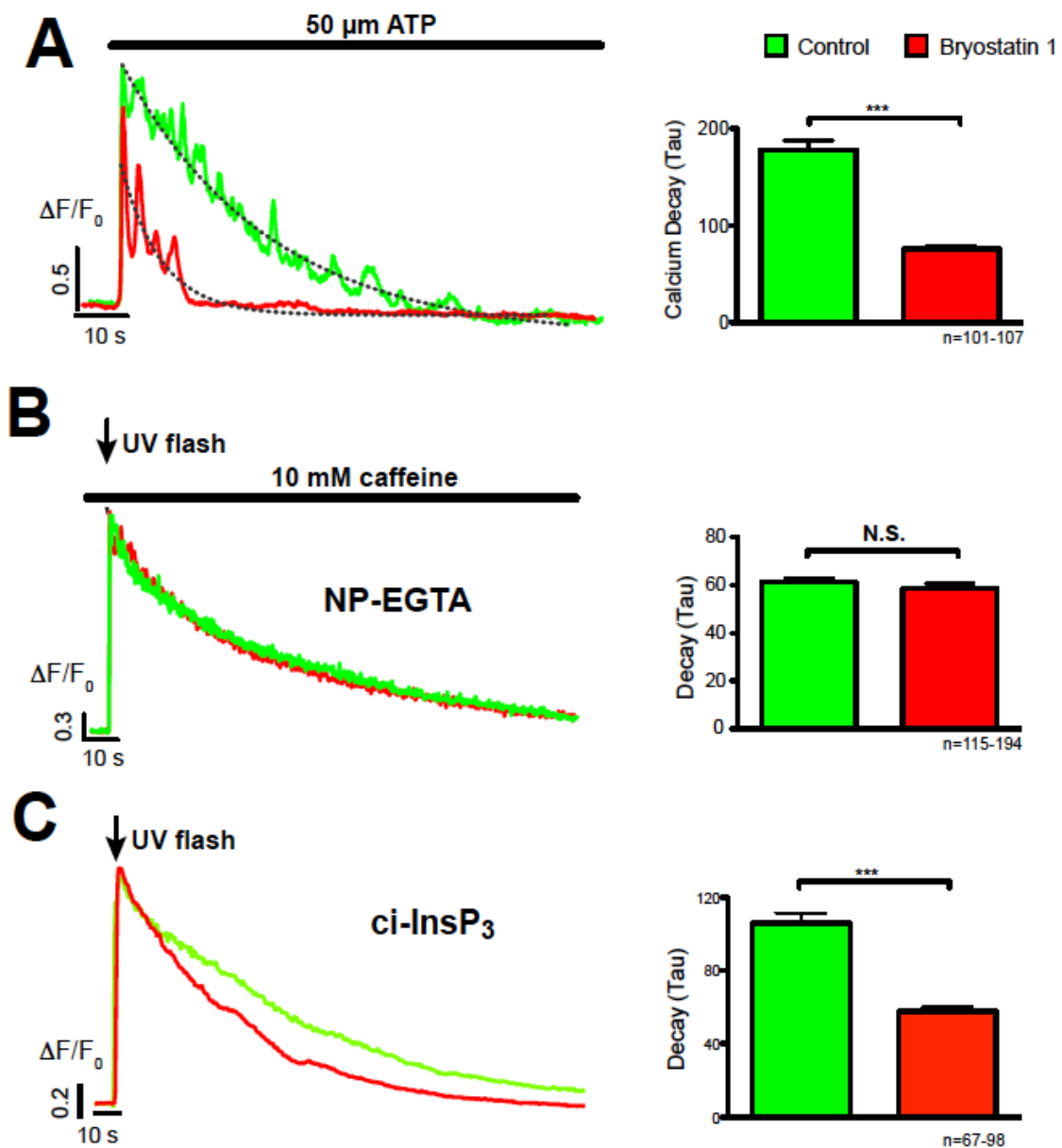


Fig. 3.3.14 Bryostatin 1 alters Ca^{2+} mobilization. (A) Fura2-loaded HEK293 cells were challenged with 50 μM ATP before and after Bryostatin 1 incubation (green and red colors, respectively). The decaying Ca^{2+} oscillations were fitted with mono-exponential equations (black dotted lines) and the obtained τ value was statistically analyzed (bar graphs). Two-tail t-test, $p < 0.001$, $n = 101-107$ in each group from 4 experiments. (B) Fluo-4 and NP-EGTA loaded HEK293 cells were pretreated with 10 mM caffeine and subjected to a UV flash to release Ca^{2+} in 0 mM Na^+ and 10 mM EGTA modified Tyrode solution. Green and red traces indicate Ca^{2+} signal in the absence of and following Bryostatin 1 incubation, respectively. The decay phase of Ca^{2+} transient was fitted with a mono exponential decay equation and the analysis of the time constant is depicted in the bar graphs. Two-tail t-test, $p > 0.05$, $n = 115-194$ in each group from 4 experiments. (C) Fluo-4 and ci-InsP₃ loaded HEK293 cells were subjected to a UV flash to release InsP₃ in 0 mM Na^+ and 10 mM EGTA modified Tyrode solution. Green and red traces indicate Ca^{2+} signal in the absence of and following Bryostatin 1 incubation, respectively. The decay phase of Ca^{2+} transient was fitted with a mono exponential decay equation and the obtained τ value was analyzed in the bar graphs. $n = 68-94$ in each group from 4 experiments.

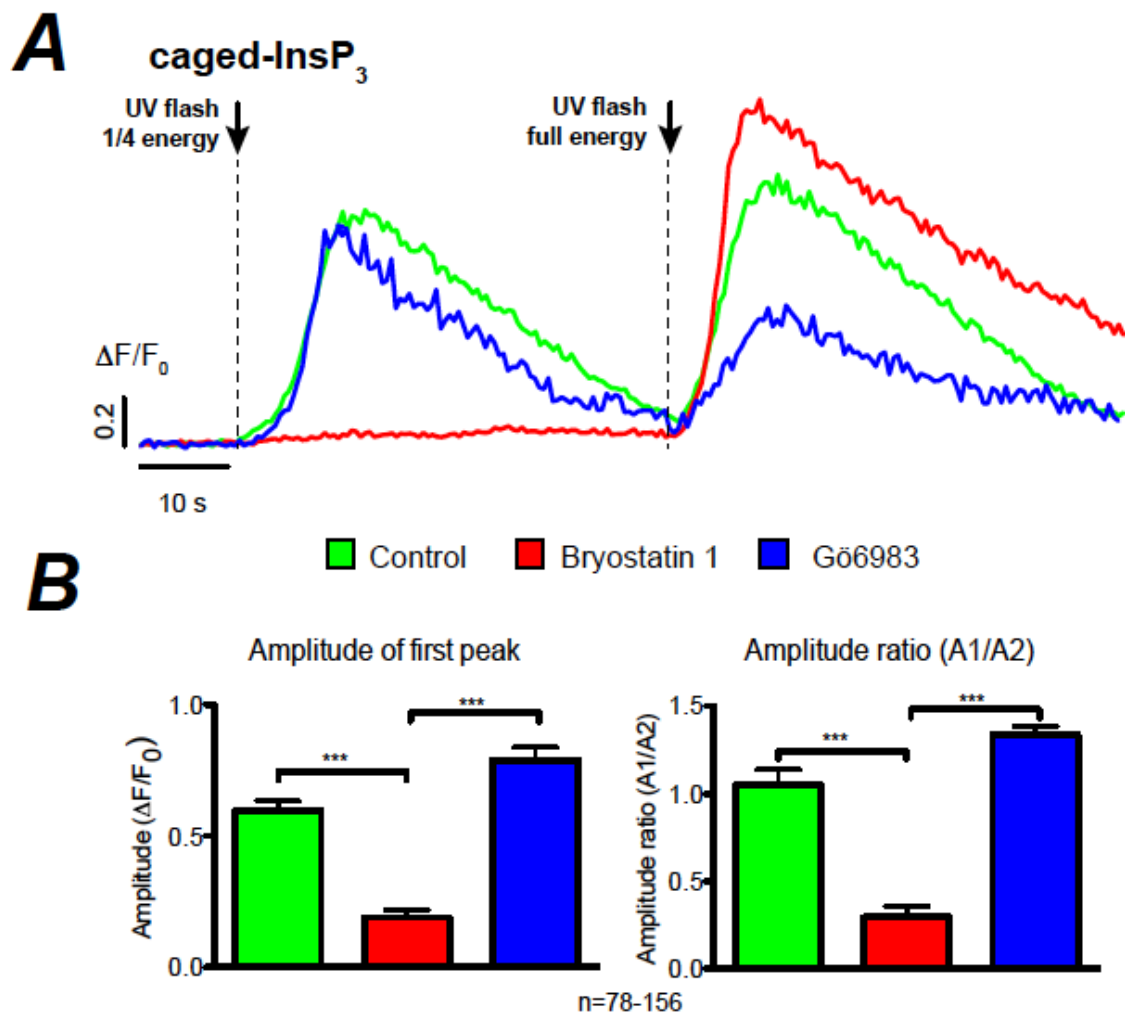


Fig. 3.3.15 Sensitivity of InsP₃R towards InsP₃ is decreased by Bryostatin 1 pre-stimulation. (A) The traces show the intracellular Ca²⁺ signal upon InsP₃ uncaging under control condition (green), with Bryostatin 1 pretreatment (red), and with Bryostatin 1 and Gö6983 treatment (blue). (B) The bar graphs show the corresponding statistical analysis of the amplitude of the 1st Ca²⁺ transient (left graph) and amplitude ratio (right graph). n=78-156 from 4 experiments.

To verify that the Bryostatin 1-induced reduction in the sensitivity of the InsP₃R towards InsP₃ was mediated by PKC δ , I thought of using PKC δ mutation with a “dead” kinase domain (PKC δ -DN) in a dominant negative approach. As reported previously [175, 176], two different mutations, PKC δ -K376R-eGFP and PKC δ -K347R_T507E-eGFP, were constructed and expressed in HEK293 cells. Both of them mutated the 347th residue from Lys to Arg at the kinase domain, but the latter also alters the 507th residue from Thr to Glu. Interestingly, PKC δ -K376R aggregated in the Golgi apparatus when expressed in HEK293 cells and the cells did not respond to Bryostatin 1 (Fig. 3.3.16. Aa), while PKC δ -K376R_T507E expressing HEK293 cells resembled the behavior of wt-PKC δ expressing cells (Fig. 3.3.16 Ab). Thus, I used PKC δ -K347R_T507E as the dominant negative mutant for further studies.

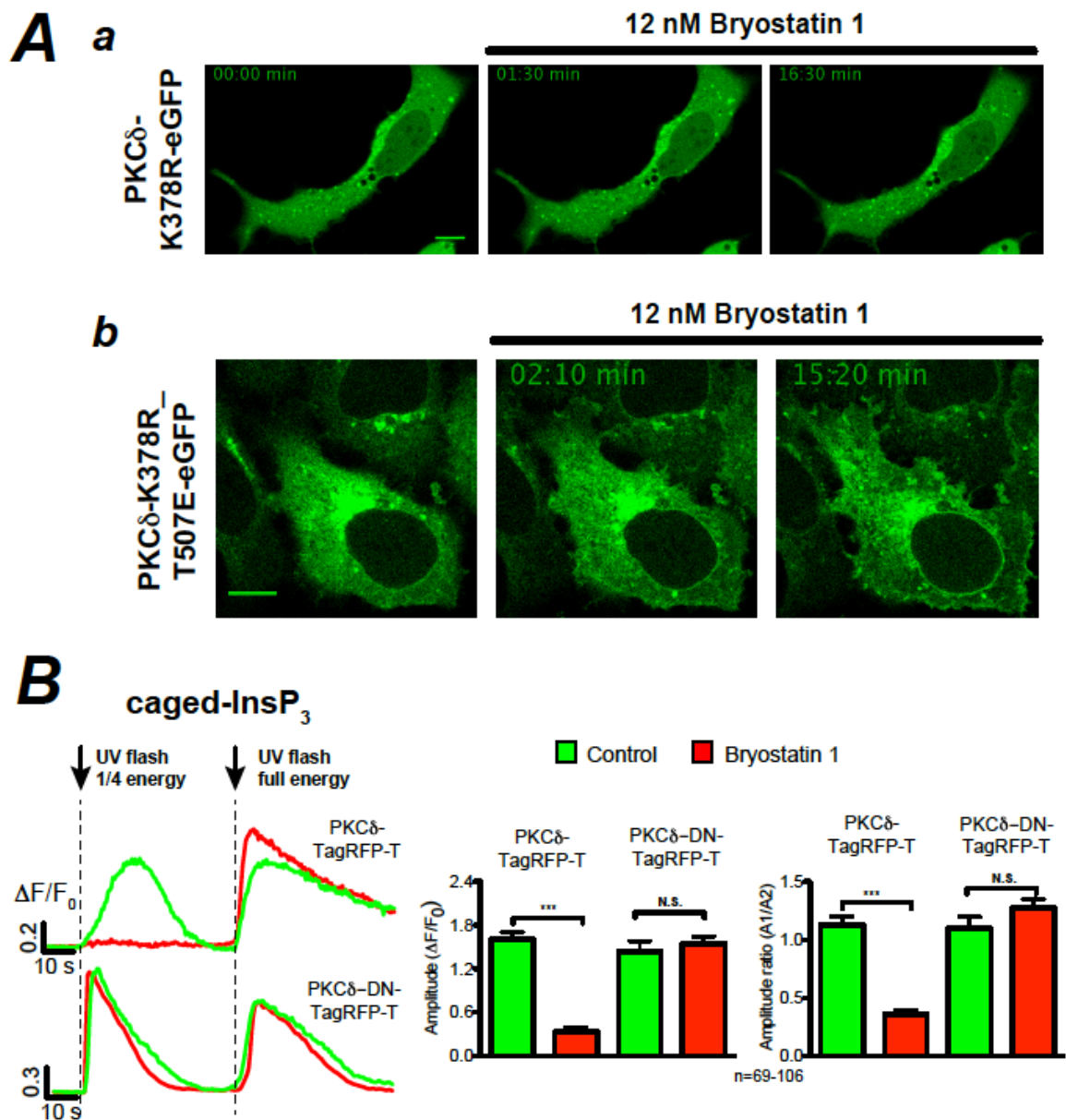


Fig. 3.3.16 PKC δ activation desensitizes the InsP₃R towards InsP₃. (A) The distribution of PKC δ -K378R and PKC δ -K378R_T507E upon Bryostatin 1 stimulation at the pointed time. The scale bars depict 10 μ m. (B) The traces shows Ca²⁺ signals obtained from wild-type (upper) and PKC δ -DN over-expressing (lower) HEK293 cells following InsP₃ uncaging with (red) or without (green) Bryostatin 1 pretreatment. The bar graphs depict the corresponding statistical analysis of the amplitude of the 1st Ca²⁺ transient (left) and 1st over 2nd ratio (right). n= 69-106 from 4 experiments.

When comparing HEK293 cells over-expressing the dominant negative mutant of PKC δ with HEK293 cells expressing the wild-type form, I found that Bryostatin 1 induced changes in global Ca²⁺ handling were abrogated (Fig. 3.3.16). While in the presence of the wild-type form, Bryostatin 1 was able to significantly reduce the amplitude of the first Ca²⁺ transient (25% UV flash energy, see Fig. 3.3.15), this effect was basically absent in cells expressing the dominant negative form of PKC δ (Fig. 3.3.16 B). This effect was also

obvious after analyzing the amplitude ratio of the first over the second Ca^{2+} transient (100% flash energy) as depicted in Fig. 3.3.16 B.

Taken together, these results strongly indicate that the ER-specific recruitment of PKC δ resulted in a reduction of the InsP $_3$ R's sensitivity towards InsP $_3$ and cause a dampening of Ca^{2+} oscillation following ATP stimulation. Thus, eventually, DAG production at the ER membrane can physiologically alter global Ca^{2+} signaling through PKC δ -mediated phosphorylation of the InsP $_3$ R. Such a modulation has the potential to physiologically or pathophysiologically alter Ca^{2+} -dependent gene expression [177, 178].

Chapter 4

DISCUSSION

4.1 PKC α translocation is diffusion-driven and independent of the cytoskeleton

4.1.1 Diffusion-driven Ca²⁺-dependent PKC α translocation

Protein kinases C are ubiquitously expressed and fulfill vital functions in almost all eukaryotic cells. Consequently, the regulation and activation mechanisms of PKC isoforms deserve detailed investigations to understand their physiological and pathophysiological functions. It is generally accepted that translocation of PKC molecules from their “resting” location to their point of activation represents an essential step in their activation mechanism. In particular for cPKCs that respond to intracellular Ca²⁺ signals [21, 87], their mobility and/or mode of translocation appears important to understand. Furthermore it was reported that the cytoskeleton plays an important role in the activation of PKC molecules [104, 122-124, 149]. Here I established a quantitative method in living cells to explore the detailed mechanisms of Ca²⁺-induced PKC α translocation to the plasma membrane and its relationship to cytoskeleton elements by means of a kilobeam laser scanning microscope, biophysical manipulation of intracellular Ca²⁺, and cell based-image analysis.

Taking advantage of the high temporal and spatial resolution offered by modern 2D confocal microscopes, I was able to observe and analyze the entire confocal cross section rather than a single line. Moreover, by using UV-flash photolysis of caged Ca²⁺ I gained independence of signaling mechanisms upstream of intracellular Ca²⁺ rises. Similarly to an earlier report [87], I was also able to identify subplasmalemmal PKC-depletion during the early stage of the translocation process (see Fig. 3.1.2), which is characteristic for a

diffusion-driven process rather than an active transport of molecules. Moreover, such an approach allowed characterization of the translocation process in a quantitative way. Detailed image analysis enabled me to delineate the accumulation of PKC α at the inner leaflet of the plasma membrane and simultaneous depletion in the neighboring cytosol. It should be noted here that the steepness of the upstroke of the membrane fluorescence can't simply be attributed to the kinetics of PKC α -membrane binding but also reflects the diffusion process of cytosolic PKC α that contributes to the accumulation. Because I was not able to distinguish these two processes, I regarded the τ value obtained from the mathematical fitting as a characteristic value to quantify the process of PKC α translocation.

4.1.2 Kinetics of oligomerized PKC α in the process of plasma membrane translocation

In eukaryotic cells, simple diffusion, facilitated diffusion, and active transport are three main mechanisms for protein transport. Simple diffusion is the result of thermal fluctuations of molecules and is often referred to as Brownian motion relying on thermodynamics of the system. Facilitated diffusion and active transport both need specific carrier proteins. Similar to simple diffusion in facilitated diffusion, molecules flow from areas of high concentration to those of lower to reach equilibrium. In active transport, molecules are transported against their concentration gradients, from areas of low concentration to those of higher concentration. Taking these considerations into account for the process of PKC α translocation, particularly from the central region of the cytosol to the subplasmalemmal cytosol, it is very important to understand the detailed diffusion mechanisms determining or contributing to this process. In the simple diffusion model and for a given concentration gradient, the rate of protein flux in living cells is mostly determined by the hydrodynamic radius of the protein, also called Stokes radius, which correlates with the molecular mass of soluble globular proteins [179]. In contrast to that, for facilitated diffusion the rate of protein movement relies on the number of carrier proteins [179].

Using two forms of oligomerized fluorescent proteins, monomer and tetramer, fused with PKC α , I analyzed the membrane accumulation by its characteristic τ value for each PKC α fusion construct. This was performed to address two questions: (i) is the photolysis assay sensitive enough to detect different diffusion rates at all and (ii) is the photolysis assay reliable enough to yield quantitative information about the translocation process. Interestingly, I obtained translocation velocity ratios for the PKC α -tetramer over the PKC α -monomer of around 4 (Fig. 3.1.5), which exactly fitted the reported ratio (3.8 ± 0.4) for the hydrodynamic radii of DsRed (tetramer) in comparison to the monomer [148].

These data not only further reassured a diffusion-driven mechanism as the main mechanism for PKC α translocation, but also strongly indicated that there is no additional carrier protein involved in this translocation process.

4.1.3 PKC α translocation is independent of an intact cytoskeleton

In simple diffusion, beside the hydrodynamic radius, the absolute temperature and the viscosity of the medium are also important determinants. In living cells at least during the course of an experiment, the temperature can be seen as constant and is therefore not relevant. In contrast, the viscosity of the medium is an important variable [179]. In my case, under resting conditions PKC α proteins reside in the cytoplasm and following Ca²⁺ increases translocate to the plasma membrane. During the course of translocation, the cytoskeleton could modulate the apparent viscosity of the cytosol, of which it constitutes a major component.

Using pharmacological approaches, I successfully depolymerized cytoskeletal components, the actin filaments and the microtubules, and analyzed possible effects such interventions might have for the relative speed of PKC α translocation. Because I did not reveal significantly different photolytic release of Ca²⁺ (Fig. 3.1.7) and no obvious morphological change of the cells (Fig. 3.1.6 and 3.1.8 A), the results from the experiments clearly indicated that neither actin filaments nor microtubules were directly responsible or involved in Ca²⁺-dependent plasma membrane translocation of PKC α .

In addition to actin filaments and microtubules, the third component of the cytoskeleton, intermediate filaments, also needs to be considered. The molecular components of intermediate filaments, however, are very variable amongst different cell types and the filaments are much more stable and durable in living cells. It still remains a challenge for those who want to manipulate them [180]. In addition, it was reported that intermediate filaments mostly participate to withstand mechanical stress rather than mediating transport [121, 181]. The putative contribution of molecular transport along intermediate filaments to PKC α translocation requires further investigations.

It's worthwhile to note here that although my results excluded the contribution of active actin filament- and microtubule-mediated PKC α transport to the translocation process and also the role passive binding might have, the possibility of interactions between PKC α and actin or tubulin can't be exclude for the resting situation, which I mentioned in the introduction section. One of the possible interpretations might be that the PKC α -Ca²⁺ binding changes the conformation of PKC α and interrupts PKC α -cytoskeleton interactions.

4.1.4 Summary and perspective

In this study, I applied PKC α -fluorescent protein fusion constructs combined with advanced optical imaging methods in living cells to demonstrate that translocation of PKC α , one member of the cPKC subfamily, appears purely diffusion-driven with no detectable contribution of filamentous transport to the membrane recruitment process, neither along the actin filaments nor along the microtubules. Since protein transport along intermediate filaments also appeared rather unlikely, PKC α recruitment to the plasma membrane can be regarded as a purely diffusion-driven process.

4.2 Self-organized clustering of membrane-bound cPKC

4.2.1 The novel theoretical model of membrane-bound cPKC

Due to the fast association and disassociation kinetics of the cPKC-plasma membrane interaction, cPKC molecules work as an ideal intracellular Ca^{2+} signal read out mechanism, which is able to respond to the large variety of cellular Ca^{2+} signals, from global Ca^{2+} waves to local Ca^{2+} events [21, 88, 89]. Furthermore, our group's previous study revealed a more complex pattern of cPKC translocation events upon threshold stimulations of cells with Ca^{2+} -mobilizing agonists. In particular, we found that a certain population of local translocation events (LTE) of PKC α that resulted from so-called Ca^{2+} puffs exceeded their lifetime by more than 5 fold [88], which can't be explained by prevalent PKC knowledge or mechanisms of biochemistry and molecular biology. Nevertheless, as of yet unknown mechanisms apparently increase PKC α 's membrane residence time, a possibly important mechanism that might foster putative PKC α -target protein interactions such as phosphorylation and thus would significantly advance signaling downstream of PKC α .

In an ongoing collaboration with the group of Prof. Karsten Kruse from the department of Theoretical Physics at the Saarland University, it was hypothesized that theoretically putative interactions between membrane-bound PKC α molecules such as they might occur in PKC α clusters could prolong membrane residence times locally and would be sufficient to explain the occurrence of long-lived LTEs.

Briefly, originating from the dynamic properties of PKC α and the biochemical principle of lipids on the plasma membrane that only the Ca^{2+} -bound PKC α is able to bind membrane but such a binding is weak if without participation of DAG, the PKC α -PKC α interaction might indeed play a critical role in prolonging PKC α 's membrane recruitment [182]. Previous reports investigating the kinetics of PKC α -PS interactions showed that the average membrane residence time of Ca^{2+} -occupied PKC α molecules is only about 50 ms [135, 183], but the phosphorylation rate of PKC α is "slow", less than 10 reactions per second [95, 125]. Thus, any mechanism that would contribute to increased membrane residence of PKC α would have the ability to foster target protein phosphorylation. In our working model, the simultaneously coupled PKC α molecules on the membrane forms clusters that extend the residence time on the inner leaflet of the plasma membrane. Furthermore we propose that PKC α at the membrane can exist in two states: 1) molecules tightly incorporated into the cluster and strongly bound to the membrane, and 2) loosely

incorporated into the cluster, weakly bound to the plasma membrane and thus presenting a “defect” in the cluster. Thus, if PKC α molecules are located at the boundary of the cluster and are in state (2) they can detach from the membrane and destabilize the cluster. If located inside the cluster, molecules in state (2) cannot detach but will increase the rate at which neighboring molecules transit into from state (1) into state (2) and thus substantially destabilize the entire cluster leading to something we refer to as avalanche-like cluster disassemble. This process is illustrated in Fig. 4.2.1. Here the mathematical modeling provides an innovative aspect for our understanding of how putative protein-protein interactions and spontaneous cluster formation increase membrane residence times and thus possibly fosters downstream signaling of PKC α .

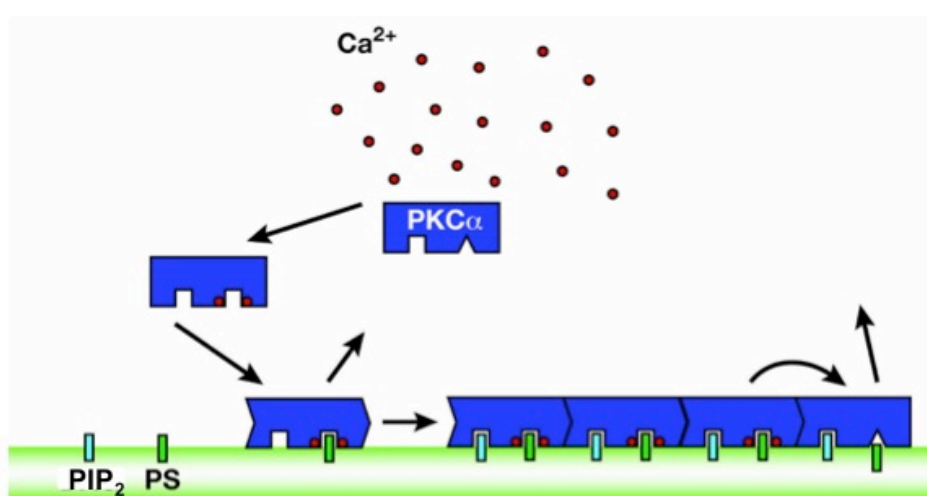


Fig. 4.2.1 Schematic representation of PKC α protein–protein interaction on the plasma membrane. The cytosolic PKC α can bind to Ca^{2+} . Ca^{2+} -PKC α can bind to PS and PIP $_2$ in the membrane and form clusters. After a Ca^{2+} decrease, Ca^{2+} can detach from strongly bound PKC α due to a conformational change of the molecule. At the boundary of the PKC α cluster, molecules not bound to Ca^{2+} can detach from the membrane. An avalanche-like dissociation would be the result.

4.2.2 Properties of PKC α -plasma membrane interactions

To support this hypothesis, the putative protein-protein interactions between membrane-bound cPKC molecules requires experimental verification. For this purpose I employed FRET measurements to quantitatively analyze putative interactions of PKC α -CFP and PKC α -eYFP on the plasma membrane of living cells.

To simultaneously monitor different cellular responses such as Ca^{2+} mobilization, protein translocation, and protein-protein interactions, I employed multiplexed spectral imaging. In addition, to more precisely quantify the energy transfer from CFP to YFP fluorescent proteins (and thus PKC α -PKC α interactions), the apparent FERT efficiency was measured and calculated, instead of simple YFP/CFP fluorescent ratios. By taking the spectral

properties of the two fluorophores and possible excitation and emission cross-talk into account, calculation of the apparent FRET efficiency help me to correct for the influence of incomplete labeling and unpaired donor and acceptor molecules [146].

My novel finding that there are transient increases in FRET between PKC α molecules following ATP stimulation of the expressing cells (Fig. 3.2.1) provided the first direct evidence that following physiological stimulation regimes intimate PKC α -PKC α interactions do indeed occur. I was even able to break down the required conditions under which this interaction occurs. In experiments using permeabilized HEK293 cells I was able to demonstrate that changes in the Ca²⁺ concentration were sufficient for PKC α -PKC α interactions to occur at the plasma membrane (Fig. 3.2.2). The fact that Ca²⁺ increases were sufficient also excluded a significant contribution of DAG to this process.

According to the principle of FRET, however, fluorescent energy transfer between two fluorophores depends on the distance of donor and acceptor and consequently FRET could come around by molecular crowding instead of specific molecular interactions [151, 152]. During the translocation process, when the cytosolic PKC α proteins are recruited from their three dimensional movement in the cytosol into the two dimensional space of the plasma membrane, the packing density of PKC α molecules substantially increases resulting in a robust drop of the distance between PKC α molecules. Therefore one has to seriously consider whether such unspecific processes between molecules undercut the distance below which FRET can occur in the absence of specific intermolecular interactions.

4.2.3 Self-organized clustering of membrane-bound PKC α

Another major finding of this series of experiments was that in the continuous presence of high Ca²⁺ concentrations “spontaneous” FRET decay occurred (Fig. 3.2.3). In addition I could demonstrate that this appeared despite a continuous strong membrane recruitment of PKC α and in a Ca²⁺-dependent manner (Fig. 3.2.3 D). My interpretation of these very important findings was that once PKC α molecules have been recruited to the plasma membrane they closely interact forming very stable clusters of PKC α . This process underlies the strong increase in apparent FRET efficiency. But how can we reconcile this notion with the spontaneous FRET decay occurring during later periods?

There are indeed a couple of possible explanations for this phenomenon. The two most prominent ones are: (i) The Ca²⁺ ionophore used (ionomycin) is exchanging Ca²⁺ ions for protons and thus especially high Ca²⁺ fluxes might be associated with decreases in the pH_i. It is well known that the spectral properties of GFP variants are pH dependent to a varying degree [184]. (ii) The decreasing FRET signal might represent changes in the way PKC α

molecules interact and is indeed the molecular correlate of the conformational switch proposed in the mathematical model for LTEs discussed above and depicted in Figure 4.2.2.

Interestingly, the original data from the simultaneous measurements of FRET and intracellular Ca^{2+} (Fig. 3.2.3 B) addressed the first concern, changes of pH_i . Here, the time course of the intracellular Ca^{2+} concentration and the apparent FRET signal displayed a prominent deviation. Despite a constant increase of Ca^{2+}_i following introduction of the high Ca^{2+}_o treatment, the FRET signal showed a complex time course, a strong upstroke in the early phase and a spontaneous decay at later time points. These data suggested an independency of the FRET decay from pH_i changes.

The other idea would indeed support the mathematical modeling suggested above in collaboration with the group of Prof. K. Kruse, namely cluster formation at the plasma membrane with strong intermolecular and plasma membrane interactions, possible switch of the molecule's state into a weakly bound mode that destabilizes the cluster and decay of the cluster size. After increasing the Ca^{2+} concentration, the PKC α concentration at the inner leaflet of the plasma membrane increases and cluster formation between large numbers of PKC α molecules takes place (strong FRET increase). The spontaneous FRET decay that I found never resulted in a total loss of FRET (*i.e.* FRET returning to pre-stimulation levels) instead it always plateaued at a higher level, suggesting that instead of detachment of the PKC α molecules the intermolecular interaction might get weaker, probably as a result of a steric switch in the PKC α molecule as incorporated in the mathematical model. Indeed, several reports seem to suggest the possibility of a different mode of plasma membrane-C2 domain interaction. In addition to the well known Ca^{2+} -C2 domain-PS interaction, these reports brought forward the additional notion of C2-PIP₂ interactions [53, 185]. Moreover, this interaction also results in a substantially altered interaction angle between the C2-domain and the leaflet of the membrane [53, 186, 187] that could give rise to the steric changes in the entire PKC α molecule and might thus be responsible for the weaker PKC α -PKC α interactions and the lower FRET levels. However, this possibility would need additional experimental attention in the future.

4.2.4 Summary and perspective

By means of multi channel fluorescent recordings and parallel measurements of FRET efficiency in living cells, I revealed a novel Ca^{2+} -dependent PKC α -PKC α interaction at the inner leaflet of the plasma membrane that also occurred transiently during physiological cell stimulations. In a mathematical model in collaboration with the group of Prof. K. Kruse, self-organization of PKC α molecules on the plasma membrane into clusters would

be a sufficient explanation for such intimate intermolecular interactions. Such processes result in an increased lifetime of the PKC α plasma membrane interaction and extended membrane residence times that would give rise to an increased chance for target protein phosphorylation by the kinase domain. Because the phosphorylation turn over of PKCs is reportedly rather low (k_{cat}/K_m $50 \text{ s}^{-1} \mu\text{M}^{-1}$) [95, 188], such a mechanism would substantially support phosphorylation and increase downstream signaling from PKC α activation.

In a more speculative way, such self-organized cluster formation might also occur in many other protein that contain C2 domains such as cPLA [189], Nedd4 [190], CAPRI [130], synaptotagmin isoforms [191-193], and more [194]. They all display Ca²⁺-dependent translocation behavior and one might thus speculate that cluster formation would result in fostered plasma membrane residence times and fostered downstream signaling in all cases.

4.3 C-domain toolkit of PKC decoding spatiotemporal signal

4.3.1 PKC α and PKC δ target distinctive compartments of the cell

Compared to the well-studied subfamily of cPKCs, detailed mechanisms of nPKC activation are still not quite clear. This is particularly true for physiological stimulation regimes [195-197]. Using live cells confocal imaging, I revealed a novel translocation pattern of PKC δ from the cytosol to intracellular membranes (Fig. 3.3.2), which I identified as the ER membrane system (Fig. 3.3.4). Such translocation was observed following physiological stimulation (ATP) but also after application of the nPKC specific activator Bryostatin 1 (Fig. 3.3.3).

The observed ER membrane recruitment of PKC δ challenges the popular translocation

regimes assumed for cPKCs and nPKCs. For both subfamilies the plasma membrane was the reported prime target [43, 49, 108, 133]. Furthermore, due to the high binding affinity of PMA to the C1 domain of cPKC and nPKC isoforms (more than 1000 fold higher than or DAG, the natural “agonist”) [86, 96, 136], PMA, the widely used PKC activator recruited all members of the cPKC and nPKC subfamilies to the plasma membrane where PMA enriches first (Fig. 3.3.1). Such an isoform equalization would deprive PKC α and PKC δ from their physiological discrimination of intracellular target membranes and target proteins. Moreover, taking into account that the PKC’s kinase domain is reportedly target unspecific [16, 22, 24], the use of phorbol esters not only results in a mis-location of PKC isoforms, but also induces mis-transduction of signal cascades by unspecific phosphorylation through various PKC isoforms [198-204]. Such mis-conduction of downstream signaling may eventually even result in mis-interpretation of experimental data. In addition, compared to the rapid dynamics of PKC α translocation induced by Ca²⁺, the intracellular membrane targeting of PKC δ showed a slow and prolonged behavior, which indicated substantially different mechanism behind, while translocation with PMA evoked recruitment were characterized by kinetics with very similar properties.

4.3.2 Following ATP stimulation PKC δ targets the ER-membrane

Employing co-expression of targeted fluorescent proteins, I was able to precisely analyze the process of PKC δ translocation in living cells. Quantitative co-localization analysis of this subcellular targeting revealed that the ER membrane was the main target for PKC δ recruitment (Fig. 3.3.4). During the analysis, I also obtained positive signals from the

Golgi, which can be explained as follows; (i) spatially: parts of the Golgi and the ER share similar locations in HEK293 cells, especially in the perinuclear region. Sometimes they are arranged in such a close proximity that optical distinction between these two organelles becomes difficult when using light microscopy; (ii) functionally: Golgi and ER are known to exchange membranes frequently through vesicular mechanisms, thus signaling that converts onto the ER membrane might also, at least to some degree, convert to the Golgi membranes. Nevertheless, despite some positive co-localization signals the relationship between PKC δ distribution and Golgi localization did not change dynamically suggesting that whatever signaling process causes ER-membrane recruitment of PKC δ was not present on the Golgi membrane. These data indicated that the Golgi membranes were at least not dynamically involved in the PKC δ recruitment.

4.3.3 ER-specific DAG production recruits PKC δ

Because DAG is the main physiological activator for nPKCs [20, 41, 43] and the existence of DAG at intracellular membranes was demonstrated directly [205, 206], I investigated the relationship between ER-specific production of DAG and PKC δ translocation. Using a combination of pharmacological and molecular biological tools, I was able to identify a novel signal cascade that was responsible for ATP-induced ER targeting (Fig. 4.3.1).

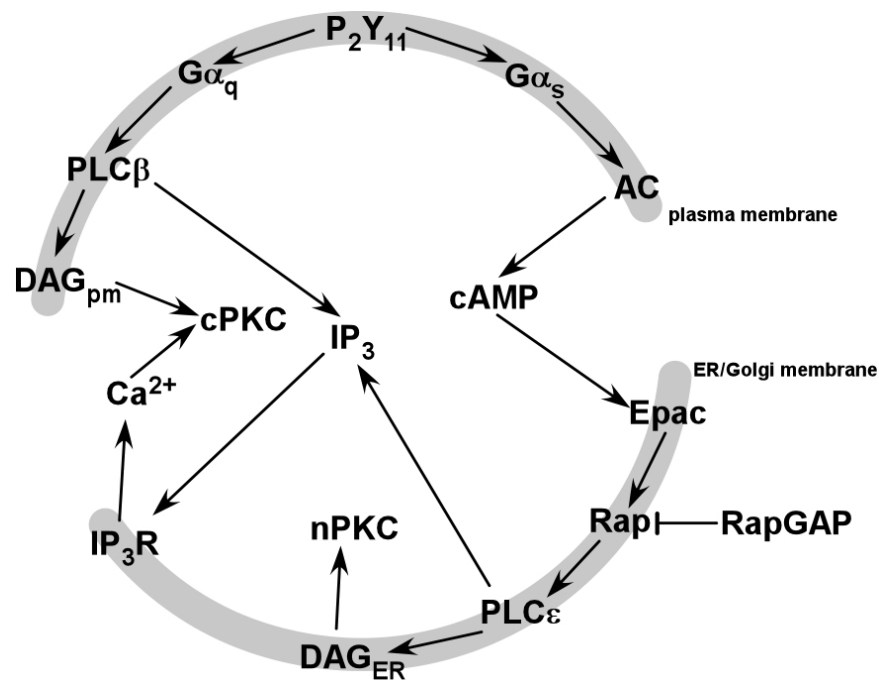


Fig. 4.3.1 Proposed scheme of signaling cascades for cPKC and nPKC activation in HEK293 cells. The upper grey region summarizes the processes on the plasma membrane, and the lower region represents those on the ER membrane.

One member of purinergic G protein-coupled receptors, the P₂Y₁₁ receptor can activate G α_s and G α_q subunits simultaneously [207] and thereby offers two possible routes for DAG production. The well-known G α_q signaling cascade originates from ligand binding over G α_q activation to lipid hydrolysis by PLC β in the plasma membrane. The activated PLC β hydrolyzes PIP₂ into DAG and InsP₃. The latter one stimulates the InsP₃R in the ER membrane and releases Ca²⁺ stored in the ER, which consequently causes cPKCs to translocate to the plasma membrane via Ca²⁺-C2 domain-plasma membrane binding. While Ca²⁺ is primarily responsible for translocation, DAG available at the plasma membrane causes cPKCs to achieve the competent activity following C1-DAG binding [15, 20, 33]. Furthermore, P₂Y₁₁ receptors can also activate G α_s subunits leading to the production of cAMP by stimulation of the adenylate cyclase (AC). After binding to cAMP, Epac subsequently activates Rap proteins by exchanging Rap-bound GDP for GTP. Interestingly, RapGAP suppresses the activated Rap proteins by exchanging GTP to GDP. Thus, the activity of Rap proteins is controlled by the balance between Epac and RapGAP proteins [155, 164]. Activated Rap proteins in turn accelerate the production of DAG in the ER membrane by stimulating PLC ϵ [208, 209]. In the end it is DAG that recruits PKC δ to the ER membrane.

Such a signaling pathway would significantly increase the versatility of cAMP signaling by extending the downstream events from cAMP-dependent activation of protein kinase A (PKA) also to the activation of nPKCs and therefore highlight the possibility of a tight regulatory interconnection of these two AGC protein kinase families.

In addition, the existing basal levels of cAMP in the cytosol might lead to a constitutive activation of the aforementioned signaling cascade resulting in a tonic, background production of DAG at the ER membrane. This residual DAG might be the reason for the partial co-localization of PKC δ and ER membrane under resting conditions (see Fig. 3.3.4). Although the activation of PLC ϵ was essential for the ER recruitment of PKC δ , other phospholipase proteins, such as PLD, still may be involved in the production of DAG [205, 210].

4.3.4 The C-domain composition of PKCs determines their translocation pattern

Presently there are two main hypotheses that try to explain the targeting of PKC isoforms, (i) binding to RACK proteins [103, 104, 108] and (ii) targeting to membrane lipids [22, 43, 91, 92]. In order to identify which one plays the key role, I constructed chimeras between PKC α and PKC δ by specific C-domain swapping. I found that regardless of the particular backbone, the Ca²⁺-sensitive C2 domain was always responsible for plasma membrane

targeting, while the C1 domain of PKC δ was both sufficient and necessary for recognizing DAG produced at the ER membrane. More specifically, using a similar approach than above, I swapped C1A and C1B domains and found that independently of the particular backbone the C1B domain of PKC δ was necessary and sufficient to cause ER targeted translocation. This notion was majorly supported by my finding that the translocation was dependent on a single amino acid known to be involved in DAG binding [40, 41]. Moreover, both Chimera II and Chimera III displayed two fold translocation with targeting, the plasma and ER membrane after ATP stimuli. This was a particular important finding, because ATP stimulation reportedly increased DAG on both membrane but the C1B domain of PKC δ distinguished between both DAGs and specifically recognized DAG on the ER membrane. Up to now this appears difficult to explain, but in contrast to the C2 domain that is known to only probe very surface of the inner leaflet of the plasma membrane, C1 domains are believed to be able to probe the lipid tails of DAGs by incorporating deeper into the lipid layer of the inner leaflet. It is important to note that beside the membrane-specific DAGs (such as DAG_{ER}), the particular DAG lipid environment of the target membranes (*e.g.*, their polarity) can also contribute to the ability of C1 domains to discriminate different target membranes [36, 136].

The alternative targeting mechanism for PKCs involves protein-protein interactions on the target membrane with the “RACK” proteins. This notion claims that each PKC isoform has a unique interaction with different substrate proteins at distinct subcellular sites by specific RACK proteins [103]. According to this “RACK theory”, however, it is difficult to explain why Chimeras II and III can quickly shuttle between two location sites (plasma and ER membrane) while Chimera I and IV can’t be recruit to any of these sites. Moreover, similar phenomena were also observed for Chimera A, B, C, and D in which only the C1A/C1B domains were exchanged and thus their structure was even more similar but they still presented entirely distinct translocation patterns upon ATP simulation (Table 3.3.1). It was even more difficult to reconcile that only a single amino acid mutation, PKC δ ^{W252K}, entirely altered translocation properties by changing protein-protein interactions as necessary for the RACK hypothesis. Thus, differential localizations of PKCs are predominately determined by their C-domain content rather than by interactions with RACKs.

4.3.5 Activation model of PKC δ translocation to the ER

Under physiological conditions, the stimulus for cPKC translocation is an intracellular Ca²⁺ increase [21, 88, 135, 211]. Although the Ca²⁺-C2 domain-plasma membrane interaction is rather weak with fast on and off rates [120], it is an important prerequisite for the C1-DAG interaction at the plasma membrane, which is much stronger but also much

more long lasting [135]. Therefore, C1-DAG interactions provide sufficient energy for cPKC activation [38, 212], although some reports appear to indicate that Ca^{2+} -C2 domain-plasma membrane interactions might already provide some energy and might be able to activate cPKCs at least partially [135]. Because PKCs are usually kept inactive by the binding of a pseudosubstrate domain to the kinase activity center, activation of PKCs can be regarded as a relief from self-inhibition [21]. With respect to the activation of nPKCs, I proposed a novel mechanism, in which production of the ER-specific DAG, DAG_{ER} , is the key for regulating nPKCs' activity. The DAG_{ER} recruits the kinase, binds to the C1B domain of nPKCs and consequently provides energy to change the conformation of nPKC structure, which eventually releases the autoinhibitory domain from the kinase core and stimulates the catalytic activity of nPKCs.

4.3.6 Local PKC phosphorylation at their distinct subcellular compartment

To measure the PKC activation in living cells, the genetically encoded PKC activity probe, CKAR, was employed and provided a real-time method to detect the dynamic phosphorylation of PKC [22, 168]. In order to analyze PKC kinase activity locally, on the plasma or on the ER membrane, local target sequences were introduced by molecular approaches. It should be noted that the CKAR-probe signal can't separate phosphorylation originating from different PKC isoforms.

Importantly, the specific targeting of PKC α and PKC δ induced spatially restricted phosphorylation events on their respective target membranes (Fig. 3.3.13 B), although the substrate peptides within pmCKAR and erCKAR were the same. This important finding not only highlights spatial specificity but also supports the notion of spatiotemporally restricted PKC activity as a major determinant for substrate specificity. Furthermore the stimulation regimes from upstream signals of DAG_{ER} generation, such as ATP, 8-pCPT-2'-O-Me-cAMP, resulted in specific phosphorylation of CKARs on the ER membrane (Fig. 3.3.13 C). The specificity for PKC δ was supported in PKC δ over-expressed HEK293 cells, in which CKAR signals on the ER membrane were substantially increased.

4.3.7 Recruitment of PKC δ reduced sensitivity of the InsP_3R towards InsP_3

To highlight the physiological relevance of the specific targeting of PKC δ , I investigated the consequence of PKC δ activation on the ER membrane. In principle, two major functions, protein modification and intracellular Ca^{2+} storage, are attributed to the ER. Here I put my emphasis on the latter one. After Bryostatin 1 treatment, a specific way to

activate nPKCs, I observed a substantial reduction of ATP-dependent Ca^{2+} oscillation, which strongly suggested a relationship between cPKC activity and Ca^{2+} signaling.

It has been reported that PKC δ can directly phosphorylate InsP₃R *in vitro* [173, 174] where it causes a decreased InsP₃ sensitivity. Taking advantage of membrane permeable caged-InsP₃, I was able to directly substantiate such *in vitro* findings *in situ* by means of graded flash-photolytic InsP₃ production.

In order to efficiently block the activity of PKC δ on the ER membrane, a competitive inhibitory strategy was employed by over-expressing a kinase-dead PKC δ that still located and translocated properly. Such an approach offered significant advantages over PKC δ RNAi techniques, because while RNAi would diminish PKC δ levels in the cell and PKC δ binding sites would be left “free” and consequently occupied by other nPKCs and cause downstream signaling, PKC δ -DN was thought to specifically compete wt-PKC δ away from its natural binding partners at the ER membrane with minimized “side effects”.

By incorporating a single point mutation, K378R, the ATP binding site in the kinase domain was destroyed, so that this kinase cannot transfer phosphate groups from ATP to substrates anymore (kinase-dead PKC δ). After expression of this mutant PKC δ , I interestingly found misallocation of this protein under resting conditions and a lack of translocation following any stimulation regime (Fig. 3.3.16 Aa). Important steps in the protein maturation of almost all PKC members are so-called auto-phosphorylation events of the protein that are critical for proper protein folding (Table 1.1 and [67]). Because the auto-phosphorylation is also required for maturation of PKC δ , I assumed that PKC δ -K378R proteins were folded incorrectly. I therefore introduced another mutant, T505E, in the Turn motif of the C-terminal tail of PKC δ , where the Glu (in the mutated PKC δ) could mimic the structure of the phosphorylated Thr (in the wt protein). This turned out to be a successful strategy, because it not only rescued the protein structure but “killed” the kinase function. Using the dominant negative PKC δ , I confirmed that PKC δ is essential for Bryostatin 1-induced desensitization of the InsP₃R towards InsP₃.

Recruitment of endogenous PKC δ to the ER will limit the positive feedback in InsP₃-dependent Ca^{2+} release from the ER by reducing the InsP₃-sensitivity of the InsP₃R. Moreover, modulation of global Ca^{2+} signals such as their duration or longevity of underlying Ca^{2+} oscillations has been shown to be effective in changing the transcription levels of Ca^{2+} regulated genes [177, 178].

4.3.8 Summary and perspective

In summary, my experiments strongly suggested the existence of a C-domain toolkit for PKCs, in which C-domains can operate independently from one another. Consequently, the C-domain composition of a particular PKC determines its translocation behavior and ultimately its target specificity. The data provided here and elsewhere [38, 213] indicate that lipids, in particular DAGs and their specific generation at the level of cellular membranes, are the major determinants of the translocation and distribution of PKCs. The interactions between such lipid-gated translocation mechanisms and putative alternative anchoring proteins [82, 104, 111] vastly increase the versatility of PKC signaling.

In conclusion, I demonstrate how cells utilize various toolkits, in particular the Ca^{2+} toolkit and the C-domain toolkit, to convert incoming stimuli into spatio-temporal complex phosphorylation patterns that are instrumental for appropriate cell signaling and responses.

References

1. Manning G: The Protein Kinase Complement of the Human Genome. *Science* 2002, 298:1912–1934.
2. Alberts B, Johnson A, Lewis J, Walter P, Raff M, Roberts K: *Molecular Biology of the Cell*. Garland Science; 2008.
3. Hunter T: Signaling--2000 and beyond. *Cell* 2000, 100:113–127.
4. Blume-Jensen P, Hunter T: Oncogenic kinase signalling. *Nature* 2001, 411:355–365.
5. Cohen P: Protein kinases--the major drug targets of the twenty-first century? *Nat Rev Drug Discov* 2002, 1:309–315.
6. Mochly-Rosen D, Das K, Grimes KV: Protein kinase C, an elusive therapeutic target? *Nat Rev Drug Discov* 2012, 11:937–957.
7. Kurokawa M, Kornbluth S: Caspases and Kinases in a Death Grip. *Cell* 2009, 138:838–854.
8. Nishizuka Y: Studies and perspectives of protein kinase C. *Science* 1986, 233:305–312.
9. Akita Y: Protein kinase C-epsilon (PKC-epsilon): its unique structure and function. *J Biochem* 2002, 132:847–852.
10. Altman A, Villalba M: Protein kinase C-theta (PKC theta): a key enzyme in T cell life and death. *J Biochem* 2002, 132:841–846.
11. Kashiwagi K: Importance of C1B Domain for Lipid Messenger-induced Targeting of Protein Kinase C. *J Biol Chem* 2002, 277:18037–18045.
12. Kawakami T, Kawakami Y, Kitaura J: Protein kinase C beta (PKC beta): normal functions and diseases. *J Biochem* 2002, 132:677–682.
13. Kikkawa U, Matsuzaki H, Yamamoto T: Protein kinase C delta (PKC delta): activation mechanisms and functions. *J Biochem* 2002, 132:831–839.
14. Nakashima S: Protein kinase C alpha (PKC alpha): regulation and biological function. *J Biochem* 2002, 132:669–675.
15. Newton AC: Protein kinase C: poised to signal. *Am J Physiol -Endoc M* 2010, 298:E395–E402.
16. Pearce LR, Komander D, Alessi DR: The nuts and bolts of AGC protein kinases. *Nat Rev Mol Cell Biol* 2010, 11:9–22.

17. Watanabe M, Chen CY, Levin DE: *Saccharomyces cerevisiae* PKC1 encodes a protein kinase C (PKC) homolog with a substrate specificity similar to that of mammalian PKC. *J Biol Chem* 1994, 269:16829–16836.
18. Madden K, Sheu YJ, Baetz K, Andrews B, Snyder M: SBF Cell Cycle Regulator as a Target of the Yeast PKC-MAP Kinase Pathway. *Science* 1997, 275:1781–1784.
19. Griner EM, Kazanietz MG: Protein kinase C and other diacylglycerol effectors in cancer. *Nat Rev Cancer* 2007, 7:281–294.
20. Steinberg SF: Structural Basis of Protein Kinase C Isoform Function. *Physiol Rev* 2008, 88:1341–1378.
21. Lipp P, Reither G: Protein Kinase C: The “Masters” of Calcium and Lipid. *Cold Spring Harb Perspect Biol* 2011, 3:a004556–a004556.
22. Gallegos LL, Newton AC: Spatiotemporal dynamics of lipid signaling: Protein kinase C as a paradigm. *IUBMB Life* 2008, 60:782–789.
23. Freeley M, Kelleher D, Long A: Regulation of Protein Kinase C function by phosphorylation on conserved and non-conserved sites. *Cell Signal* 2011, 23:753–762.
24. Newton AC: Protein kinase C: structural and spatial regulation by phosphorylation, cofactors, and macromolecular interactions. *Chem Rev* 2001, 101:2353–2364.
25. Rosse C, Linch M, Kermorgant S, Cameron AJM, Boeckeler K, Parker PJ: PKC and the control of localized signal dynamics. *Nat Rev Mol Cell Biol* 2010, 11:103–112.
26. Dutil EM, Newton AC: Dual role of pseudosubstrate in the coordinated regulation of protein kinase C by phosphorylation and diacylglycerol. *J Biol Chem* 2000, 275:10697–10701.
27. Ron D, Mochly-Rosen D: An Autoregulatory Region in Protein-Kinase-C - the Pseudoanchoring Site. *Proc Natl Acad Sci USA* 1995, 92:492–496.
28. Anthonen MW, Andersen S, Solhaug A, Johansen B: Atypical lambda /iota PKC Conveys 5-Lipoxygenase/Leukotriene B4-mediated Cross-talk between Phospholipase A2s Regulating NF-kappa B Activation in Response to Tumor Necrosis Factor-alpha and Interleukin-1beta. *J Biol Chem* 2001, 276:35344–35351.
29. Petit I, Goichberg P, Spiegel A, Peled A, Brodie C, Seger R, Nagler A, Alon R, Lapidot T: Atypical PKC-zeta regulates SDF-1-mediated migration and development of human CD34+ progenitor cells. *J Clin Invest* 2005, 115:168–176.
30. Orr JW, Keranen LM, Newton AC: Reversible exposure of the pseudosubstrate domain of protein kinase C by phosphatidylserine and diacylglycerol. *J Biol Chem* 1992, 267:15263–15266.
31. Orr JW, Newton AC: Intrapeptide regulation of protein kinase C. *J Biol Chem* 1994, 269:8383–8387.
32. Keranen LM, Newton AC: Ca²⁺ differentially regulates conventional protein kinase Cs' membrane interaction and activation. *J Biol Chem* 1997, 272:25959–25967.
33. Leonard TA, Rózycki B, Saidi LF, Hummer G, Hurley JH: Crystal Structure and Allosteric Activation of Protein Kinase C βII. *Cell* 2011, 144:55–66.

34. Hommel U, Zurini M, Luyten M: Solution structure of a cysteine rich domain of rat protein kinase C. *Nat Struct Biol* 1994, 1:383–387.
35. Cho W: Membrane Targeting by C1 and C2 Domains. *J Biol Chem* 2001, 276:32407–32410.
36. Gomez-Fernandez JC, Torrecillas A, Corbalan-Garcia S: Diacylglycerols as activators of protein kinase C (Review). *Mol Membr Biol* 2004, 21:339–349.
37. Hurley JH, Misra S: Signaling and subcellular targeting by membrane-binding domains. *Annu Rev Biophys Biomol Struct* 2000, 29:49–79.
38. Ananthanarayanan B, Stahelin RV, Digman MA, Cho W: Activation mechanisms of conventional protein kinase C isoforms are determined by the ligand affinity and conformational flexibility of their C1 domains. *J Biol Chem* 2003, 278:46886–46894.
39. VALLENTIN A, Prévostel C, Fauquier T, Bonnefont X, Joubert D: Membrane targeting and cytoplasmic sequestration in the spatiotemporal localization of human protein kinase C alpha. *J Biol Chem* 2000, 275:6014–6021.
40. Wang QJ: Role of Hydrophobic Residues in the C1b Domain of Protein Kinase C delta on Ligand and Phospholipid Interactions. *J Biol Chem* 2001, 276:19580–19587.
41. Dries DR, Gallegos LL, Newton AC: A Single Residue in the C1 Domain Sensitizes Novel Protein Kinase C Isoforms to Cellular Diacylglycerol Production. *J Biol Chem* 2007, 282:826–830.
42. Stahelin RV: Mechanism of Diacylglycerol-induced Membrane Targeting and Activation of Protein Kinase C. *J Biol Chem* 2004, 279:29501–29512.
43. Stahelin RV, Digman MA, Medkova M, Ananthanarayanan B, Melowic HR, Rafter JD, Cho W: Diacylglycerol-induced membrane targeting and activation of protein kinase Cepsilon: mechanistic differences between protein kinases Cdelta and Cepsilon. *J Biol Chem* 2005, 280:19784–19793.
44. Melowic HR, Stahelin RV, Blatner NR, Tian W, Hayashi K, Altman A, Cho W: Mechanism of diacylglycerol-induced membrane targeting and activation of protein kinase Ctheta. *J Biol Chem* 2007, 282:21467–21476.
45. Giorgione JR, Lin JH, McCammon JA, Newton AC: Increased membrane affinity of the C1 domain of protein kinase Cdelta compensates for the lack of involvement of its C2 domain in membrane recruitment. *J Biol Chem* 2006, 281:1660–1669.
46. Slater SJ, Seiz JL, Cook AC, Buzas CJ, Malinowski SA, Kershner JL, Stagliano BA, Stubbs CD: Regulation of PKC alpha activity by C1-C2 domain interactions. *J Biol Chem* 2002, 277:15277–15285.
47. Stahelin RV, Wang J, Blatner NR, Rafter JD, Murray D, Cho W: The origin of C1A-C2 interdomain interactions in protein kinase Calpha. *J Biol Chem* 2005, 280:36452–36463.
48. Kajimoto T: Ceramide-induced Apoptosis by Translocation, Phosphorylation, and Activation of Protein Kinase C in the Golgi Complex. *J Biol Chem* 2003, 279:12668–12676.
49. Wang QJ, Fang TW, Fenick D, Garfield SH, Bienfait B, Marquez VE, Blumberg PM: The lipophilicity of phorbol esters as a critical factor in determining the pattern of translocation of protein kinase C delta fused to green fluorescent protein. *J Biol Chem*

2000, 275:12136–12146.

50. Perander M, Bjorkoy G, Johansen T: Nuclear import and export signals enable rapid nucleocytoplasmic shuttling of the atypical protein kinase C lambda. *J Biol Chem* 2001, 276:13015–13024.
51. Medkova M, Cho W: Mutagenesis of the C2 domain of protein kinase C-alpha. Differential roles of Ca²⁺ ligands and membrane binding residues. *J Biol Chem* 1998, 273:17544–17552.
52. Corbalan-Garcia S, Garcia-Garcia J, Rodríguez-Alfaro JA, Gomez-Fernandez JC: A new phosphatidylinositol 4,5-bisphosphate-binding site located in the C2 domain of protein kinase Calpha. *J Biol Chem* 2003, 278:4972–4980.
53. Evans JH, Murray D, Leslie CC, Falke JJ: Specific translocation of protein kinase Calpha to the plasma membrane requires both Ca²⁺ and PIP2 recognition by its C2 domain. *Mol Biol Cell* 2006, 17:56–66.
54. Stahelin RV, Rafter JD, Das S, Cho W: The molecular basis of differential subcellular localization of C2 domains of protein kinase C-alpha and group IVa cytosolic phospholipase A2. *J Biol Chem* 2003, 278:12452–12460.
55. Knighton DR, Zheng JH, Eyck Ten LF, Ashford VA, Xuong NH, Taylor SS, Sowadski JM: Crystal structure of the catalytic subunit of cyclic adenosine monophosphate-dependent protein kinase. *Science* 1991, 253:407–414.
56. Yang J, Cron P, Thompson V, Good VM, Hess D, Hemmings BA, Barford D: Molecular mechanism for the regulation of protein kinase B/Akt by hydrophobic motif phosphorylation. *Mol Cell* 2002, 9:1227–1240.
57. Emrick MA, Lee T, Starkey PJ, Mumby MC, Resing KA, Ahn NG: The gatekeeper residue controls autoactivation of ERK2 via a pathway of intramolecular connectivity. *Proc Natl Acad Sci USA* 2006, 103:18101–18106.
58. Garske AL, Peters U, Cortesi AT, Perez JL, Shokat KM: Chemical genetic strategy for targeting protein kinases based on covalent complementarity. *Proc Natl Acad Sci USA* 2011, 108:15046–15052.
59. Chalfant CE, Mischak H, Watson JE, Winkler BC, Goodnight J, Farese RV, Cooper DR: Regulation of alternative splicing of protein kinase C beta by insulin. *J Biol Chem* 1995, 270:13326–13332.
60. Babwah AV, Dale LB, Ferguson SSG: Protein kinase C isoform-specific differences in the spatial-temporal regulation and decoding of metabotropic glutamate receptor1a-stimulated second messenger responses. *J Biol Chem* 2003, 278:5419–5426.
61. Goodnight JA, Mischak H, Kolch W, Mushinski JF: Immunocytochemical localization of eight protein kinase C isozymes overexpressed in NIH 3T3 fibroblasts. Isoform-specific association with microfilaments, Golgi, endoplasmic reticulum, and nuclear and cell membranes. *J Biol Chem* 1995, 270:9991–10001.
62. Yeong SS, Zhu Y, Smith D, Verma C, Lim WG, Tan BJ, Li QT, Cheung NS, Cai M, Zhu Y-Z, Zhou S-F, Tan S-L, Duan W: The last 10 amino acid residues beyond the hydrophobic motif are critical for the catalytic competence and function of protein kinase Calpha. *J*

Biol Chem 2006, 281:30768–30781.

63. Zhu Y, Smith D, Verma C, Lim WG, Tan BJ, Armstrong JS, Zhou S, Chan E, Tan S-L, Zhu Y-Z, Cheung NS, Duan W: The very C-terminus of protein kinase Cepsilon is critical for the full catalytic competence but its hydrophobic motif is dispensable for the interaction with 3-phosphoinositide-dependent kinase-1. *Cell Signal* 2006, 18:807–818.
64. Hauge C, Antal TL, Hirschberg D, Doehn U, Thorup K, Idrissova L, Hansen K, Jensen ON, Jørgensen TJ, Biondi RM, Frödin M: Mechanism for activation of the growth factor-activated AGC kinases by turn motif phosphorylation. *Embo J* 2007, 26:2251–2261.
65. Stensman H: Autophosphorylation Suppresses Whereas Kinase Inhibition Augments the Translocation of Protein Kinase C in Response to Diacylglycerol. *J Biol Chem* 2004, 279:40576–40583.
66. DeVries TA, Neville MC, Reyland ME: Nuclear import of PKC delta is required for apoptosis: identification of a novel nuclear import sequence. *Embo J* 2002, 21:6050–6060.
67. Newton AC: Regulation of the ABC kinases by phosphorylation: protein kinase C as a paradigm. *Biochem J* 2003, 370:361–371.
68. Parker PJ, Parkinson SJ: AGC protein kinase phosphorylation and protein kinase C. *Biochem Soc Trans* 2001, 29:860–863.
69. Gould CM, Kannan N, Taylor SS, Newton AC: The chaperones Hsp90 and Cdc37 mediate the maturation and stabilization of protein kinase C through a conserved PXXP motif in the C-terminal tail. *J Biol Chem* 2009, 284:4921–4935.
70. Cancer Genome Atlas Research Network: Comprehensive genomic characterization defines human glioblastoma genes and core pathways. *Nature* 2008, 455:1061–1068.
71. Tsutakawa SE, Medzihradsky KF, Flint AJ, Burlingame AL, Koshland DE: Determination of in vivo phosphorylation sites in protein kinase C. *J Biol Chem* 1995, 270:26807–26812.
72. Keranen LM, Dutil EM, Newton AC: Protein kinase C is regulated in vivo by three functionally distinct phosphorylations. *Curr Biol* 1995, 5:1394–1403.
73. Chou MM, Hou W, Johnson J, Graham LK, Lee MH, Chen CS, Newton AC, Schaffhausen BS, Toker A: Regulation of protein kinase C zeta by PI 3-kinase and PDK-1. *Curr Biol* 1998, 8:1069–1077.
74. Dutil EM, Toker A, Newton AC: Regulation of conventional protein kinase C isozymes by phosphoinositide-dependent kinase 1 (PDK-1). *Curr Biol* 1998, 8:1366–1375.
75. Le Good JA, Ziegler WH, Parekh DB, Alessi DR, Cohen P, Parker PJ: Protein kinase C isotypes controlled by phosphoinositide 3-kinase through the protein kinase PDK1. *Science* 1998, 281:2042–2045.
76. Sonnenburg ED, Gao T, Newton AC: The phosphoinositide-dependent kinase, PDK-1, phosphorylates conventional protein kinase C isozymes by a mechanism that is independent of phosphoinositide 3-kinase. *J Biol Chem* 2001, 276:45289–45297.
77. Cazaubon S, Bornancin F, Parker PJ: Threonine-497 is a critical site for permissive activation of protein kinase C alpha. *Biochem J* 1994, 301 (Pt 2):443–448.
78. Orr JW, Newton AC: Requirement for negative charge on “activation loop” of protein kinase C.

J Biol Chem 1994, 269:27715–27718.

79. Balendran A, Hare GR, Kieloch A, Williams MR, Alessi DR: Further evidence that 3-phosphoinositide-dependent protein kinase-1 (PDK1) is required for the stability and phosphorylation of protein kinase C (PKC) isoforms. *FEBS Lett* 2000, 484:217–223.
80. Bornancin F, Parker PJ: Phosphorylation of threonine 638 critically controls the dephosphorylation and inactivation of protein kinase Calpha. *Curr Biol* 1996, 6:1114–1123.
81. Facchinetti V, Ouyang W, Wei H, Soto N, Lazorchak A, Gould CM, Lowry C, Newton AC, Mao Y, Miao RQ, Sessa WC, Qin J, Zhang P, Su B, Jacinto E: The mammalian target of rapamycin complex 2 controls folding and stability of Akt and protein kinase C. *Embo J* 2008, 27:1932–1943.
82. Ikenoue T, Inoki K, Yang Q, Zhou X, Guan K-L: Essential function of TORC2 in PKC and Akt turn motif phosphorylation, maturation and signalling. *Embo J* 2008, 27:1919–1931.
83. Jacinto E, Lorberg A: TOR regulation of AGC kinases in yeast and mammals. *Biochem J* 2008, 410:19–37.
84. Behn-Krappa A, Newton AC: The hydrophobic phosphorylation motif of conventional protein kinase C is regulated by autophosphorylation. *Curr Biol* 1999, 9:728–737.
85. Ziegler WH, Parekh DB, Le Good JA, Whelan RD, Kelly JJ, Frech M, Hemmings BA, Parker PJ: Rapamycin-sensitive phosphorylation of PKC on a carboxy-terminal site by an atypical PKC complex. *Curr Biol* 1999, 9:522–529.
86. Giorgione JR, Newton AC: Measuring the binding of protein kinase C to sucrose-loaded vesicles. 2003, 233:105–113.
87. Schaefer M, Albrecht N, Hofmann T, Gudermann T, Schultz G: Diffusion-limited translocation mechanism of protein kinase C isoforms. *FASEB J* 2001, 15:1634–1636.
88. Reither G, Schaefer M, Lipp P: PKCalpha: a versatile key for decoding the cellular calcium toolkit. *J Cell Biol* 2006, 174:521–533.
89. Oancea E, Meyer T: Protein kinase C as a molecular machine for decoding calcium and diacylglycerol signals. *Cell* 1998, 95:307–318.
90. Kohout SC, Corbalan-Garcia S, Torrecillas A, Gomez-Fernandez JC, Falke JJ: C2 domains of protein kinase C isoforms alpha, beta, and gamma: activation parameters and calcium stoichiometries of the membrane-bound state. *Biochemistry* 2002, 41:11411–11424.
91. Johnson JE, Giorgione JR, Newton AC: The C1 and C2 domains of protein kinase C are independent membrane targeting modules, with specificity for phosphatidylserine conferred by the C1 domain. *Biochemistry* 2000, 39:11360–11369.
92. Giorgione JR, Hysell M, Harvey DF, Newton AC: Contribution of the C1A and C1B domains to the membrane interaction of protein kinase C. *Biochemistry* 2003, 42:11194–11202.
93. Fujii K, Zhu G, Liu Y, Hallam J, Chen L, Herrero J, Shaw S: Kinase peptide specificity: improved determination and relevance to protein phosphorylation. *Proc Natl Acad Sci USA* 2004, 101:13744–13749.
94. Nolen B, Taylor S, Ghosh G: Regulation of protein kinases; controlling activity through

- activation segment conformation. *Mol Cell* 2004, 15:661–675.
95. Newton AC: Protein kinase C: structure, function, and regulation. *J Biol Chem* 1995, 270:28495–28498.
 96. Dries DR, Newton AC: Kinetic analysis of the interaction of the C1 domain of protein kinase C with lipid membranes by stopped-flow spectroscopy. *J Biol Chem* 2008, 283:7885–7893.
 97. Hansra G, Garcia-Paramio P, Prévostel C, Whelan RD, Bornancin F, Parker PJ: Multisite dephosphorylation and desensitization of conventional protein kinase C isoforms. *Biochem J* 1999, 342 (Pt 2):337–344.
 98. Dutil EM, Keranen LM, DePaoli-Roach AA, Newton AC: In vivo regulation of protein kinase C by trans-phosphorylation followed by autophosphorylation. *J Biol Chem* 1994, 269:29359–29362.
 99. Brognard J, Newton AC: PHLiPPing the switch on Akt and protein kinase C signaling. *Trends Endocrinol Metab* 2008, 19:223–230.
 100. Cheng W, Wang L, Zhang R, Du P, Yang B, Zhuang H, Tang B, Yao C, Yu M, Wang Y, Zhang J, Yin W, Li J, Zheng W, Lu M, Hua Z: Regulation of protein kinase C inactivation by Fas-associated protein with death domain. *J Biol Chem* 2012, 287:26126–26135.
 101. Leontieva OV, Black JD: Identification of two distinct pathways of protein kinase C α down-regulation in intestinal epithelial cells. *J Biol Chem* 2004, 279:5788–5801.
 102. Mochly-Rosen D, Gordon AS: Anchoring proteins for protein kinase C: a means for isozyme selectivity. *FASEB J* 1998, 12:35–42.
 103. Churchill E, Budas G, Vallentin A, Koyanagi T, Mochly-Rosen D: PKC Isozymes in Chronic Cardiac Disease: Possible Therapeutic Targets? *Annu Rev Pharmacol Toxicol* 2008, 48:569–599.
 104. Mochly-Rosen D, Khaner H, Lopez J: Identification of intracellular receptor proteins for activated protein kinase C. *Proc Natl Acad Sci USA* 1991, 88:3997–4000.
 105. Stebbins EG, Mochly-Rosen D: Binding specificity for RACK1 resides in the V5 region of beta II protein kinase C. *J Biol Chem* 2001, 276:29644–29650.
 106. Ron D, Luo J, Mochly-Rosen D: C2 region-derived peptides inhibit translocation and function of beta protein kinase C in vivo. *J Biol Chem* 1995, 270:24180–24187.
 107. Kheifets V, Bright R, Inagaki K, Schechtman D, Mochly-Rosen D: Protein kinase C delta (deltaPKC)-annexin V interaction: a required step in deltaPKC translocation and function. *J Biol Chem* 2006, 281:23218–23226.
 108. Schechtman D, Craske ML, Kheifets V, Meyer T, Schechtman J, Mochly-Rosen D: A critical intramolecular interaction for protein kinase Cepsilon translocation. *J Biol Chem* 2004, 279:15831–15840.
 109. LIRON T, Chen L, Khaner H, VALLENTIN A, Mochly-Rosen D: Rational design of a selective antagonist of ϵ protein kinase C derived from the selective allosteric agonist, pseudo-RACK peptide. *J Mol Cell Cardiol* 2007, 42:835–841.
 110. Perkins GA, Wang L, Huang LJ, Humphries K, Yao VJ, Martone M, Deerinck TJ, Barraclough DM, Violin JD, Smith D, Newton A, Scott JD, Taylor SS, Ellisman MH: PKA, PKC, and

- AKAP localization in and around the neuromuscular junction. *BMC Neurosci* 2001, 2:17.
111. Hoshi N, Langeberg LK, Gould CM, Newton AC, Scott JD: Interaction with AKAP79 Modifies the Cellular Pharmacology of PKC. *Mol Cell* 2010, 37:541–550.
 112. Fu H, Subramanian RR, Masters SC: 14-3-3 proteins: structure, function, and regulation. *Annu Rev Pharmacol Toxicol* 2000, 40:617–647.
 113. Nguyen TA, Takemoto LJ, Takemoto DJ: Inhibition of gap junction activity through the release of the C1B domain of protein kinase C γ (PKC γ) from 14-3-3: identification of PKC γ -binding sites. *J Biol Chem* 2004, 279:52714–52725.
 114. Keenan C, Kelleher D: Protein Kinase C and the Cytoskeleton. *Cell Signal* 1998, 10:225–232.
 115. Larsson C: Protein kinase C and the regulation of the actin cytoskeleton. *Cell Signal* 2006, 18:276–284.
 116. Akita Y: Protein kinase C ϵ : multiple roles in the function of, and signaling mediated by, the cytoskeleton. *FEBS J* 2008, 275:3995–4004.
 117. Prekeris R, Hernandez RM, Mayhew MW, White MK, Terrian DM: Molecular analysis of the interactions between protein kinase C- ϵ and filamentous actin. *J Biol Chem* 1998, 273:26790–26798.
 118. Anilkumar N, Parsons M, Monk R, Ng T, Adams JC: Interaction of fascin and protein kinase C α : a novel intersection in cell adhesion and motility. *Embo J* 2003, 22:5390–5402.
 119. Chen D, Purohit A, Halilovic E, Doxsey SJ, Newton AC: Centrosomal anchoring of protein kinase C β II by pericentrin controls microtubule organization, spindle function, and cytokinesis. *J Biol Chem* 2003, 279:4829–4839.
 120. Nalefski EA, Newton AC: Membrane binding kinetics of protein kinase C β II mediated by the C2 domain. *Biochemistry* 2001, 40:13216–13229.
 121. Doherty GJ, McMahon HT: Mediation, modulation, and consequences of membrane-cytoskeleton interactions. *Annu Rev Biophys* 2008, 37:65–95.
 122. Papadopoulos V, Hall PF: Isolation and characterization of protein kinase C from Y-1 adrenal cell cytoskeleton. *J Cell Biol* 1989, 108:553–567.
 123. Szalay J, Bruno P, Bhati R, Adjodha J, Schueler D, Summerville V, Vazeos R: Associations of PKC isoforms with the cytoskeleton of B16F10 melanoma cells. *J Histochem Cytochem* 2001, 49:49–66.
 124. Evans JH, Falke JJ: Ca $^{2+}$ influx is an essential component of the positive-feedback loop that maintains leading-edge structure and activity in macrophages. *Proc Natl Acad Sci USA* 2007, 104:16176–16181.
 125. House C, Kemp BE: Protein kinase C contains a pseudosubstrate prototope in its regulatory domain. *Science* 1987, 238:1726–1728.
 126. Bootman M, Niggli E, Berridge M, Lipp P: Imaging the hierarchical Ca $^{2+}$ signalling system in HeLa cells. *J Physiol* 1997, 499 (Pt 2):307–314.
 127. Bootman MD, Berridge MJ, Lipp P: Cooking with calcium: The recipes for composing global signals from elementary events. *Cell* 1997, 91:367–373.

128. Schievella AR, Regier MK, Smith WL, Lin LL: Calcium-mediated translocation of cytosolic phospholipase A2 to the nuclear envelope and endoplasmic reticulum. *J Biol Chem* 1995, 270:30749–30754.
129. Stein A, Radhakrishnan A, Riedel D, Fasshauer D, Jahn R: Synaptotagmin activates membrane fusion through a Ca²⁺-dependent trans interaction with phospholipids. *Nat Struct Mol Biol* 2007, 14:904–911.
130. Dai Y, Walker SA, de Vet E, Cook S, Welch HCE, Lockyer PJ: Ca²⁺-dependent Monomer and Dimer Formation Switches CAPRI Protein between Ras GTPase-activating Protein (GAP) and RapGAP Activities. *J Biol Chem* 2011, 286:19905–19916.
131. Oancea E, Teruel MN, Quest AFG, Meyer T: Green fluorescent protein (GFP)-tagged cysteine-rich domains from protein kinase C as fluorescent indicators for diacylglycerol signaling in living cells. *J Cell Biol* 1998, 140:485–498.
132. Collazos A, Diouf B, Guérineau NC, Quittau-Prévostel C, Peter M, Coudane F, Hollande F, Joubert D: A spatiotemporally coordinated cascade of protein kinase C activation controls isoform-selective translocation. *Mol Cell Biol* 2006, 26:2247–2261.
133. Lenz JC, Reusch HP, Albrecht N, Schultz G, Schaefer M: Ca²⁺-controlled competitive diacylglycerol binding of protein kinase C isoenzymes in living cells. *J Cell Biol* 2002, 159:291–302.
134. Verdaguer N, Corbalan-Garcia S, Ochoa WF, Fita I, Gomez-Fernandez JC: Ca²⁺ bridges the C2 membrane-binding domain of protein kinase C α directly to phosphatidylserine. *Embo J* 1999, 18:6329–6338.
135. Bolsover SR, Gomez-Fernandez JC, Corbalan-Garcia S: Role of the Ca²⁺/phosphatidylserine binding region of the C2 domain in the translocation of protein kinase C α to the plasma membrane. *J Biol Chem* 2003, 278:10282–10290.
136. Sanchez-Bautista S, Corbalan-Garcia S, Perez-Lara A, Gomez-Fernandez JC: A Comparison of the Membrane Binding Properties of C1B Domains of PKC γ , PKC δ , and PKC ϵ . *Biophys J* 2009, 96:3638–3647.
137. Shirai Y, Kashiwagi K, Yagi K, Sakai N, Saito N: Distinct effects of fatty acids on translocation of γ - and ϵ -subspecies of protein kinase C. *J Cell Biol* 1998, 143:511–521.
138. Shaner NC, Lin MZ, McKeown MR, Steinbach PA, Hazelwood KL, Davidson MW, Tsien RY: Improving the photostability of bright monomeric orange and red fluorescent proteins. *Nat Meth* 2008, 5:545–551.
139. Violin JD, Zhang J, Tsien RY, Newton AC: A genetically encoded fluorescent reporter reveals oscillatory phosphorylation by protein kinase C. *J Cell Biol* 2003, 161:899–909.
140. Borgese N, Gazzoni I, Barberi M, Colombo S, Pedrazzini E: Targeting of a tail-anchored protein to endoplasmic reticulum and mitochondrial outer membrane by independent but competing pathways. *Mol Biol Cell* 2001, 12:2482–2496.
141. Li Y, Asuri S, Rebhun JF, Castro AF, Parnavitana NC, Quilliam LA: The RAP1 guanine nucleotide exchange factor Epac2 couples cyclic AMP and Ras signals at the plasma membrane. *J Biol Chem* 2006, 281:2506–2514.

142. Yabuki T, Motoda Y, Hanada K, Nunokawa E, Saito M, Seki E, Inoue M, Kigawa T, Yokoyama S: A robust two-step PCR method of template DNA production for high-throughput cell-free protein synthesis. *J Struct Funct Genomics* 2007, 8:173–191.
143. Bulbarelli A, Sprocati T, Barberi M, Pedrazzini E, Borgese N: Trafficking of tail-anchored proteins: transport from the endoplasmic reticulum to the plasma membrane and sorting between surface domains in polarised epithelial cells. *J Cell Sci* 2002, 115:1689–1702.
144. Ronchi P, Colombo S, Francolini M, Borgese N: Transmembrane domain-dependent partitioning of membrane proteins within the endoplasmic reticulum. *J Cell Biol* 2008, 181:105–118.
145. Luisier F, Vonesch C, Blu T, Unser M: Fast interscale wavelet denoising of Poisson-corrupted images. *Signal Process* 2010, 90:415–427.
146. Wlodarczyk J, Woehler A, Kobe F, Ponimaskin E, Zeug A, Neher E: Analysis of FRET Signals in the Presence of Free Donors and Acceptors. *Biophys J* 2008, 94:986–1000.
147. Verkhusha VV, Lukyanov KA: The molecular properties and applications of Anthozoa fluorescent proteins and chromoproteins. *Nat Biotechnol* 2004, 22:289–296.
148. Heikal A, Hess S, Baird G, Tsien R, Webb W: Molecular spectroscopy and dynamics of intrinsically fluorescent proteins: Coral red (dsRed) and yellow (Citrine) (vol 97, pg 11996, 2000). *Proc Natl Acad Sci USA* 2000, 97:14831–14831.
149. Mochly-Rosen D, Henrich CJ, Cheever L, Khaner H, Simpson PC: A protein kinase C isozyme is translocated to cytoskeletal elements on activation. *Cell Regul* 1990, 1:693–706.
150. Torchia J, Yi Q, Sen AK: Carbachol-stimulated phosphorylation of the Na-K-Cl cotransporter of avian salt gland. Requirement for Ca²⁺ and PKC Activation. *J Biol Chem* 1994, 269:29778–29784.
151. Wouters FS, Verveer PJ, Bastiaens PI: Imaging biochemistry inside cells. *Trends Cell Biol* 2001, 11:203–211.
152. Esposito A, Tiffert T, Mauritz JMA, Schlachter S, Bannister LH, Kaminski CF, Lew VL: FRET imaging of hemoglobin concentration in Plasmodium falciparum-infected red cells. *PLoS ONE* 2008, 3:e3780.
153. Berkow RL, Kraft AS: Bryostatin, a non-phorbol macrocyclic lactone, activates intact human polymorphonuclear leukocytes and binds to the phorbol ester receptor. *Biochem Biophys Res Commun* 1985, 131:1109–1116.
154. Wender PA, Baryza JL, Brenner SE, DeChristopher BA, Loy BA, Schrier AJ, Verma VA: Design, synthesis, and evaluation of potent bryostatin analogs that modulate PKC translocation selectivity. *Proc Natl Acad Sci USA* 2011, 108:6721–6726.
155. Schmidt M, Evellin S, Weernink PA, Dorp vom F, Rehmann H, Lomasney JW, Jakobs KH: A new phospholipase-C-calcium signalling pathway mediated by cyclic AMP and a Rap GTPase. *Nat Cell Biol* 2001, 3:1020–1024.
156. Gloerich M, Bos JL: Epac: Defining a New Mechanism for cAMP Action. *Annu Rev Pharmacol Toxicol* 2010, 50:355–375.

157. Kang G, Joseph JW, Chepurny OG, Monaco M, Wheeler MB, Bos JL, Schwede F, Genieser HG, Holz GG: Epac-selective cAMP Analog 8-pCPT-2'-O-Me-cAMP as a Stimulus for Ca²⁺-induced Ca²⁺ Release and Exocytosis in Pancreatic beta -Cells. *J Biol Chem* 2002, 278:8279–8285.
158. Holz GG, Chepurny OG, Schwede F: Epac-selective cAMP analogs: New tools with which to evaluate the signal transduction properties of cAMP-regulated guanine nucleotide exchange factors. *Cell Signal* 2008, 20:10–20.
159. van Hooren KWEM, van Agtmaal EL, Fernandez-Borja M, van Mourik JA, Voorberg J, Bierings R: The Epac-Rap1 signaling pathway controls cAMP-mediated exocytosis of Weibel-Palade bodies in endothelial cells. *J Biol Chem* 2012, 287:24713–24720.
160. de Rooij J, Zwartkruis FJT, Verheijen MH, Cool RH, Nijman SM, Wittinghofer A, Bos JL: Epac is a Rap1 guanine-nucleotide-exchange factor directly activated by cyclic AMP. *Nature* 1998, 396:474–477.
161. Branham MT, Bustos MA, De Blas GA, Rehmann H, Zarelli VEP, Treviño CL, Darszon A, Mayorga LS, Tomes CN: Epac activates the small G proteins Rap1 and Rab3A to achieve exocytosis. *J Biol Chem* 2009, 284:24825–24839.
162. Breckler M, Berthouze M, Laurent A-CC, Crozatier B, Morel E, Lezoualc'h F: Rap-linked cAMP signaling Epac proteins: compartmentation, functioning and disease implications. *Cell Signal* 2011, 23:1257–1266.
163. Lacabaratz-Porret C, Corvazier E, Kovács T, Bobe R, Bredoux R, Launay S, Papp B, Enouf J: Platelet sarco/endoplasmic reticulum Ca²⁺-ATPase isoform 3b and Rap 1b: interrelation and regulation in physiopathology. *Biochem J* 1998, 332 (Pt 1):173–181.
164. Harden TK, Sondek J: Regulation of phospholipase C isozymes by ras superfamily GTPases. *Annu Rev Pharmacol Toxicol* 2006, 46:355–379.
165. Jeon TJ, Lee DJ, Lee S, Weeks G, Firtel RA: Regulation of Rap1 activity by RapGAP1 controls cell adhesion at the front of chemotaxing cells. *J Cell Biol* 2007, 179:833–843.
166. Scrima A, Thomas C, Deaconescu D, Wittinghofer A: The Rap-RapGAP complex: GTP hydrolysis without catalytic glutamine and arginine residues. *Embo J* 2008, 27:1145–1153.
167. Kajimoto T, Sawamura S, Tohyama Y, Mori Y, Newton AC: Protein kinase C δ -specific activity reporter reveals agonist-evoked nuclear activity controlled by Src family of kinases. *J Biol Chem* 2010, 285:41896–41910.
168. Gallegos LL, Kunkel MT, Newton AC: Targeting Protein Kinase C Activity Reporter to Discrete Intracellular Regions Reveals Spatiotemporal Differences in Agonist-dependent Signaling. *J Biol Chem* 2006, 281:30947–30956.
169. Stempka L, Schnölzer M, Radke S, Rincke G, Marks F, Gschwendt M: Requirements of protein kinase cdelta for catalytic function. Role of glutamic acid 500 and autophosphorylation on serine 643. *J Biol Chem* 1999, 274:8886–8892.
170. Welling A, Hofmann F, Wegener JW: Inhibition of L-Type Cav1.2 Ca²⁺ Channels by 2,(4-Morpholinyl)-8-phenyl-4H-1-benzopyran-4-one (LY294002) and 2-[1-(3-Dimethylaminopropyl)-5-methoxyindol-3-yl]-3-(1H-indol-3-yl) Maleimide (Go6983). *Mol*

Pharmacol 2004, 67:541–544.

171. Ehrlich BE, Kaftan E, Bezprozvannaya S, Bezprozvanny I: The pharmacology of intracellular Ca (2+)-release channels. *Trends Pharmacol Sci* 1994, 15:145.
172. Racke FK, Nemeth EF: Cytosolic Calcium Homeostasis in Bovine Parathyroid Cells and Its Modulation by Protein-Kinase-C. *J Physiol* 1993, 468:141–162.
173. Matter N, Ritz MF, Freyermuth S, Rogue P, Malviya AN: Stimulation of nuclear protein kinase C leads to phosphorylation of nuclear inositol 1, 4, 5-trisphosphate receptor and accelerated calcium release by inositol 1, 4, 5-trisphosphate from isolated rat liver nuclei. *J Biol Chem* 1993, 268:732–736.
174. Vermassen E, Fissore RA, Nadif Kasri N, Vanderheyden V, Callewaert G, Missiaen L, Parys JB, Smedt HD: Regulation of the phosphorylation of the inositol 1,4,5-trisphosphate receptor by protein kinase C. *Biochemi Biophys Res Commun* 2004, 319:888–893.
175. Li W, Yu JC, Shin DY, Pierce JH: Characterization of a protein kinase C-delta (PKC-delta) ATP binding mutant. An inactive enzyme that competitively inhibits wild type PKC-delta enzymatic activity. *J Biol Chem* 1995, 270:8311–8318.
176. Sumandea MP, Rybin VO, Hinken AC, Wang C, Kobayashi T, Harleton E, Sievert G, Balke CW, Feinmark SJ, Solaro RJ, Steinberg SF: Tyrosine phosphorylation modifies protein kinase C delta-dependent phosphorylation of cardiac troponin I. *J Biol Chem* 2008, 283:22680–22689.
177. Dolmetsch RE, Lewis RS, Goodnow CC, Healy JJ: Differential activation of transcription factors induced by Ca²⁺ response amplitude and duration. *Nature* 1997, 386:855–858.
178. Berridge MJ, Bootman MD, Roderick HL: Calcium signalling: Dynamics, homeostasis and remodelling. *Nat Rev Mol Cell Biol* 2003, 4:517–529.
179. Miyawaki A: Proteins on the move: insights gained from fluorescent protein technologies. *Nat Rev Mol Cell Biol* 2011, 12:656–668.
180. Herrmann H, Bär H, Kreplak L, Strelkov SV, Aebi U: Intermediate filaments: from cell architecture to nanomechanics. *Nat Rev Mol Cell Biol* 2007, 8:562–573.
181. Lazarides E: Intermediate filaments: a chemically heterogeneous, developmentally regulated class of proteins. *Annu Rev Biochem* 1982, 51:219–250.
182. Huang SM, Leventhal PS, Wiepz GJ, Bertics PJ: Calcium and phosphatidylserine stimulate the self-association of conventional protein kinase C isoforms. *Biochemistry* 1999, 38:12020–12027.
183. Manna D, Bhardwaj N, Vora MS, Stahelin RV, Lu H, Cho W: Differential roles of phosphatidylserine, PtdIns(4,5)P₂, and PtdIns(3,4,5)P₃ in plasma membrane targeting of C2 domains. Molecular dynamics simulation, membrane binding, and cell translocation studies of the PKC α C2 domain. *J Biol Chem* 2008, 283:26047–26058.
184. Elsliger MA, Wachter RM, Hanson GT, Kallio K, Remington SJ: Structural and spectral response of green fluorescent protein variants to changes in pH. *Biochemistry* 1999, 38:5296–5301.
185. Corbin JA, Evans JH, Landgraf KE, Falke JJ: Mechanism of Specific Membrane Targeting by

- C2 Domains: Localized Pools of Target Lipids Enhance Ca²⁺-Affinity †. *Biochemistry* 2007, 46:4322–4336.
186. Landgraf KE, Malmberg NJ, Falke JJ: Effect of PIP₂ binding on the membrane docking geometry of PKC alpha C2 domain: an EPR site-directed spin-labeling and relaxation study. *Biochemistry* 2008, 47:8301–8316.
 187. Lai C-L, Landgraf KE, Voth GA, Falke JJ: Membrane docking geometry and target lipid stoichiometry of membrane-bound PKC α C2 domain: a combined molecular dynamics and experimental study. *J Mol Biol* 2010, 402:301–310.
 188. Yeh R-H, Yan X, Cammer M, Bresnick AR, Lawrence DS: Real time visualization of protein kinase activity in living cells. *J Biol Chem* 2002, 277:11527–11532.
 189. Clark JD, Lin LL, Kriz RW, Ramesha CS, Sultzman LA, Lin AY, Milona N, Knopf JL: A novel arachidonic acid-selective cytosolic PLA₂ contains a Ca(2+)-dependent translocation domain with homology to PKC and GAP. *Cell* 1991, 65:1043–1051.
 190. Plant PJ: The C2 Domain of the Ubiquitin Protein Ligase Nedd4 Mediates Ca²⁺-dependent Plasma Membrane Localization. *J Biol Chem* 1997, 272:32329–32336.
 191. Chapman ER: Synaptotagmin: a Ca(2+) sensor that triggers exocytosis? *Nat Rev Mol Cell Biol* 2002, 3:498–508.
 192. Chapman ER: How Does Synaptotagmin Trigger Neurotransmitter Release? *Annu Rev Biochem* 2008, 77:615–641.
 193. Jahn R, Fasshauer D: Molecular machines governing exocytosis of synaptic vesicles. *Nature* 2012, 490:201–207.
 194. Zhang D, Aravind L: Identification of novel families and classification of the C2 domain superfamily elucidate the origin and evolution of membrane targeting activities in eukaryotes. *Gene* 2010, 469:18–30.
 195. Denning MF, Wang YH, Nickoloff BJ, Wrone-Smith T: Protein kinase C delta is activated by caspase-dependent proteolysis during ultraviolet radiation-induced apoptosis of human keratinocytes. *J Biol Chem* 1998, 273:29995–30002.
 196. Majumder PK, Pandey P, Sun X, Cheng K, Datta R, Saxena S, Kharbanda S, Kufe D: Mitochondrial translocation of protein kinase C delta in phorbol ester-induced cytochrome c release and apoptosis. *J Biol Chem* 2000, 275:21793–21796.
 197. Qi X, Mochly-Rosen D: The PKCdelta -Abl complex communicates ER stress to the mitochondria - an essential step in subsequent apoptosis. *J Cell Sci* 2008, 121:804–813.
 198. Braz JC, Gregory K, Pathak A, Zhao W, Sahin B, Klevitsky R, Kimball TF, Lorenz JN, Nairn AC, Liggett SB, Bodi I, Wang S, Schwartz A, Lakatta EG, DePaoli-Roach AA, Robbins J, Hewett TE, Bibb JA, Westfall MV, Kranias EG, Molkentin JD: PKC-alpha regulates cardiac contractility and propensity toward heart failure. *Nat Med* 2004, 10:248–254.
 199. Srivastava J, Procyk KJ, Iturrioz X, Parker PJ: Phosphorylation is required for PMA- and cell-cycle-induced degradation of protein kinase Cdelta. *Biochem J* 2002, 368:349–355.
 200. Rybin VO, Sabri A, Short J, Braz JC, Molkentin JD, Steinberg SF: Cross-regulation of novel protein kinase C (PKC) isoform function in cardiomyocytes. Role of PKC epsilon in

- activation loop phosphorylations and PKC delta in hydrophobic motif phosphorylations. *J Biol Chem* 2003, 278:14555–14564.
201. Holden NS, Squires PE, Kaur M, Bland R, Jones CE, Newton R: Phorbol ester-stimulated NF-kappaB-dependent transcription: roles for isoforms of novel protein kinase C. *Cell Signal* 2008, 20:1338–1348.
 202. Oestreich EA, Malik S, Goonasekera SA, Blaxall BC, Kelley GG, Dirksen RT, Smrcka AV: Epac and phospholipase Cepsilon regulate Ca²⁺ release in the heart by activation of protein kinase Cepsilon and calcium-calmodulin kinase II. *J Biol Chem* 2009, 284:1514–1522.
 203. Kveiborg M, Instrell R, Rowlands C, Howell M, Parker PJ: PKC α and PKC δ regulate ADAM17-mediated ectodomain shedding of heparin binding-EGF through separate pathways. *PLoS ONE* 2011, 6:e17168.
 204. Chen L, Meng Q, Jing X, Xu P, Luo D: A role for protein kinase C in the regulation of membrane fluidity and Ca²⁺(+) flux at the endoplasmic reticulum and plasma membranes of HEK293 and Jurkat cells. *Cell Signal* 2011, 23:497–505.
 205. Sato M, Ueda Y, Umezawa Y: Imaging diacylglycerol dynamics at organelle membranes. *Nat Meth* 2006, 3:797–799.
 206. van Meer G, Voelker DR, Feigenson GW: Membrane lipids: where they are and how they behave. *Nat Rev Mol Cell Biol* 2008, 9:112–124.
 207. van der Weyden L, Conigrave AD, Morris MB: Signal transduction and white cell maturation via extracellular ATP and the P2Y₁₁ receptor. *Immunol Cell Biol* 2000, 78:369–374.
 208. Song C: Regulation of a Novel Human Phospholipase C, PLCepsilon, through Membrane Targeting by Ras. *J Biol Chem* 2000, 276:2752–2757.
 209. Citro S, Malik S, Oestreich EA, Radeff-Huang J, Kelley GG, Smrcka AV, Brown JH: Phospholipase Cepsilon is a nexus for Rho and Rap-mediated G protein-coupled receptor-induced astrocyte proliferation. *Proc Natl Acad Sci USA* 2007, 104:15543–15548.
 210. Brindley DN, Pilquil C, Sariahmetoglu M, Reue K: Phosphatidate degradation: Phosphatidate phosphatases (lipins) and lipid phosphate phosphatases. *Biochim Biophys Acta* 2009, 1791:956–961.
 211. Sutton RB, Sprang SR: Structure of the protein kinase C β phospholipid-binding C2 domain complexed with Ca²⁺. *Structure* 1998, 6:1395–1405.
 212. Colon-Gonzalez F, Kazanietz MG: C1 domains exposed: From diacylglycerol binding to protein–protein interactions. *Biochim Biophys Acta* 2006, 1761:827–837.
 213. Bittova L, Stahelin RV, Cho W: Roles of Ionic Residues of the C1 Domain in Protein Kinase C-alpha Activation and the Origin of Phosphatidylserine Specificity. *J Biol Chem* 2000, 276:4218–4226.

Publications

During PhD period

1. **Hui X**, Reither G, Kaestner L, Lipp P. (2014) Targeted activation of conventional and novel protein kinase C through differential translocation patterns. Mol Cell Biol submitted.
2. Lipp P, **Hui X**, Reither G, Kaestner L. (2014) Multichannel Imaging of Cellular Signaling: Interplay of Ca²⁺ and Conventional Protein Kinase C. In: J. Parys, M. Bootman, D. Yule, & G. Bultynck, (Eds.), Calcium Techniques: A Laboratory Manual (pp126-129). New York, Cold Spring Harbor Laboratory Press

Before PhD study

1. Zhao Y, Wang X, Wang T, Hu X, **Hui X**, Yan M, Gao Q, Chen T, Li J, Yao M, Wan D, Gu J, Fan J, He X (2011). Acetylcholinesterase, a key prognostic predictor for hepatocellular carcinoma, suppresses cell growth and induces chemosensitization. Hepatology; 53(2): 493-503.
2. Gao F, **Hui X**, He X, Wan D, Gu J (2008). Dysfunction of murine dendritic cells induced by incubation with tumor cells. Cell Mol Immunol.; 5(2): 133-40.
3. **Hui X**, Gao J, Xie X, Suto N, Ogiku T, Wang MW (2005). A robust homogeneous binding assay for alpha4beta2 nicotinic acetylcholine receptor. Acta Pharmacol Sin.; 26(10): 1175-80.
4. Ji QG, Gao J, Wang J, Yang C, **Hui X**, Yan X, Wu X, Xie Y, Wang MW. Benzothieno[3,2-b]indole derivatives as potent selective estrogen receptor modulators. Bioorg Med Chem Lett. 2005 Jun 2; 15(11): 2891-2893.

Acknowledgments

Time flies without any notice. After nearly four years PhD study, I finally reached the point that need to summarise my research work. When looking back, I really enjoyed the time and will cherish the memory of these days. Here I would like to express my deepest and sincerest appreciation to all the people who helped me, especially to those bellow.

First of all, I would like to thank Prof. Dr. Peter Lipp, my supervisor, for giving me this great opportunity to work in this lab. During my PhD study, he directly instructed my research work, offered so much valuable advices, and offered countless time and efforts in my research articles and this dissertation. His optimism, cheerfulness, and encouragement inspire me for further adventure in the field of scientific research.

I would also like to express my deep gratitude to Dr. Lars Kaestner for his sophisticated instrument support but mostly for his original and brilliant ideas for experimental design from his special physical aspect.

I would also like to thank Prof. Dr. Markus Hoth and Dr. Barbara Niemeyer for accepting to be members of my thesis committee, for efficient discussions and constant support.

My thankfulness also gives to Dr. Anke Scholz and Dr. Sandra Ruppenthal for their unselfish helps in molecular cloning and cell maintaining.

My great appreciation and friendship also goes to Dr. Qinghai Tian. His nice offering of software programming and macros for data analysis extremely improve work efficiency and save lot of time.

I also thank to Mr Benjamin Sauer for his proficient instruments maintaining and warm-hearted helps in my everyday-life, to Ms Tanya Kuhn for routine experimental support, and to Ms. Karin Schumacher for administrative support.

Many thanks also gives to all members I didn't mention above in our group for their constant support and collegiality for the pleasant and comfortable atmosphere.

Besides I would like to express thankfulness to my co-operators, Prof. Karsten Kruse and Mr Mike Bonny from the department of Theoretical Physics for their excellent theoretical simulation and interpretation, Dr. Gregor Reither for his kindly gifts of many biological material.

Finally, I would like to thank my wife and parents for their continuous loving and supports in my decisions.